DEVELOPMENT OF ARTIFICIAL NEURAL NETWORK-BASED MODEL FOR ASSESSMENT OF SOLAR ENERGY RESOURCES AND IMPLEMENTATION OF OFF-GRID SOLAR POWER SYSTEM

BY

OLUBUSADE JOSEPH EYITAYO

PhD/SPS/2017/993

DEPARTMENT OF PHYSICS SCHOOL OF PHYSICAL SCIENCES FEDERAL UNIVERSITY OF TECHNOLOGY MINNA

JULY, 2023

DEVELOPMENT OF ARTIFICIAL NEURAL NETWORK-BASED MODEL

FOR ASSESSMENT OF SOLAR ENERGY RESOURCES AND

IMPLEMENTATION OF OFF-GRID SOLAR POWER SYSTEM

BY

OLUBUSADE JOSEPH EYITAYO

PhD/SPS/2017/993

THESIS SUBMITTED TO THE POSTGRADUATE SCHOOL FEDERAL UNIVERSITY OF TECHNOLOGY MINNA, NIGERIA IN PARTIAL FULFILMENT OF THE REQUIREMENT FOR THE AWARD OF THE DEGREE OF DOCTORATE OF PHILOSOPHY (PhD) IN APPLIED ATMOSPHERIC PHYSICS

JULY, 2023

DECLARATION

I hereby declare that this thesis titled “Development of Artificial Neural Network-Based

Model for Assessment of Solar Energy Resources and Implementation of Off-Grid Solar Power System" is a collection of my original research work and it has not been presented for any other qualification anywhere. Information from other sources (published or unpublished) has been duly acknowledge.

Joseph E. Olubusade …….

PhD/SPS/2017/993 Signature & Date

Federal University of Technology,

Minna, Nigeria

CERTIFICATION

The thesis titled “Development of Artificial Neural Network-Based Model for

Assessment of Solar Energy Resources and Implementation of Off-Grid Solar Power System” by OLUBUSADE, Joseph Eyitayo (PhD/SPS/2017/993) meets the regulation governing the award of the degree of PhD of the Federal University of Technology, Minna and it is approved for its contribution to scientific knowledge and literary presentation.

Prof. O. D. Oyedum …….

Major Supervisor Signature & Date

Prof. M. A. Aibinu …….

Co-Supervisor Signature & Date

Dr. J. A. Ezenwora …….

Co-Supervisor Signature & Date

Dr. A. S. Moses …….

Head of Department Signature & Date

Prof. M. Jiya …….

Dean, School of Physical Sciences Signature & Date

Engr. Prof. O. K. Abubakre ……. Dean,
Postgraduate School Signature & Date

DEDICATION

This thesis is dedicated to the Almighty God for the gift of life, and to the souls of my deceased beloved: father (Michael Olugbade Olubusade), mother (Margaret Folayemi Olubusade) and sister (Helen Oluseeke Olubusade). May you all find peace with your maker.

ACKNOWLEDGEMENT

True people brighten prosperity and lighten adversity by taking parts. My Major Supervisor Prof. O. D. Oyedum. His love, persistent supports, guidance, devotion and words of wisdom in different spheres of life are my motivation. His fatherly relationship is the major cause of my joy today. The resilience supports from Prof. A. M. Aibinu, even at mid nights with his inspiration can never be forgotten. Dr. J. A. Ezenwora, your commitment, care and time will forever be remembered. I am glad and proud to extract from their pool of knowledge.

The success of this work is also tied to the love, concerns and supports received from the following scholars: The Head of Department, Dr. A. S. Moses, Dr. J. Eichie, Dr. G. Aku,

Dr. K. Igwe, Dr. L. Olarinoye, Dr. M. Dada, Dr. T. Folorunso, Dr. L. Olatomiwa, Dr. J. Ojeniyi, Dr. M. Olomiyesan, members of PhD Clinic, other great Professors, Doctors, academic / non-academic staff, colleagues and students from the Department of Physics, Federal University of Technology, Minna and beyond whose names are numerous to mention.

Mrs. Ene Esther Olubusade, the woman behind my success is not only acknowledged but equally congratulated for the successful completion of my PhD research. Her golden love, understanding and modesty will forever be treasured. My profound gratitude also goes to the following people, without which my Joy would not have been to the fullest: Miss Judith O. Olubusade, Mrs. Omoyemi Olubusade-Ajibola, Mrs. Omotola Olorunsogo, Mrs. Evelyn Kasa, Mrs. Elizabeth Arowolo, Miss Abosede Arowolo, Dr. Mary Adepoju, Mr. Vincent Nkama, Mrs. Remi Adebayo, Mr. Okpako, Mr. Olanrewaju and Mrs. Blessing (Badamosi), the entire Akor family, the good people of El-Amin International School, Priests, Church members / leaders, Pastors, Prophets and everyone that had in one way or the other contributed to my success.

However, the graph of my life remains non-linear. On this note, I appreciate all friends and foes for the various impacts they have made in my life. In their respective love and detestation, I have realised the reasons for my existence. I love you all.

ABSTRACT

Energy poverty is a brick-wall between man and modern technology, especially in the developing regions of the world. Total electricity generation in Nigeria has been kept far below 10, 000 MW and Nigeria would require above 200,000 MW to meet up with the electricity demand of about 200 million people. Regrettably, a major fraction of the power generated is driven by fossil fuels. In order to guarantee emission-free, affordable and sustainable electricity in Nigeria, there is need to embrace solar as an alternative energy source. Solar energy exists freely in nature, it is abundant and inexhaustible. To access this resource, a precise knowledge of Global Solar Radiation (GSR) at surface level is a requisite. This study is therefore aimed at assessing the potential of solar energy resources for power generation in the North-Central Nigeria using surface meteorological data. A 25-year (1993 to 2018) monthly average data of global solar radiation, relative humidity, amount of cloud, minimum and maximum temperature were obtained from the database of the United States' National Aeronautics and Space Agency for each of the states. A soft computing model was developed using Artificial Neural Network (ANN). Relative humidity, temperature change and solar flux are the input nodes, while the measured GSR is the output to the network which has 49 hidden neurons. Supervised learning algorithm was employed with a feed-forward back propagation architecture and LevenbergMarquard training algorithm. Non-linear and linear activation functions were used at the first and second layers of the network respectively, through which a training state of 0.98 and a testing state of 0.97 regression values were attained. The developed model was used along-side thirteen existing empirical models to estimate global solar radiation. Their results were compared using statistical metrics which include Mean Absolute Error (MAE), Mean Bias Error (MBE), Mean Squared Error (MSE), Root Mean Squared Error (RMSE) and Coefficient of Correlation (R). MAE, MBE, MSE, RMSE and R values for the model are respectively given as: 0.242, 0.026, 0.079, 0.281 and 0.856 for Abuja; 0.247, -0.043, 0.077, 0.277 and 0.825 for Benue; 0.294, -0.25, 0.136, 0.369

and 0.757 for kogi; 0.323, -0.171, 0.156, 0.395 and 0.704 for Kwara; 0.195, 0.092, 0.058, 0.240 and

0.919 for Nasarawa; 0.353, -0.035, 0.175, 0.419 and 0.665 for Niger; and 0.320, -0.053, 0.148, 0.385 and 0.871 for Plateau State. HOMER was used to simulate and optimise different system configurations using four components, including photovoltaic solar module, diesel generator, battery and controller. 1,137, 984, 1,004, 1,050, 1,130, 1,171 and 1,155 power system configurations are feasible for Abuja, Benue, Kogi, Kwara, Nasarawa, Niger and Plateau respectively. The optimisation report showed that system combination of a photovoltaic solar module, a diesel generator, strings of battery and a controller is the best for the region, providing unit cost of energy as low as 0.017$, 0.021$, 0.022$, 0.020$, 0.019$, 0.017$ and 0.018$ for Abuja, Benue, Kogi, Kwara, Nasarawa, Niger and Plateau respectively. A system configuration that is of 100% renewable input consumed no diesel and this automatically implies that the system has zero (0) emission. It is also noteworthy that the unmet load for all the simulated results is zero (0). Rather, excess electricity was produced which could be sold out to serve other load demands. Hence, the study concluded that the abundant solar energy resources in the region guarantees an enabling environment for the inclusion of solar energy technologies in generating clean, cheap and sustainable electricity. Government, interested individuals and investors are therefore encouraged to take advantage of the findings in order to create a healthy and wealthy nation.

Table of Contents

List of Tables Table

Page

 List of Figures

Figure **Page**

List of Symbols and Abbreviations

Δ	Change / variation
δ	Solar declination
Γ	Factor of monthly variation of extra-terrestrial solar radiation
K	Factor of latitude, solar declination and the mean sunrise hour angle
ω_s	Sunset hour angle
φ	Latitude of the site
φ_1	Activation function of the first layer
φ_2	Activation function of the second layer
b_j	Input bias associated with the j^{th} neuron of the first layer
b_k, b_2	Output bias associated with the k^{th} neuron of the second layer

C_{ld}	Cloud amount
dn	Day number of the year
H_2O	Water
I_{rr}	Solar flux
T_{max}	Maximum temperature
T_{min}	Minimum temperature
T	Temperature
AE	Absolute Error
AI	Artificial Intelligence
EGSR	Estimated Global Solar Radiation
ANFIS	Adaptive Neuro-Fuzzy Inference System
ANN	Artificial Neural Network
B	Battery
Bat	Battery
BNN	Biological Neural Network
C	Controller
CO_2	Carbon dioxide
COE	Unit Cost of Energy
Ctl	Controller
ECN	Electricity Corporation of Nigeria
EGSR	Estimated Global Solar Radiation
FCT	Federal Capital Territory
G	Diesel generator
Gen	Diesel generator
GSR	Global Solar Radiation
HOMER	Hybrid Optimisation Model for Electric Renewable
I_{sc}	Solar constant = 1,367 Wm^{-2}
IW	Input weight (w_{ij})
logsig	Logistic sigmoid
LW	Layered weight (w_{jk})

MABE	Mean Absolute Bias Error
MAE	Mean Absolute Error
MBE	Mean Bias Error
Md	Model
MGSR	Measured Global Solar Radiation
MNN	Multi-layer Neural Network
MSE	Mean Squared Error
NCSN	North Central States of Nigeria
NDA	Niger Dams Authority
NEPA	National Electric Power Authority
NPC	Net Present Cost
NPC	Nigeria Population Commission
NREL	National Renewable Energy Laboratory
OC	Operation cost
P	Photovoltaic module
PHCN	Power Holding Company of Nigeria
PV	Photovoltaic / Solar Module
R	Coefficient of Correlation
RBFN	Radial Basic Function Network
ReLU	Rectified Linear Unit
RH	Relative Humidity
RMSE	Root Mean Squared Error
s_o	Average day length
SAE	Sum Absolute Error
SCM	Soft Computing Model
SNN	Single-layer Neural Network
SSE	Sum Squared Error
tanh	Hyperbolic tangent
w_{ij}	Adjustable weight connecting the input layer to the hidden layer
w_{jk}	Adjustable weight connecting the hidden layer to the output layer

x_i Set of input data to the ANN (for $1 \leq i \leq n$ and n = 3)

y_1 Output of the first layer

y_2 Output of the second layer,

CHAPTER ONE

1.0 INTRODUCTION

1.1 Background to the Study

Economic development is largely related to energy development (Hermann, 2001). Presently, most of the world's energy supplies on a large scale are generated using fossil fuels which in turn pose many threats to lives. Globally, there is huge demand for energy which is propelled by growing human population (Suleiman, 2010).

According to history, Nigeria's electricity grid has been based on hydro power which is one of the conventional means of generating power on a large-scale. But over the years, the use of hydropower in Nigeria's energy grid has declined as more attention is given to natural gas for the generation of electricity. The natural gas, apart from being a nonrenewable form of energy, is limited by so many factors which place power generation in a situation of dependence.

Renewable energy sources involve continuous transformation and development of energy from raw form into useful form. Renewable energy sources include solar, biomass, wind, tidal, water, and geothermal. Renewable energy sources are more favourable compared to other sources of energy. For instance, solar energy is free, inexhaustible, needs no fuel and does not release greenhouse gases. A world that relies on the ever-diminishing supply of fossil fuels will not last. High dependency on power generation through fossil fuels might be limited by the scarcity in supply of natural gas which sometimes may have to be imported (Rapier, 2020). So, the development of renewable energy technologies in generating power will not only guarantee energy security but also help in decarbonising and purify the atmosphere. Nevertheless, there are many hurdles on the quest to fossil fuel independence, few among these include economic issue, social issue, structural issue and political issue.

The energy from the sun is the prime source of energy flowing into the universal ecosystem (Qiang, 2003). After reflection and absorption of part of the energy in the sky, about 10^5 TW hit the Earth's surface and are transformed to various forms of energy (GCEP, 2006). Solar radiation is enormous and constitutes about 6×10^3-portion of the current world-wide energy usage which is projected to be 13.7 TW (IEA, 2004).

The pursuit to providing satisfactory energy for the general public is still a global subject, more especially in the developing and the underdeveloped parts of the world. According to the last population update by the Nigeria Population Commission (NPC), Nigeria's population is assessed to be about 200 million. Out of this population, a good number of this population are not fortunate to connect to the power grid (Punch, 2022), while many of those who have access to the grid are crying over epileptic power supply (Sambo *et al*., 2014). Energy is unavoidable for any human activity in this generation. As a result of this, the demand for power-generating sets increases daily. On the other hand, people with little or no access to power of any form resort to the use of coal, burning fire woods, and other forms of fossil fuels. However, cutting down of trees to make fire woods, burning of fuels to run a generating set and the likes, have many pronounced adverse impacts on the ecosystem. These include deforestation, global warming, desertification, erosion pollution, depletion of the ozone layer and flood, to mention but a few.

Little or no availability of power supply in a nation is a source of social and economic poverty (Fagbenle *et al*., 2011). For a couple of years back in Nigeria, the diminishing nature of the power sector has resulted into closure of workshops, industries and firms (Punch, 2020). Some proprietors have relocated to nearby countries where power can easily be accessed, thereby increasing the rate of unemployment and unproductivity in Nigeria. For Nigeria to experience a total breakthrough from its present state of economic depression, the issue of power supply must be well addressed so as to optimise power output.

Nigeria is blessed with enormous un-utilised solar energy resources that can address the limited power supply and lack of power supply as the case may be. Therefore, a proper study to assess the potential of solar energy resources is crucial. When this is properly done, it will significantly improve the quality and efficacy of power distribution and consumption, both within the urban and rural communities. Proper harvesting of renewable energy resources will considerably contribute to solving the power problem of Nigeria. Nevertheless, generation and transmission of power through power grids are often confronted with some challenges which in-turn limit the amount of generated power available to consumers (Iwayemi, 2008). More so, extending grid to all parts of the country will require a huge budgetary allocation. Hence, appropriate application of solar energy is key to a sustainable energy supply, which could be adopted as a stand-alone application or as power grid application as the case demands.

1.2 The Sun

The sun is a massive luminous object of glowing gas. It is an average star in the centre of the solar system. The sun gives life to the Earth by growing its plants, feeding its animals, preserving its foods, heating and illuminating its land, sea and atmosphere, generating its winds and tides, circulating its water and above all, producing its fossil fuels (Coleman and Davidson, 2015). The sun has a diameter which is estimated to be about 109 times wider than that of the Earth while its mass is about 3.3×10^5 times more than the mass of the Earth. On average, the distance of the sun from the Earth is about 1.5×10^8 km. Sometimes, these estimations seem not precise, owing to the fact that the sun has no true surface. There is nothing concrete about the solar disk and the constituent matter of the apparent surface is rarefied, which could sometimes be considered as a vacuum.

According to report, the sun was formed as a result of gravitational collapse of matter within a region of massive molecular cloud. Approximately, the sun is said to have existed

for 5×10^9 years. Based on estimation, the sun will continue to exist for the next 5 billion years, implying that the sun has a half-life of approximately 5×10^9 years. The age of the sun is predicted with the aid of computer models of stellar evolution and through nucleocosmo-chronology (Bonanno *et al*., 2008). Solar technologies apply and not limited to: cooling and heating technologies, provision of warm water for private and commercial purposes, operating engines and pumps, desalinating water for human consumption, initiating chemical processes and generating electricity to mention a few (Ullah *et al.*, 2013).

1.2.1 Definition of common terms associated with solar radiation

i. **Absorbed radiation:** When solar radiation impinges on particles or molecules of matter, it is either scattered, sent back towards the source, retained in the form of heat or transmitted. The process whereby the radiation is retained is known as absorption. Ozone, water (in the three states), methane, carbon dioxide, nitrogen and oxygen to mention but a few are good absorbers of radiant energy and are otherwise known as green-house gases. However, different spectrum of the solar radiation is captured differently by different particles or molecules of matter.

ii. **Clearness index:** This term describes the fraction of solar radiation at ground level to the solar radiation at the top of the atmosphere (extra-terrestrial radiation).

iii. **Diffuse radiation:** This is the component of solar radiation that is either scattered or reflected on the Earth's surface. Scattering in the atmosphere occurs when solar rays hit particles of matter in their paths. This is a phenomenon that explains why the sky is blue in the noon time, and red at

sunrise and sunset. Diffuse radiation does not include the ground-reflected radiation as in the case of inclined receiving plane (Wald, 2018).

iv. **Direct radiation:** This is the component of the solar radiation that travels in parallel lines directly from the sun to the Earth's surface without any interception. That is, the incident solar radiation received at the Earth's surface normal to the sun's rays. The maximum direct solar beam that could be received on clear sky at sea level on the surface is approximately 1000 Wm^{-2} (Olomiyesan, 2016b).

v. **Extra-terrestrial radiation:** This describes the solar radiation from the sun which is incident on a horizontal surface at the top of the atmosphere. This implies, the solar radiation recorded outside the atmosphere of the Earth. vi. **Global solar radiation (GSR):** This is the total solar radiation at the surface which is comprising of the direct, diffuse and the reflected radiations. vii. **Radiosity:** This is the term that describes the rate per unit surface area through which a radiant energy leaves a surface in relation to its transmission, reflection and emission.

viii. **Reflected radiation:** This explains how incident solar radiation is redirected back to space after striking a hard surface or some particles of matter in the atmosphere. Reflectivity varies for different matter particles and this is termed 'albedo'. Cloud is accountable for most reflections in the atmosphere (Pidwirny, 2006).

ix. **Solar constant:** This is the magnitude of solar irradiation that is received per unit time, per unit surface area which is normal to the solar radiation at the exterior boundary of the atmosphere at the average Sun-Earth distance. The solar constant however varies with the distance of the Earth from the sun. It is highest (1,400 Wm^{-}

^{2}) around December 21st, when the Earth is at its nearest position to the sun and minimum (1,310 Wm^{-2}) around June 21st, when the Earth is farthest from the sun. Its average value is often used as solar constant.

x. **Solar irradiance:** This simply indicates the radiating power of the sun per unit area on the Earth's surface (Wm^{-2}).

xi. **Solar irradiation:** This describes the radiating energy of the sun over a unit surface area on the Earth. It is otherwise known as solar insolation, measured in Jm^{-2} (Wald, 2018).

1.3 Statement of the Research Problem

In this era, energy is essential for any meaningful transformation to take place. In Nigeria, power availability diminishes daily with increasing human population. The generated 4,000 MW (Gerretsen, 2018) is not sufficient to sustain the economy of a state. Hydropower and fossil fuels are the major sources of the generated power.

Hydropower involves the use of dammed water to power a generator. About 90% of the power generated in developing countries are gotten from hydropower (Bartle, 2002). The stagnant water in the dam has higher temperature than a flowing river. It contains excess sediments and nutrients which cultivate more algae and aquatic weeds. In addition, methane (green-house gas) is often produced and released into the atmosphere. The construction of dams affects land use, migration and population of wildlife and aquatic animals, it alters the weather condition of the environment and involves huge government revenue allocation for maintenance.

A severe flood was recorded in 2012, in which about 30 out of the 36 States in Nigeria were affected (Daily Trust, 2018). A similar case was recorded in the year 2018 in which many lives and valuables were lost to flood (Vanguard, 2018). In the same vein, the world recorded the peak flood in the year 2022, and Nigeria was one of the highest hit countries

across the globe (The Guardian, 2022; Reliefweb, 2022; Telesur, 2022; World Economic forum, 2022). The cause of the severe flood in Nigeria is majorly attributed to the release of excess water from dams.

Despite the huge losses recorded from the use of hydropower, some major parts of the country still suffer from epileptic power supply, while many others do not even have access to the grid. As a result of this, citizens try to adopt various means of making power available by using fossil fuels. The use of fossil fuels involves the transformation of chemical energy to various other forms which impose many threats on the ecosystem. More so, fossil fuel is not readily available and requires huge financial commitments for its exploration, exploitation and consumption. Yet, over dependence on fossil consumption leads to the scarcity of the product.

Above all, nature has blessed Nigeria with much renewable and non-renewable energy resources to enable it stand and compete economically with any nation across the globe, but lack of the required amount of energy has limited the development of Nigeria. For Nigeria to generate cheap and clean energy that will be sustainable, there is need to harvest the energy from the sun. To achieve this, good knowledge of solar insolation at the point of application is a requisite. Pyranometer, an instrument used to measure the direct solar insolation is hard to come by. The scarcity of the equipment can be attributed to high cost of purchase, cost of installation, cost of calibration and maintenance. Aside these facts, issues of missing data are often recorded by users. As a result, many researchers have developed models that will predict values for solar irradiation, but many of these developed models are erroneous (Teke *et al*., 2015), which can be attributed to model adaptations to specific regions and sometimes methodology. Therefore, there is a need to develop an adaptable model of better accuracy than the existing models.

1.4 Study Area

The research is conducted in North-Central Nigeria (NCN). This includes the Federal Capital Territory (FCT) and six other states, which are geographically situated in the middle belt region of Nigeria. In the course of this study, the FCT is assumed as a state. Then, North-Central States of Nigeria (NCSN) will be referenced as seven states, covering from the west, around the convergence of River Benue and River Niger. The states therefore include, Abuja, Benue, Kwara, Kogi, Niger, Nasarawa and Plateau. The zone is rich in natural land structures and claims some of Nigeria's major tourist attractions. In addition, the middle belt comprises of people with different ethnic groups, speaking different languages. The significant ethnic groups within the zone include the Igala, the Igbira, the Idoma, the Tiv, the Yoruba, the Gbagyi, the Nupe, the Berom, the Mangu, the Mada-Eggon and the Gwandara. Figure 1.1 shows the map of Nigeria with the various zones, Figure 1.2 shows the NCSN, while Figure 1.3 is a map of the NCSN showing the seven states.

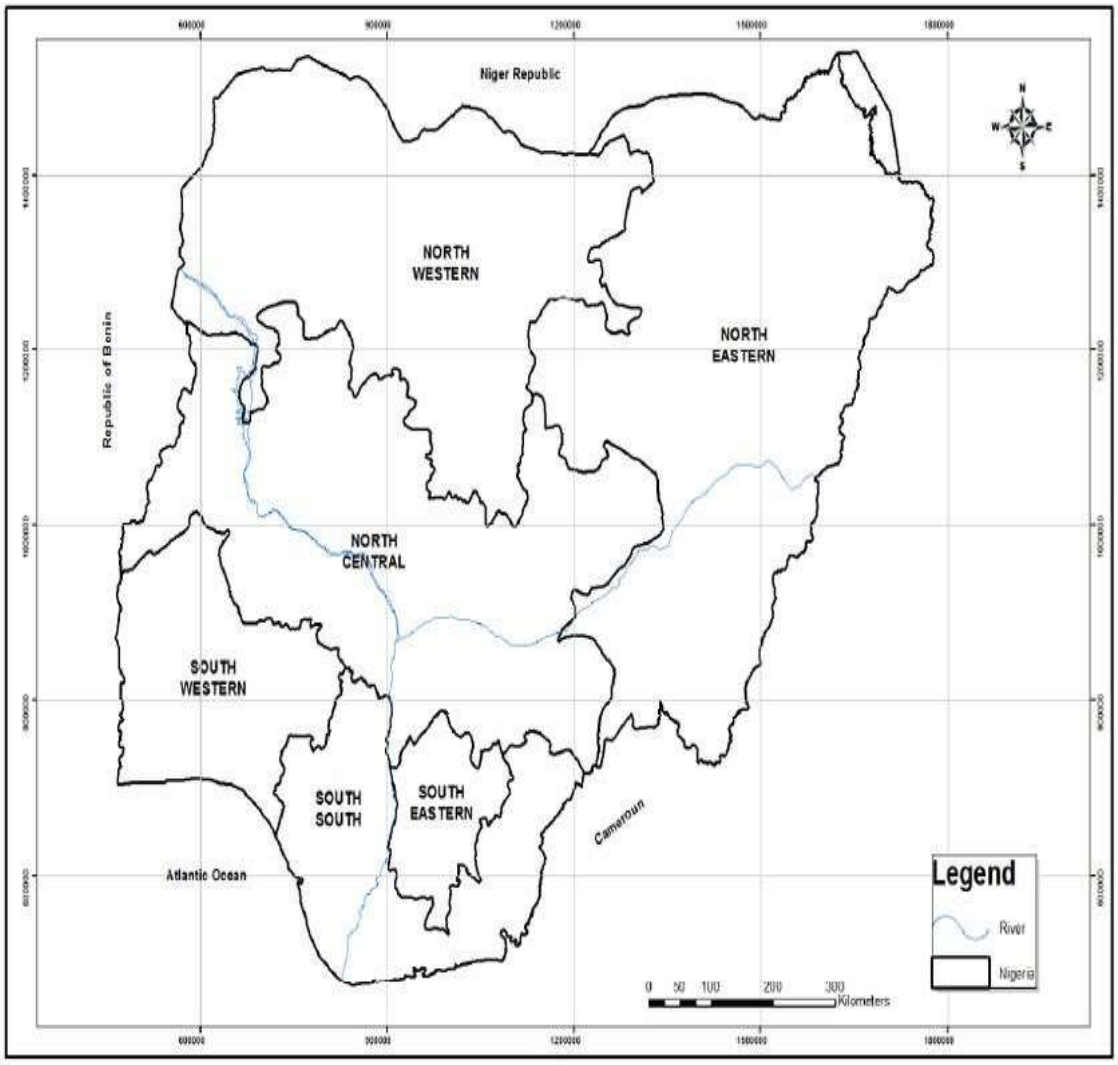

Figure 1.1: The six geographical zones of Nigeria (Source: Bovwe *et al.*, 2016).

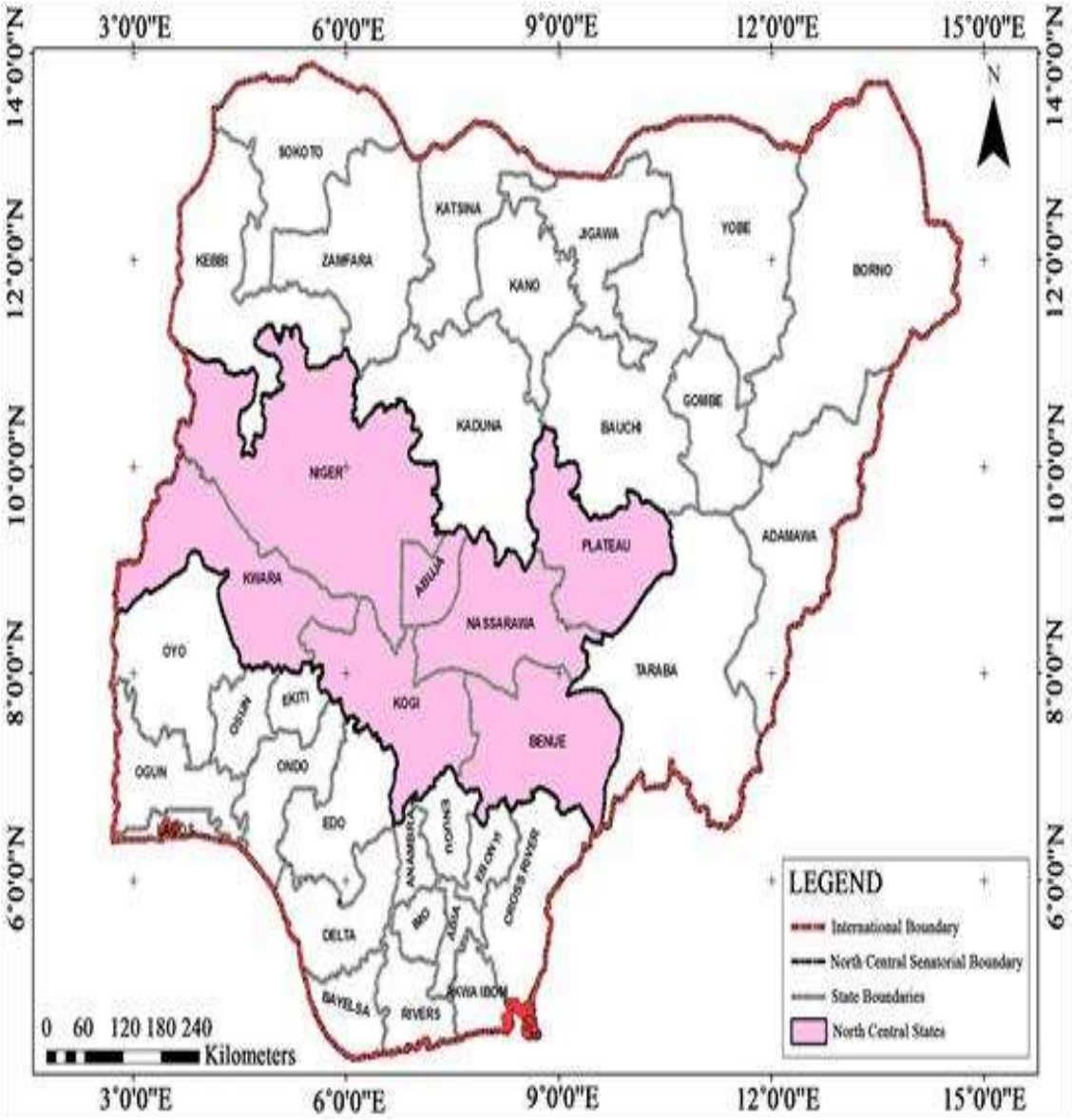

Figure 1.2: The North-Central Zone of Nigeria (Source: Ideki and Weli, 2019).

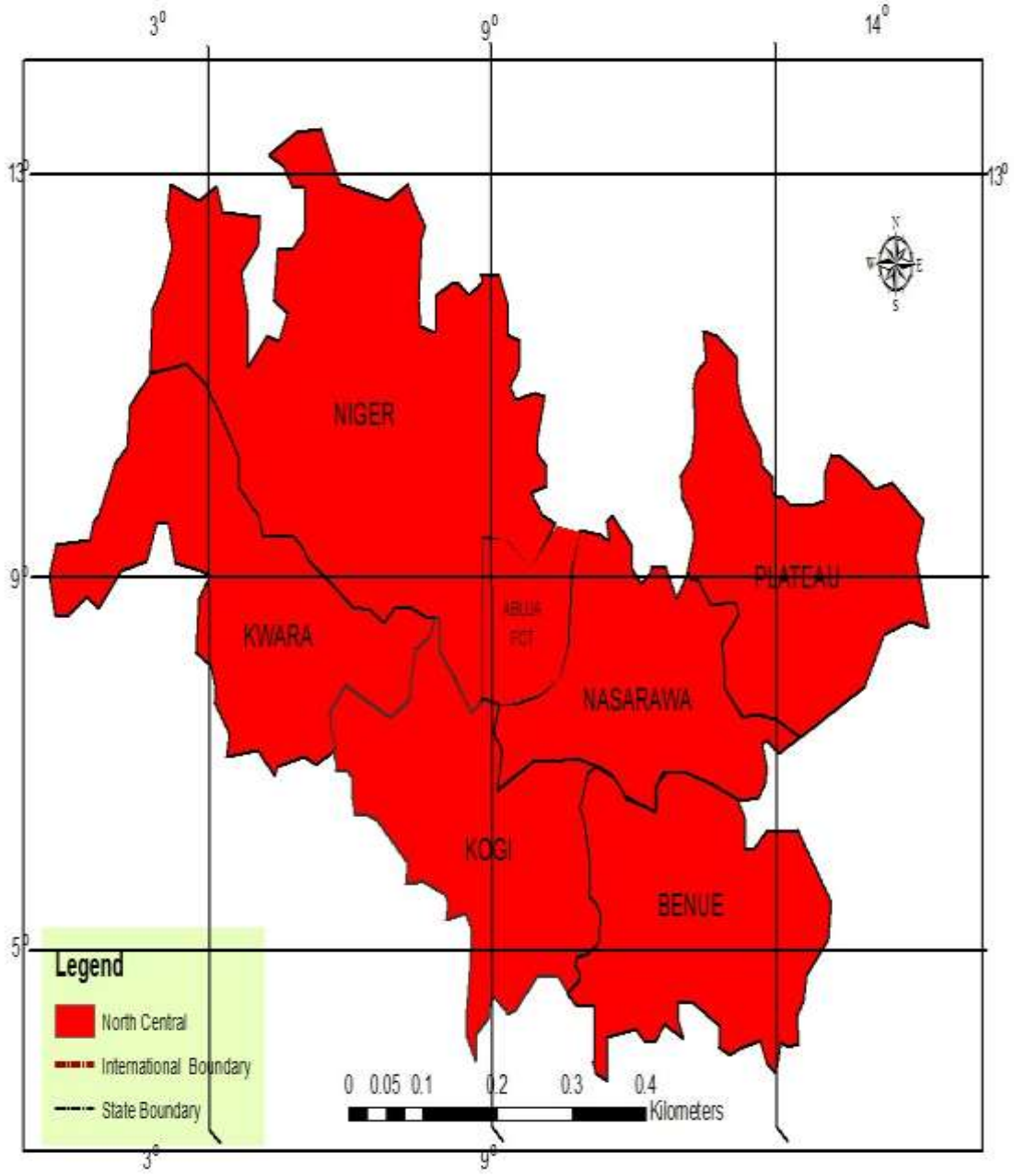

Figure 1.3: States in the North-Central Zone of Nigeria (Source: Author).

Abuja: Abuja which is referred to as center of power is the Federal Capital Territory of Nigeria. It spans over an area that is tactically located at the center of Nigeria to signify neutrality and national unity. The area covered is about 7,569 square kilometers, while its geographical coordinates fall within latitude 9.07 and longitude 7.49 with an average

altitude of 245 meters above sea level. Abuja shares a boundary on the north with Kaduna State, on the south with Kogi state, on the west with Niger state and on the east with Nasarawa State (Wikipedia, 2021).

Benue State: The state is called the food-basket of the nation, having Makurdi as its state capital. Benue State is positioned in the Guinea Savannah region of Nigeria's Middle Belt zone. The main ethnic groups include Tiv, Idoma, Igede, Etulo and Abakwa. Benue State falls within latitude 7.73 and longitude 8.53 with a mean average of 152 meters above sea level. The total area is about 30,755 square kilometers. Benue State shares boundaries with Taraba State to the east, Kogi State to the west, Cross River State to the south, Enugu State to the south-west Nasarawa State to the north and international boundary with the Republic of Cameroon to the south-east (Wikipedia, 2021).

Kogi State: Kogi state is referred to as the confluence state, having its capital as Lokoja. It is called the confluence state because of its location at the meeting point of river Niger and river Benue. The confluence state comprises of a wooded savanna region which is divided by the southward flowing river Niger. Kogi State is located on latitude 7.75 and longitude 6.82 which covers an area of about 20, 389 square kilometers with an average altitude of 55 meters above sea level. The main ethnic group in the State include, the Igala, the Ebira the Okun and the Yoruba. Kogi shares borders with Abuja and Niger State to the north, Nasarawa State to the north-east, Enugu, Anambra, and Delta to the south, Benue to the east, and Ondo, Ekiti, and Kwara to the west (Wikipedia, 2021).

Kwara State: It is referred to as the state of Harmony. The ethnic groups include Yoruba, Bariba, Nupe, Busa, Baatonun and Fulani. The state is located in the western region of the NCSN having Ilorin as its state capital. The state has boundaries with Benin to the west, Kogi to the east, Niger to the north and Ekiti, Osun, and Oyo to the south. Kwara

State is positioned on latitude 8.50 and longitude 4.55 with an average altitude of 305 meters above sea level. It covers about 23,822 square kilometers lying in-between the forest and the guinea savannah zones of Nigeria (Wikipedia, 2021).

Nasarawa State: Nasarawa State is referred to as home of solid minerals with its capital as Lafia. Nasarawa State is located between latitude 8.48 and longitude 8.52. The state is bounded by states like Kaduna in the North, Taraba and Benue in the south, Kogi and the Federal Capital Territory in the West and Plateau in the East. The state spans over an entire area of about 29,063 square kilometers with a mean height of about 193 meters above sea level. The major ethnic majority in the state include the Hausa, Aho, Alago, Gwandara, Bassa, Agatu, Eggon, Ake and Kanuri (Wikipedia, 2021).

Niger State: Niger State is referred to as the power state, having Minna as its state capital. The state takes its name after river Niger, which forms one of its main borders. Niger State is positioned on latitude 9.58 and longitude 6.55 with an average height of about 164 meters above sea level. It covers about 76,363 square kilometers, making it the largest state in Nigeria. Due to the position of the state, the two major hydroelectric power stations in Nigeria are located within the state, these include Shiroro and Kanji dam, which is the reason why it is referred to as the power state. The recognised ethnic groups in the state include Gbagyi, Nupe, Kadara, Barab, Koro, Kambari, Kakanda, Dukawa, Gwada Gana, Dibo, Hausa, Kamuku, Pangu, and Ingwai (Wikipedia, 2021).

Plateau State: Plateau State is discussed as the home of peace and tourism, having Jos as its state capital. Plateau State consists mainly of undulating uplands of an average height of 1200 meters. Owing to the presence of rugged hills and numerous rock formations, some of the rivers and streams have formed appealing landscape scenery, which also make the state fascinating for tourism. Its location is between latitude 9.89 and longitude 8.86. The total land mass is about 26,899 square kilometres, sharing borders

with Bauchi State to the north-east, Kaduna to the north-west, Taraba to the south-east and Nasarawa to the south-west. There are over forty ethnic groups in the state, these include the Afizere, Aten, Mupun, Ron-Kulere, Bache, Ngas, Jarawa, Bogghom, Tarok, Kofyar, Buji, Chip, Talet, Gashish, Irigwe, Montol, Amo, Mushere, Piapung, Anaguta, Mwaghavul, Pyem, Berom, Fier, Jukun, Goemai and Youm (Wikipedia, 2021).

1.4.1 Climatology of the study area

North-central geographical zone of Nigeria covers six states and the FCT. It is positioned between latitudes $6^0 30''$ N and $11^0 20''$ N and longitudes 7^0E and 10^0E, spreading over a total landmass of about 296,898 square kilometres (Adelaja *et al*., 2021). NCN experiences a typical tropical climate with two distinguished seasons (wet and dry season). The wet season is also known as the rainy season. It is a period of rainfall and lasts for an average period of six months, which is usually between May and October, with a mean annual rainfall ranging between 1,500 mm to 1,800 mm (Olayemi *et al*., 2014; Adelaja *et al*., 2021). The dry season is a period that is marked for no rainfall. The dry season is usually between the months of December and March. November and April are the transitional periods between the two seasons.

The activity of rainfall is usually at its peak in the month of August and this is accompanied by a mild temperature, while February is marked for the peak activity of the dry season which is accompanied by high temperature. On average, the annual temperature of NCN ranges between 20^{o}C to 35^{o}C. Furthermore, the dry season is characterised by a short period of cold and dry weather condition which is commonly known as harmattan. Harmattan is brought about by the northeast trade wind and generally begins in the month of November and ends in the month of January (Olayemi *et al*., 2014). The vegetation of NCN is of the Guinea Savanna type. As a result of the prevailing vegetation coupled with the existence of river Niger and river Benue, the region

is endowed with huge mineral deposits and is famous for agricultural practices (Adelaja *et al*., 2021).

The wet season is defined by low solar insolation, low air temperature, high relative humidity and vast cloud cover. On the other hand, the dry season is defined by high solar insolation, high air temperature, low relative humidity and little or no cloud cover.

1.5 Aim and Objectives of the Study

The study is aimed at developing an Artificial Neural Network (ANN) based model to assess solar energy resources for implementation of off-grid solar power system.

The aim of the study will be achieved through the following objectives:

i. to develop ANN-based model for calculating GSR.
ii. to estimate GSR using the proposed model and some existing empirical models for comparison with measured GSR values.
iii. to conduct feasibility study and techno-economic analysis of household off-grid solar power systems for NCSN.

1.6 Justification of the Study

In this era, almost all activities require energy. Be it reading, cooking, washing, spraying, communicating, milling, mixing, building, blending/grinding, cutting, weaving, playing music and many more require energy in one way or the other. Energy crisis in Nigeria is at a critical level in which the supply of energy diminishes daily with increasing human population. Hence, there is the need to explore the accessible energy resources. Energy from the sun is the most abundant and most evenly distributed energy source all over the globe. Within an hour, the magnitude of solar radiation reaching the surface is sufficient to cater for the total annual global energy demand (Abedelhak *et al*., 2013). More importantly the use of photovoltaic (PV) cells in generating electricity requires little or

no network distribution, it is durable, easy to install, low cost of maintenance is involved and it can be used at any location. In addition, solar energy technologies have huge potential to mitigate global warming. However, solar radiation is sometimes unpredictable and its potential for present and future use has to be carefully assessed.

NCSN is considered for the study because, it is the most sensitive part of the nation. It does not only accommodate the FCT, but, links other geographical regions together and it is known for massive agricultural activities which has the potential to provide food security for the nation and neighbouring countries. Therefore, results obtained from the study will be of immense benefit to governmental and non-governmental agencies, solar energy system engineers, farmers, researchers and individuals that are interested in solar applications.

1.7 Scope and Limitation of the Study

The study covers the North-Central states of Nigeria including Abuja, the FCT. In the course of the study, Abuja assumes the position of a state, thereby making a total of seven states. NCSN is considered for the study owing to its potential to facilitate national development. In view of this, a SCM is developed to assess GSR in the region. The study only considered ANN as one of the available SCM tools. A grid point data accessed from NASA is used for the study. The data is hence extrapolated to other places on assumption that it is homogenous. The research application focuses more on power generation, greenhouse gas emission and techno-economic analysis of different off-grid power system configurations.

CHAPTER TWO

2.0 LITERATURE REVIEW

2.1 Etymology of Energy

The term ‘energy’ refers to the ability to work. It is not something we can see, hear, touch, or smell. It is not made of anything, but describes an attribute of matter (Smith, 1998) which can exist in different forms. Energy emanated from two Greek words *en* and *ergon*, implying work inside a body. The compound word is *ἐνέργεια (enérgeia)*. *Enérgeia* as established by Aristotle between 322 BC and 384 BC simply means ‘being at work’ and has no direct translation to English language (Crosbie, 2000). According to Max Planck, energy is defined as the capability of a system to produce outside activity. Nothing on Earth could ensue or survive without energy. Plants and animals need energy to carry out their metabolic processes, just as a machine also needs energy to operate. However, the nature (form, state) in which the energy can exist and be utilised in order to achieve a useful work varies. This is therefore a justification to the law of conservation of energy, which states that “the magnitude of energy in a closed or isolated system remains unchanged”. This is to say that energy is not created and cannot be totally destroyed but can be changed to different forms. The forms of energy include, electrical, mechanical, solar, wind, nuclear, atomic, biomass, hydro, sound, light, electromagnetic and thermal, to mention but just a few.

In his 1802 lectures to the Royal Society, Thomas Young was the first man to use energy in a modern way. He described energy from the idea of *vis-visa*, which means, living force (Smith, 1998). This idea was defined by Leibniz as the product of the mass of a body and the square of its velocity (Thomas, 1807). Leibniz further stated that the term *vis-viva* is conserved. The erg is a unit of energy equivalent to 10^{-7} joules It is used in the centimetre-gram-second (cgs) system of units.

2.2 Exergy Concept of the Sun

In the year 1956, Zoran Rant was first to use the word *Exergy* as a name for available energy (Martinez, 2011). The word was a combination of two Greek words *ex* (meaning from or outer) and *ergon* (meaning work or force). Exergy could summarily be defined as the maximum work potential of a given system. That is, a measure of the maximum useful work that a system can deliver at a given state in a defined environment. It could also be referred to as the potential entropy of a system (measure of how clumped energy is spread out).

Thermodynamics explains that the total heat of a system cannot be completely converted into useful work, hence, exergy is more of a theoretical concept describing energy quality and energy utilisation (Zamfirescu and Dincer, 2009). Considering two identical metal slabs *a* and *b* from Figure 2.1. Slab *a* is heated (red hot) while slab *b* is kept at a low temperature. Since the degree of entropy is higher in slab *a*, then, when brought closer together, heat energy flows from slab *a* to slab *b* and as a result, work is said to be done. As the process continues, more energy will be transformed or (and) transferred between the slabs until the available energy will no longer have the potential to be used for further work.

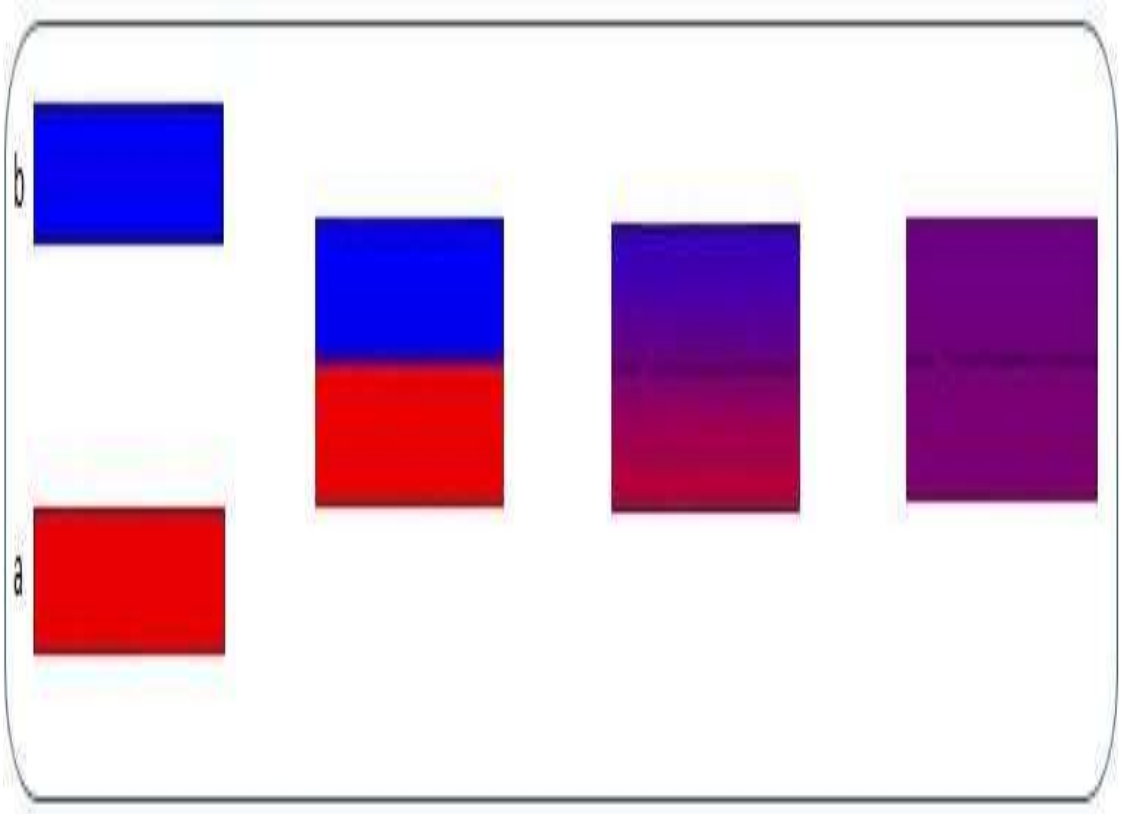

Figure 2.1: Energy flow between two identical slabs (Source: Author). If slab *a* is a heat system and slab *b* is the environment, then, this implies that a thermal equilibrium has been achieved between the system and its environment. This state is termed the dead state and the remaining energy in the system that has no potential to drive further process is known as anergy. Temperature gradients between the slabs depicts work-done, therefore, the efficiency (E_{ff}) of a system with quantity (Q) of heat is given as the fraction of temperature gradient (ΔT) between the system (T_a) and the environment (T_b), and to the temperature of the system (T_a).

$$E_{ff} = {}^{\Delta T}{}_{Ta} = {}^{T_a - T_a}{}_{T_a}{}^{T_b} \times 100 \quad (2.1)$$

$$E_{ff} = 1 - {}^{T}{}_{T}{}^{T_a}{}_{a}{}^{b} \times 100 \quad (2.2)$$

The exergy of a system as it undergoes an irreversible process is not conserved (it is destroyed), which is in contrary to the law of conservation of energy. When we burn our fossils and other sources of fuel, we could no longer use them again. However, exergy

"E_{xr}" describes energy quality or energy efficiency (Ahmet, 2014) and it is expressed as:

$$E_{xr} = Q\ [1 - \ _{T}T_{a}b] \tag{2.3}$$

The universe is faced with the problem of global warming and some other problems associated with it, these are the consequences of the nature of the energy we use. The universe has lots of clumped, clean and free energy sources from the sun which has not been put into use. Insolation is the topmost source of energy in the global ecosystem. After reflection and absorption of part of the energy in the atmosphere, about 100,000 TW hit the Earth's surface and are transformed to various forms of energy (GCEP, 2006). Solar radiation constitutes approximately 6,000-fold of the global energy requirements, which is estimated to be 13.7 TW (IEA, 2004). It will get to a dead state, but not until all its potentials are totally spread (given off) to its environment. When this happens, the exergy of the sun will be said to be destroyed (Zargut *et al*., 1988).

According to early engineers (Ahmet, 2014), the concept of exergy was developed to provide vital information to improve the efficacy of systems. In order to make the available solar radiation more valuable, therefore, the knowledge of its maximum potential is essential. For a radiating system (black body). The energy (E) of the radiating body is given by:

$$E = \sigma T^4 \tag{2.4}$$

while the exergy (E_{xr}) of a radiating body is given by:

$$E_{xr} = \sigma [T_4 - 4\_\_\_\_T_3 3T_o + T_3 0_4] \quad (2.5)$$

(Enrico and Goran, 2007).

where, σ is Stefan Boltzmann constant (5.67×10^{-8} W/m^{2}K^4), T (K) is temperature of the system (radiating body), T_o is temperature of the environment, E and E_{xr} are measured in watt per square meter.

Bodies which do not absorb all the radiation incident on them are referred to as grey bodies. However, most bodies fall into this category since they cannot absorb radiation of all wavelengths.

$$E_{grey} = \varepsilon\sigma T^4 \quad (2.6)$$

where, E_{grey} is the energy of a grey body, ε is known as the emission coefficient, σ is Stefan Boltzmann constant and T is its temperature in Kelvin.

2.3 Structure and Composition of the Sun

The sun is part of the milky-way. The milky way constitutes a spiral composed of over 10^{11} stars and the sun is our closest star. Hydrogen makes up for about 73% of the total mass of the sun, helium constitutes about 25%, while oxygen, iron, neon and carbon accounts for the remaining 2% when taking all together. The sun is a gigantic ball of hot gas, having its own atmosphere just as the Earth. It is subjected to the action of gravity which is balanced by the pressure exerted by the gas, so that an equilibrium size is maintained. The core of the sun covers from its centre to about twenty percent of the solar radius, with an extreme pressure that is about 3.4×10^{11} times higher than that of the Earth at sea level (Hufbauer, 1991). The structure of the sun is shown in Figure 2.2.

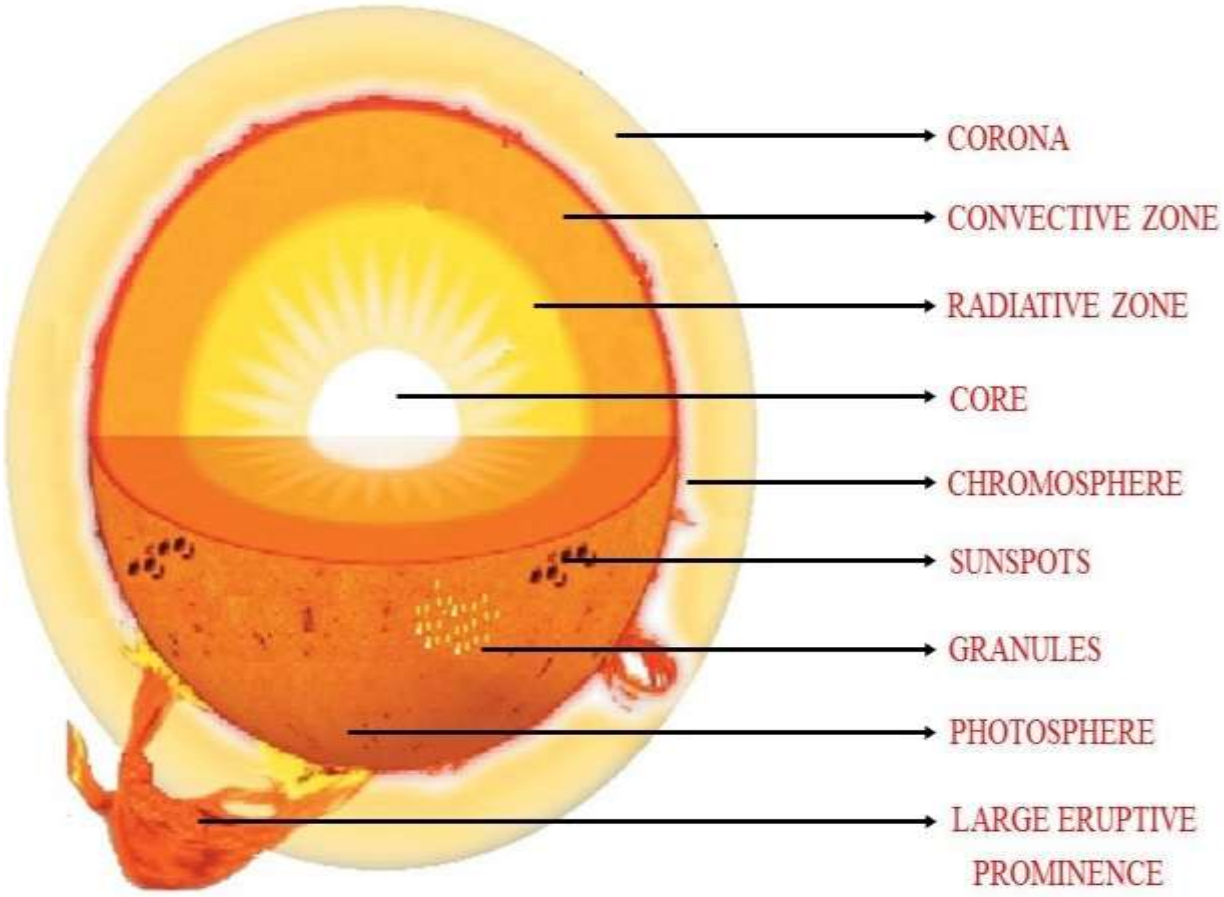

Figure 2.2: Structure of the Sun (Source: Author).

The structure and the composition of the sun shall be discussed under the following subheadings:

1. Solar interior
2. Solar atmosphere

2.3.1 Solar interior

The solar interior constitutes mainly the inner component of the sun. Classification is based on energy transport mechanism. It includes the core, the radiative zone and the convective zone.

2.3.1.1 *The core*

The core as the name implies is the innermost part of the sun. The temperature and density of the sun are highest in the core. The temperature in the core ranges between 15×10^6 K to 40×10^6 K, while the gases are highly compressed at density that ranges between 106 gcm^{-3} to 150 gcm^{-3}. The core constitutes about one-fifth of the solar radius (Garcia *et al*., 2007). A nuclear fusion reaction occurs at the core due to the high temperature and pressure recorded. During this nuclear reaction, four hydrogen nuclei are converted to helium nuclei through a process known as proton-proton chain reaction (Broggini, 2003), which is accompanied by the release of huge amount of energy.

Within the core, proton-proton chain reaction takes place about 9.2×10^{37} times per second, converting about 3.7×10^{38} protons into alpha particles (Phillips, 1995).

Solar thermonuclear reaction: Thermonuclear fusion is a process involving thermal and nuclear energy. Nuclear fusion is a process in which an atom is transformed into a different atom by gaining proton. It is important to note that the fusion chain reaction involve smaller nuclides, combining to form larger stable ones. Amidst this process, enormous amount of thermal energy is released. In the core, the rate of fusion reaction is constant and it is at equilibrium. A slight change in the rate of reaction would result to an increase in the temperature of the core and consequently cause the sun to expand, thereby reducing its density and the rate of nuclear reactions. On the other hand, a slight decrease in the rate of reaction would result to a decrease in temperature which will cool the sun and consequently make it contract, thereby increasing its density and the rate of nuclear reactions. The vast energy released during the fusion process is gotten from lost mass of the individual fused nucleons. According to Einstein's mass-energy equation, the conversion of matter into energy is controlled by the equation:

$$E = mc^2 \quad (2.7)$$ where, E is the energy, m is the lost mass and c is the speed of light.

In stars, most fusion reactions begin with hydrogen atoms combining to form helium atoms. The reaction chain continues as more atoms like helium and beryllium combine to form larger atoms. The combination process will not end until all the atoms are converted to ion. At this stage, fusion process can no longer take place because the energy required for fusion is much more than the energy released by the atoms. Hence, the star is said to be dead. Heat is given off in a nuclear fusion reaction that involves atomic nuclides with atomic masses lesser than that of iron (exothermic reaction). Contrarywise, heat is required or will be absorbed in a nuclear fusion reaction that involves atomic nuclides with atomic masses greater than that of iron (endothermic reaction).

Proton-proton chain reaction: Proton–proton nuclear chain reaction is predominant in dwarf stars (Jiachen, 2018). That is, stars that are equal in mass to the sun or less massive than the sun. For proton-proton chain reaction to occur, there must be sufficient temperature to overcome the repulsive force between the parent protons. The temperature required to start a proton-proton reaction is about 4×10^6 ^oC. In the fusion of protonproton, diprotons are more often the product of the reaction and not deuterium. Since the produced diprotons are in their unstable states, they often decay back into parent protons.

During the process, the energy released is about 27 MeV per cycle.

$$^1_2 H + {}^1_1 H \rightarrow {}^2_1 D + {}^0_{+1} e \quad (2.8)$$

$$^2_1 D + {}^1_1 H \rightarrow {}^3_2 He \quad (2.9)$$

$$^3_2 He + {}^1_1 H \rightarrow {}^4_2 He + {}^0_{+1} e \quad (2.10)$$

$$4\,{}^{1}_{1}H \rightarrow {}^{4}_{2}He + 2\,{}^{0}_{+1}e \quad (2.11)$$

Carbon-nitrogen-oxygen cycle: The carbon-nitrogen-oxygen fusion reaction is commonly known as the carbon-nitrogen cycle. It is predominant in stars that are more massive than the sun (Salaris and Cassisi, 2005). The carbon-nitrogen cycle is similar to the proton-proton cycle because their end products are the same, but the carbon-nitrogen cycle involves mainly carbon and nitrogen while the later involves only proton. It is a catalytic cycle. The minimum temperature required to start the carbon-nitrogen cycle is about 1.6×10^7 °C. The process thus becomes more domineering in the star with increasing temperature.

$$^{12}_{6}C + {}^{1}_{1}H \rightarrow {}^{13}_{7}N \quad (2.12)$$

$$^{13}_{7}N \rightarrow {}^{13}_{6}C + {}^{0}_{+1}e \quad (2.13)$$

$$^{13}_{6}C + {}^{1}_{1}H \rightarrow {}^{14}_{7}N \quad (2.14)$$

$$^{14}_{7}N + {}^{1}_{1}H \rightarrow {}^{15}_{8}O \quad (2.15)$$

$$^{15}_{8}O \rightarrow {}^{15}_{7}N + {}^{0}_{+1}e \quad (2.16)$$

$$^{15}_{7}N + {}^{1}_{1}H \rightarrow {}^{12}_{6}C + {}^{4}_{2}He \quad (2.17)$$

$$4\,{}^{1}_{1}H \rightarrow {}^{4}_{2}He + 2\,{}^{0}_{+1}e \quad (2.18)$$

2.3.1.2 *Radiative zone*

The radiative zone derives its name from its means of transferring energy. The enormous energy generated in the core during the nuclear reaction contains a huge magnitude of gamma rays which are transferred through the radiative zone. Within the radiative zone, gamma rays collide with atoms and the atoms absorb the energy of the rays which are further radiated outward in the form of electromagnetic waves. The radiative zone covers from the core to approximately 70 % of the radius of the sun. Within this zone, heat is

radiated which is the major mode of energy transmission (NASA, 2013). Temperature fades with increasing distance from the core. The temperature and density ranges between 2×10^6 K to 7×10^6 K, and 0.2 gcm^{-3} to 20 gcm^{-3} respectively (NASA, 2007).

2.3.1.3 *Convective zone*

The convective zone constitutes up to 30 % of the interior part of the sun. It is characterised by lower temperature and density when compared to the radiative zone. Owing to the presence of lower temperature and density, heat cannot be transferred outward through radiation, but the density of the plasma is sufficient to develop convection currents which move outward to the surface. Hence, the means of energy transfer in the convective zone is through convection. Tachocline is the transition zone between the radiative zone and the convective zone (Tobias, 2005).

2.3.2 Solar atmosphere

The solar atmosphere includes the photosphere, the chromosphere, the corona and the heliosphere.

2.3.2.1 *Photosphere*

The photosphere (implying sphere of light) is found at the lower part of the sun's atmosphere. It is the source of visible radiation and the part of the sun that can be seen from the Earth. It is majorly known for emitting visible and infrared radiations. The energy from the sun gets to the Earth through the photosphere. Temperature in this zone ranges between 4×10^3 K to 6×10^3 K. The photosphere is made up of heterogenous gas of low density, which form granulations and sunspots. This heterogenous gas results from the convection currents flowing out of the convective zone.

Granulations are referred to as patterns of bright grainy markings on the sun's surface. They are tiny cellular features that cover the surface of the sun where there are no

Sunspots. Granulations are formed when hot fluid at the top of the convection cells rises up in the bright areas and spread out at the surface. Granules are continuously produced, having a half-life of about 10 minutes per granule. They sink inward along the dark lanes when cooled and new granules emerge to replace the old ones. There are also supergranules which can last for about 24 to 48 hours.

Sunspots are referred to as dark regions on the exterior of the sun. The number of sunspots changes cyclically along the surface and the variation is referred to as solar cycle.

According to Wolf, sunspot index can be determined using the relation:

$$R = K(10g_r + F) \tag{2.19}$$

where, R is the sunspot index, g_r is sunspot groups, F is individual sunspot and K is the correlation factor (Mandrini, 2012). The correlation factor is aimed at correcting anomalies between observers, telescopes and the environment. Samuel Schawe discovers the sunspot cycle in the year 1843. He named it the Schawe cycle. From observations, Schawe concluded that sunspot cycle has an average life cycle of about 11.1 years.

2.3.2.2 *Chromosphere*

The chromosphere is an irregular layer with temperature ranging between 4,400 ^{o}C to about 80,000 ^{o}C. Energy transferred in this region is achieved through various mechanisms which include hydrodynamics, acoustic and magneto-acoustic. The lower chromosphere has diverse features like spicules, bright plagues, dark filaments, chromospheric network and bright prominences.

2.3.2.3 *Corona*

Corona is the name given to the sun's outer atmosphere. It can be seen during a total eclipse as a white crown surrounding the sun. The corona has no true shape. Its shape changes with the solar cycle and continually increase in size, thereby giving rise to the

formation of the solar wind (National Research Council, 2004). Its average temperature ranges from 10^6 ^oC to 2×10^6 ^oC. Some of the features of the corona include streamers, loops, coronal holes and plumes.

2.3.2.4 *Heliosphere*

The heliosphere refers to the outer atmosphere of the Sun. It is the boundary that marks the end of the Sun's magnetic field in space. A current of wind brooks out from the Sun's upper atmosphere in different directions, filling the space between the planets in the solar system. This wind is referred to as the solar wind. Solar wind is a torrent of charged particles originating from the sun's upper atmosphere. This stream of charged particle is majorly composed of protons and electrons (magnetic plasma) with varying speed and temperature. Owing to the possession of high speed and temperature, they acquire high kinetic energy which enables them to escape the Sun's gravity. These magnetic plasmas making up the solar wind does not mix with other magnetic plasmas between the stars in our galaxy. Thereby forming a bubblelike atmosphere that protects our solar system from the majority of galactic cosmic radiations (Wilcox Solar Observatory, 2006).

2.4 Characteristics of Insolation

At the surface, the sun's gravity is about 273 kgm/s^2. The sun has a spectral type G2V with an absolute visual magnitude of 4.85 and a luminous intensity of about 3.83×10^{23} watt (Mandrini, 2012). Considering size and luminosity, the sun is a dwarf star. The sun completes its revolution in orbit round the centre of the milky way in about 2.25×10^8 years, with an average velocity of about 220 km/s (Mandrini, 2012). For a whole year, the energy which the sun unleashes on the Earth in an hour is sufficient to cater for the world's total energy need. The energy from the sun radiates in all directions. The total solar radiation reaching the surface of the Earth is termed the insolation, which is a short form for 'incident solar radiation'. A nuclear reaction takes place in the sun, which is the

fusion of hydrogen nuclei into helium nuclei. This nuclear reaction continues and enables the sun to generate its enormous energy as more matter is converted into energy. About four billion kilograms of matter is converted per second (Roger and Merlin, 2006). The internal temperature of the sun is over forty million degrees Celsius. At its surface, the gases are at about six thousand degrees Celsius out of which the highest percentage of the radiation is ultraviolet. However, only about fifty percent of this radiation gets to the surface of the Earth, as much of the radiation is absorbed in the Earth's upper atmosphere by oxygen, nitrogen and ozone, while some of the longer wavelength radiations are selectively absorbed by H_2O vapour and CO_2 gas in the lower atmosphere.

The percentage of radiation that is reflected by the Earth and its atmosphere is referred to as albedo. The heating portion of the sun's radiation is mainly found within the infrared region of the electromagnetic spectrum, while the greater percentage of the infrared radiation reaching the surface is retained mainly by CO_2 gas and H_2O vapour, which is later re-radiated back to the Earth. This process of re-radiation of heat back to the Earth's surface is the main cause of global warming. To have a state of temperature equilibrium at the surface of the Earth, energy inflow must equate the energy outflow. Consequently, excessive circulation of carbon dioxide within the atmosphere results in surplus heat retention within the atmosphere which is the reason for global warming.

According to literature (Roger and Merlin, 2006), an approximate of 1,360 Wm^{-2} can be recorded on the surface. This value is termed the solar constant. Solar constant is affected by geographical location, season of the year, time of the day, the amount of cloud at a particular time and largely on the thickness of the atmosphere. The geographical (latitude) and the seasonal factors are owing to the geometry of the Earth's orbit as it revolves round the sun. This orbit in which the Earth revolves round the sun is not a perfect circle and the axis in which the Earth spins is tilted at an angle of 23.5^0. Thus, the north pole is titled

toward the sun during the northern hemisphere's summer and away from the sun is the winter.

2.5 Spectra Emissive Power of the Sun

The sun is a black body at a temperature of about 5,527 ^{o}C. The energy which the Earth receives from the sun is a function of the Sun-Earth distance, which increases with decreasing distance. Plank describes the energy density of a radiating surface as;

$$E_d = \frac{3.7414400 \times 10^{8}}{\lambda^{5}\left[exp\left(\frac{\quad}{\quad}\right) - 1\right]} \qquad (2.20)$$

where, E_d is the energy density at the surface, λ is wavelength and T is its temperature.

The energy density of the Earth from the sun is given by:

$$E_D = \left(\frac{R}{D}\right)^{2} E \qquad (2.21)$$

where, E_D is the energy density of the Earth from the sun, R is the radius of the Earth, D is the sun-Earth distance and $\left(\frac{R}{D}\right)^{2}$ is the solar factor.

The light provided by the sun lies between the visible light region of the electromagnetic spectrum. According to the fundamental theory of waves, light is referred to as a continuous wave with different wavelengths. The speed c, wavelength λ and frequency f of the visible light are related by;

$$c = f\lambda \qquad (2.22)$$

Also, speed c, permittivity of free space $_o$ and permeability of free space μ_o are related by;

$$c = \frac{1}{\sqrt{\mu_o \varepsilon_o}} \qquad (2.23)$$

As sunlight enters the Earth's atmosphere, some portion of it is absorbed, some are reflected back into space, some are scattered while some get to the Earth's surface. At certain wavelength, significant amount of sunlight is absorbed by different molecules in the atmosphere. For instance, ozone absorbs sunlight in the ultraviolet region. Carbon dioxide and water vapour absorb sunlight in the infrared and visible region. Sunlight is also affected by atmospheric thickness, which is the volume of the atmosphere. As shown in Figure 2.3. Therefore, knowledge about the air mass ratio is of utmost importance. The air mass ratio is given by;

$$A_m = \sqrt{1 + \left(\frac{S}{h}\right)^2} \tag{2.24}$$

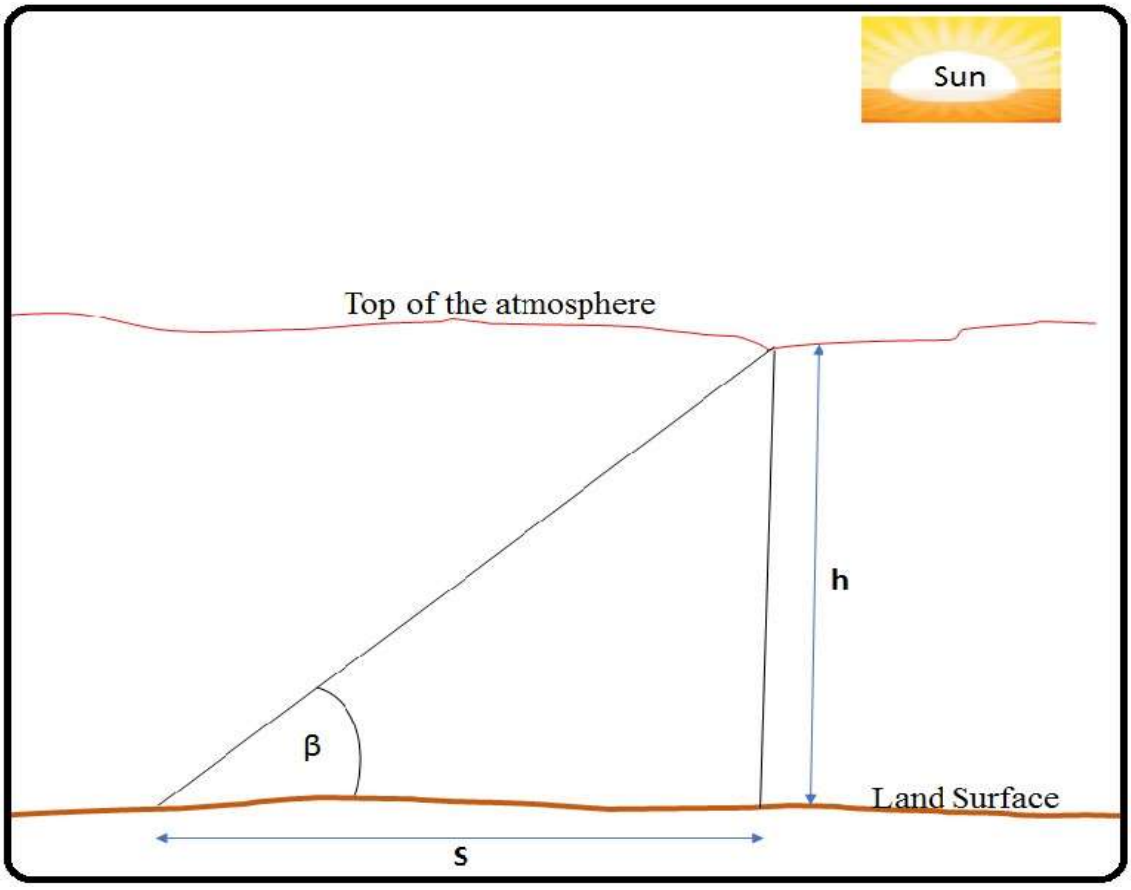

Figure 2.3: Air mass ratio (Source: Author).

also,

$$A_m = \sin^1\beta \tag{2.25}$$

where, h = height of object β

= altitude angle of the sun

S = length of shadow of object

2.6 Solar Spectrum

Sunlight is an unceasing wave of different wavelengths. The light wave reaching the Earth from the sun has a wavelength between 2×10^{-7} m to 2×10^{-6} m, which is within the visible light region of the electromagnetic spectrum as shown in Figure 2.4. Each wavelength has its equivalent frequency and energy (Scofield, 2009). The frequency and energy of a wave increases with diminishing wavelength, and on the other hand, the frequency and energy of a wave diminishes with increasing wavelength. The mathematical relationship between energy (E) and wavelength (λ) is given by:

$$E = \frac{hc}{\lambda} \tag{2.26}$$

where, h is plank's constant (6.626×10^{-34} Js), c is the speed of sunlight in vacuum. Combining equations (2.5 and 2.9) will give rise to equation 2.10, where f is the frequency of sunlight.

$$E = hf \tag{2.27}$$

In the same vein, equations 2.6 and 2.9 can be combined to obtain:

$$E = \frac{h}{\lambda\sqrt{\mu_o\varepsilon_o}} \tag{2.28}$$

where, μ_o and $_o$ are permeability of free space and permittivity of free space respectively.

According to Stefan Boltzmann, radiation emitted by a body is directly proportional to the radiation it will absorb and both the frequency and the energy radiated are functions of the body's temperature. Thus,

(Energy flux)E_f = $PA\text{-}(power(surface\ radiated\ area))$ (2.29)

P = $\alpha\sigma AT^4$ (2.30) $E_f = \sigma T^4$ (2.31)

where, σ is Stefan-Boltzmann constant (5.67×10^{-8} W/m^{2}K^4), T is temperature (K), α is emissivity, which is a dimensionless fudge factor (Scofield, 2009). The Stefan's constant σ accounts for the fact that a surface has to transmit light of specific wavelengths. Its value ranges between 0 and 1, while a perfect emitter or absorber has a value of 1. Equation (2.31) above is referred to as the Stefan-Boltzmann's law.

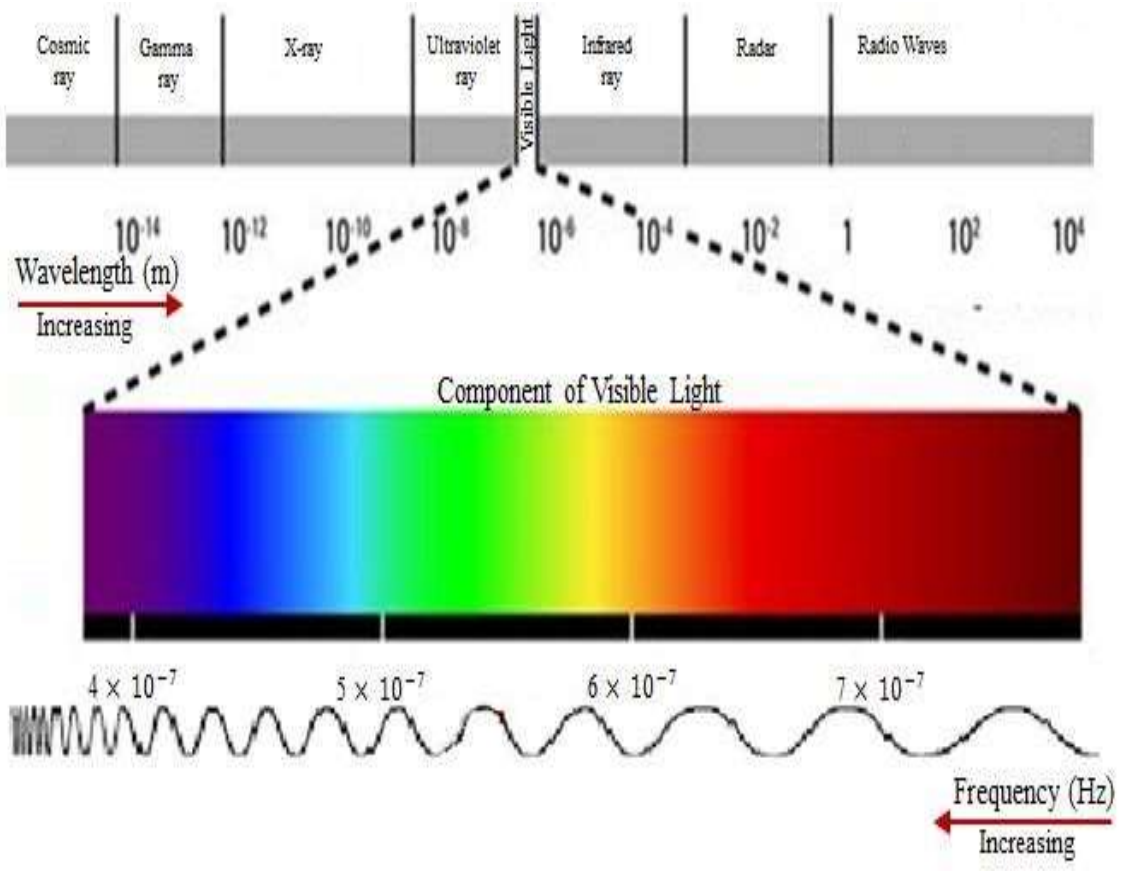

Figure 2.4: Electromagnetic spectrum (Source: Author).

Since the sun is a good emitter of heat, definitely, it is also a good absorber of heat and it is therefore referred to as a perfect black body. Reflectivity is a characteristic of bright surfaces, while absorption is a characteristic of dull (black) surfaces. When radiations are incident on bright surfaces, they bounce back to the direction of the source, but are captured when incident on dull surfaces. A surface of high reflective characteristics will absorb less radiation and therefore will emit less radiation. The light emitted by the sun is mostly found in the visible region of the electromagnetic spectrum, cresting close to the wavelength of yellow light. While the heat emitted by the sun is found within the infrared and the ultraviolet regions of the electromagnetic spectrum. However, waves of high frequencies will radiate more energy compared to waves of low frequencies. That is, the energy of a radiating body increases with increasing frequency. The power spectral density (P_τ) of a radiating body is represented as:

$$P_\tau = 2\overline{\pi\lambda C52h\,[e(\underline{\hbar\alpha C(\lambda)})\,\overline{\lambda KT} - 1]} \tag{2.32}$$

where, k is the Boltzmann's constant (1.38×10^{-23} J/K), $\alpha(\lambda)$ is the wavelength dependent emissivity, c is the speed of light in free space, h is the Plank's constant, T is the absolute temperature and λ is the wavelength.

Considering the Earth to be a sphere of radius R_e, with surface area A_e and temperature T_e, the rate at which power is given off from the Earth's surface is given by:

$$P_e = \sigma A_e T_e^4 \tag{2.33}$$

where, P_e is the power loss/given off, σ is the Stefan-Boltzmann's constant, π is a dimensionless constant which accounts for the curvature of the Earth ($\pi = \frac{22}{7}$).

If $A_e = 4\pi R_e^2$ (2.34) then, equation (2.32) becomes:

$$P_e = 4\pi\sigma R_e^2 T_e^4 \quad (2.35)$$

If on the other hand, the sun has R_s as its radius, T_s as its surface temperature and d as the sun-Earth distance, then the intensity of solar radiation I_s reaching the Earth's surface is given by:

$$I_s = \sigma T_s^4 \left({}_R d_s\right)^2 \quad (2.36)$$

Abedelhak *et al*. (2013) estimated GSR in Troyes-Barberey city in France using linear model, quadratic model and cubic model. Their comparative studies between the estimated and the measured GSR showed that linear model which gave most favourable estimate of GSR is the best in the region.

Soft Computing Models (SCMs) are developed on the basis of information processing in human body system (Eichie *et al.*, 2016). There are lots of complex information processing taking place in the human system which are all geared towards accomplishing various tasks. But in human, both logical and intuitive information processing are required. Computers are only able to process information logically, but their ability to process information intuitively cannot be compared with that of the human system. The following features are required for a computer system to process information like that of human, they include: openness, robustness and real time processing.

Openness describes the competence of the system to adjust and handle challenges encountered on its own. Robustness describes the stability and resilience of a system to changes or imperfections, while the real time processing describes the capacity of a

system to respond promptly to changes. Therefore, any information processing system that could support these three features is referred to as a real-world computing system (Chaudhuri and Chattopadhyay, 2005).

Soft computing is a good example of real-world computing system. Razmjoo *et al*. (2016) used Angstrom-Prescott model for determining the monthly GSR in Ahvaz and Abadan cities of Iran. Coefficients a and b were obtained as 0.30 and 0.49 for Abadan, and 031 and 0.47 for Ahvaz correspondingly. Olatomiwa *et al.* (2015) employed Adaptive NeuroFuzzy Inference System (ANFIS) to predict solar radiation using monthly mean; sunshine duration, maximum temperature and minimum temperature. Results gotten from ANFIS were compared with the results from empirical model, but, ANFIS predicted GSR better than the empirical model. Kumar *et al*., 2012) estimated monthly solar radiation using ANN and multiple regression models. Result for the two models were compared, it was concluded that the ANN performed better than the multiple regression models. Reasoning that the mean absolute percentage error values of the ANN models are lower than those of the multiple regression models. Also, the values of the coefficient of correlation are higher for the ANN compared to the multiple regression models, which is in agreement with the work of Yadav and Chandel (2013). In the same vein, Mohanty *et al*. (2016) reviewed the application of (GSR) models with correctional and SCM for the estimation of GSR. On this note, existing models were classified into two categories. The first category falls under empirical model while others fall under SCM. SCM is further classed as ANN, ANFIS and Radial Basis Function Network (RBFN). Having reviewed more than one hundred and ten research works, the authors concluded that soft comporting models are more accurate by giving minimum errors. Quej *et al.*, 2017) employed there SCMs to estimate daily GSR in a warm sub-humid region. They provided a new empirical model to predict daily GSR at six different stations in Mexico. Their newly developed model gave good accuracy in all the six stations. Hence, results showed

that models that combine temperature rainfall and air humidity perform better than models that use only temperature as input parameter. Furthermore, Fadare *et al*. (2010) modelled the potential of solar energy in Africa, using ANN. The researchers examined the viability of an ANNbased model for the determination of GSR in Africa. They concluded that ANN-based models are accurate and reliable for the estimation of GSR in Africa.

Generations back, computers are designed to obey a set of commands for the purpose of completing a task. As a result of this, the computer is unable to offer solution to any problem on its own, unless the series of instructions to follow are provided. This therefore restricts the capacity of conventional computers to resolving problems that already have solutions. This implies that they cannot solve problems without clue to the solution.

ANN is introduced to put an end to the duplication of solutions. They learn from examples just like the human brain does and cannot be programmed to carry out a specific task. They learn from examples and experience to solving a problem that we do not know how to solve. The building block of a neural network is artificial which works much the same way the biological neuron does. Just as a new born baby learns from his or her experience, the network is trained to learn but in a faster manner.

Considering many variables and phenomena, the atmosphere is a highly complierdynamic and non-linear system in which the interactions between different parameters often display chaotic features (Henderson and Wells, 1988; Sharifi *et al*., 1990; Stehlik, 1999; Sivakumar *et al*., 1998). According to Sivakumar (2020), the complexity encountered while analysing atmospheric data is as a result of the intrinsic non-linearity and the chaos. ANN is more suited to analyse such complex system (Maqsood *et al*., 2002).

2.7 Classification of Solid Matter

A solid describes a condition of matter of three-dimensional rigid structure, which is formed from the arrangement of atoms, ions and molecules. Unlike the other states of

matter, the relative forces of attraction between atoms, ions or molecules of a solid is high. However, some solids have their atoms, ions or molecules arranged in a repeating regular pattern. These solids are referred to as crystalline solids. On the other hand, some solids do not have their atoms, ions or molecules arranged in a repeating regular pattern. These solids are known as non-crystalline or amorphous solids.

Considering the conductive and resistive properties of solids, Solid materials with good conducting and poor resisting properties are called conductors, while solids with poor conducting and good resisting properties are called insulators. The relationship between the conductivity (σ) and the resistivity (ρ) of a solid matter is inverse. It is given as;

$$\sigma = \frac{1}{\rho} \tag{2.37}$$

2.7.1 Conductor

Conducting devices allow electrical and thermal energy to flow through them. A good conducting device is characterised by high conductivity and low resistivity, thereby allowing the free flow of electric charges. Metals and most crystalline substances are good examples of conducting devices. Metals generally are between group I to group III on the periodic table and are generally referred to as donors because of their mobile valence electrons. The conductivity (σ) $\approx 10^2$ to 10^8 Sm^{-1}, while the resistivity (ρ) $\approx 10^{-2}$ to 10^{-8} Ωm. Figures 2.5 describes the energy band theory of a conductor.

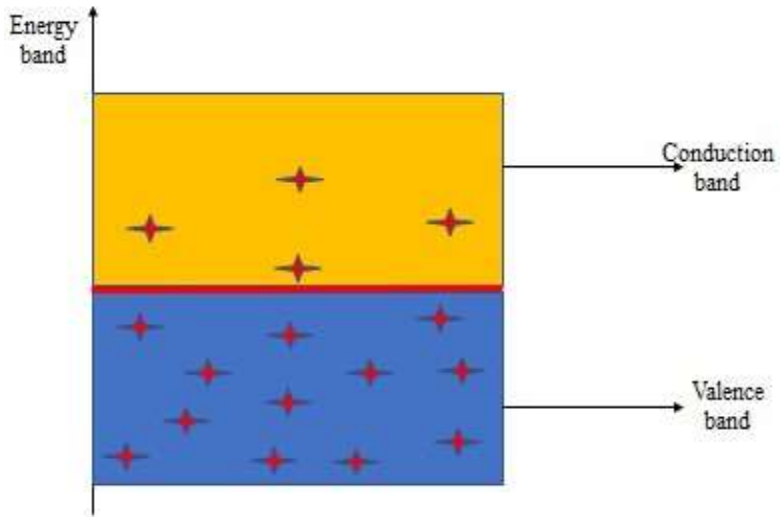

Figure 2.5: Energy band of a conductor (Source: Author).

2.7.2 Insulator

An insulating device is characterised by high resistivity and low conductivity, thereby creating a high opposition to the flow of electrical and thermal energy. Dry wood, cotton, plastic, glass, mica, paper and diamond to mention a few are insulators. Insulators are electron acceptors, having high affinity for electrons. The electrons in the valence band are bound to the parent atoms and as a result of this, electrons are not free to move like in the case of conductors. The conductivity (σ) $\approx 10^{-11}$ to 10^{-19} Sm^{-1}, while the resistivity (ρ) $\approx 10^{11}$ to 10^{19} Ωm. Figure 2.6 describes the energy band of an insulator.

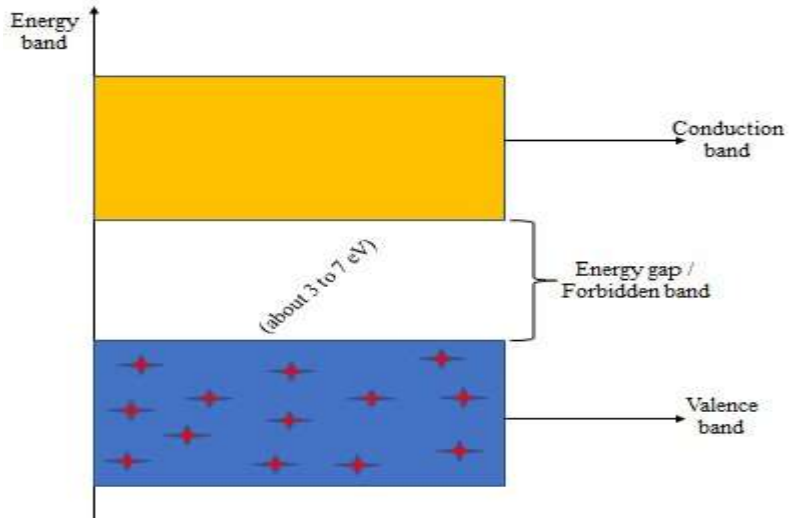

Figure 2.6: Energy band of an insulator (Source: Author).

2.7.3 Semiconductor

Semiconductors are group of materials whose conducting and resisting properties are intermediate between conductors and insulators. Semiconductor devices are employed in the modern day's technology because of their outstanding properties, more especially in the design of solid-state electronics. For semiconducting devices, conductivity (σ) $\approx 10^{5}$ to 10^{-6} Sm^{-1}, while resistivity (ρ) $\approx 10^{-5}$ to 10^{6} Ωm. Figure 2.7 describes the energy band of a semiconductor.

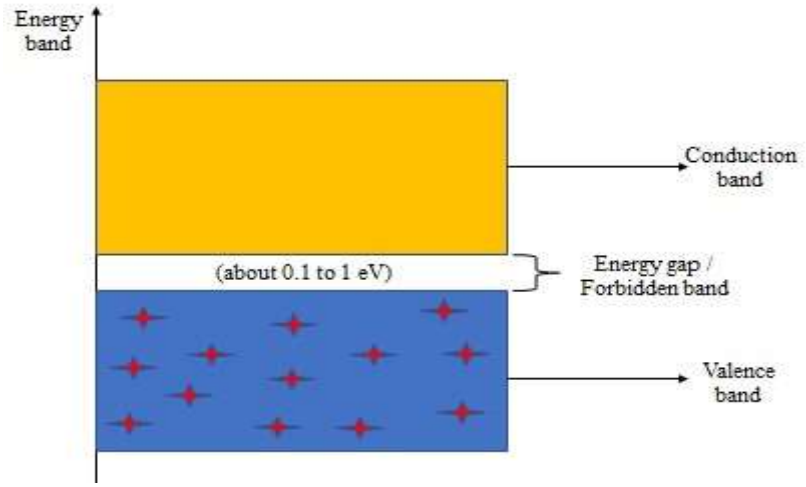

Figure 2.7: Energy Band of a Semiconductor (Source: Author).

Valency is the ability of an atom to combine with another atom. Valence electrons are the electrons that can be found in the outermost energy level of an atom. In a crystalline solid, every electron has a specified position with a particular order of arrangement, and each electron occupies different energy level. The available energy levels are of different energy magnitudes which form energy bands. The energy band that makes up the energy levels of the valence electrons is known as the valence band, while the energy band that makes up the energy levels of the conduction electrons is known as the conduction band. The conduction band is therefore a delocalised band of energy levels in a crystalline solid, which is partly filled with electrons. Electrons migrate from the valence band into the

conduction band if the least energy level in the conduction band is lower than the highest level in the valence band.

In the case of a conductor as seen in Figure 2.5, there is no energy gap between the valence and the conduction bands. The conduction band overlaps the valence band, which therefore paves way for easy transition of electrons between the two bands. Figure 2.6 describes the energy band theory of an insulator. In an insulator, there is a wide energy gap (forbidden gap) between the valence and the conduction bands. The presence of this wide energy gap, which is usually between 3 to 7 eV makes it difficult for free electrons to migrate into the conduction band. Still on the same note, Figure 2.7 explains the energy band theory of an insulator. In a semiconducting device, there is a small energy gap between the valence and the conduction bands which is usually between (0.1 to 1 eV). The small gap can easily be bridged by thermal application or through other forms of excitation. Hence, an increase in temperature increases conductivity in semiconductors, while the reverse is the case for conductors.

Semiconductors in their pure form are known as intrinsic semiconductors and in their impure form are known as extrinsic semiconductors (Kittel, 2004). Semiconductor devices are metalloid, they have four valence electrons in their outermost shell. They are group 4 elements on the periodic table and exhibit covalent bonding. Silicon is the most famous among the semiconductors owing to its abundance and simplicity. A typical unit cell of the crystal structure of silicon is shown in Figure 2.8.

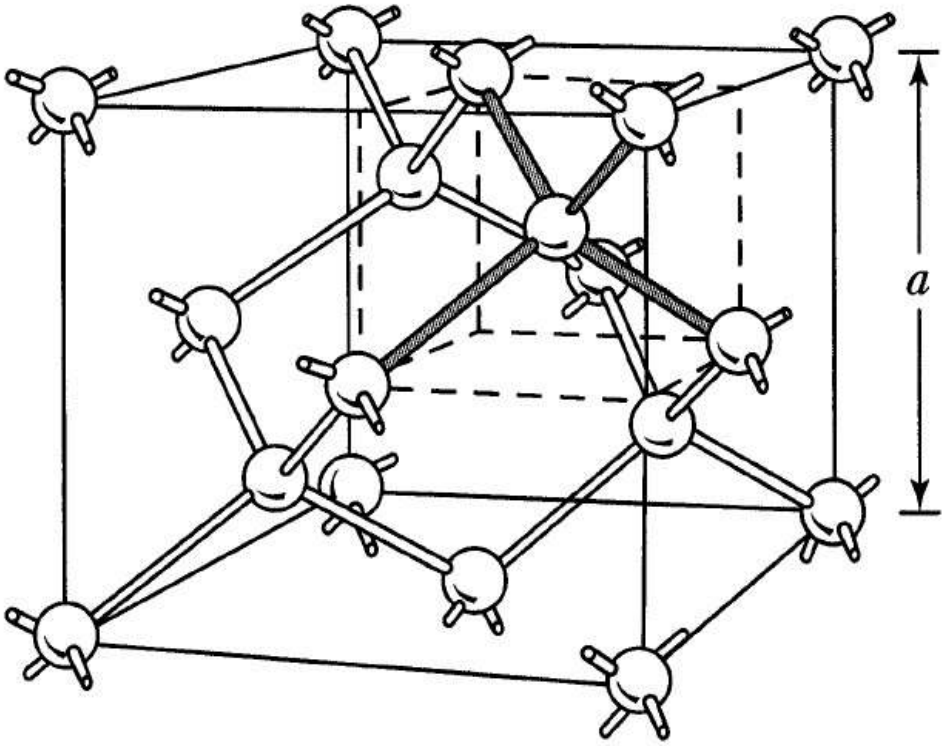

Figure 2.8: The unit cell of the silicon crystal (Source: Pisanty, 2018).

2.7.3.1 *Intrinsic semiconductor*

An intrinsic semiconductor is a pure form of semiconductor. The number of electrons and holes that make up the material dictates its behaviour. Both the electrons and holes are equally divided thereby making it a neutral crystal. Electrons transit between the valence and the conduction band as a result of thermal excitation (*Sze, 1981)*. When these electrons jump, they leave holes behind in the valence band, which will later be filled by other electrons in the valence band through a process called recombination. This process is reversible. For an intrinsic semiconductor, impurity composition should be less than 1 part in 100 million parts of the Semiconductor (Nada, 2017). This is shown in Figure 2.9.

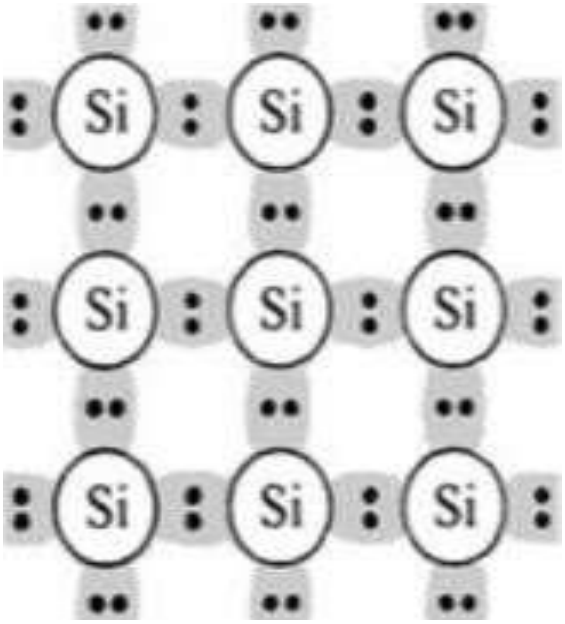

Figure 2.9: Pure silicon crystal (Source: Author).

However, the conductivity of a semiconductor does not solely depend on the number of carrier electrons and holes, but on the charge density, which is described as the number of carriers per unit volume (Nada, 2017). The carrier concentration of an intrinsic semiconductor is not the same for all materials and varies with temperature. At room temperature, an intrinsic semiconductor is an insulator.

If n is the number of electrons, p is the number of holes and n_i is the carrier concentration of an intrinsic semiconductor, then,

$$n_i = n = p \tag{2.38}$$

The specific conductance (σ_i) of an intrinsic semiconductor is the addition of conductivity of the electrons (σ_n) and conductivity of the holes (σ_p)

$$\sigma_i = \sigma_n + \sigma_p \tag{2.39}$$

$$\sigma_i = n_i e\mu_n + n_i e\mu_p \tag{2.40}$$ $$\sigma_i = n_i e(\mu_n + \mu_p) \tag{2.41}$$

where, μ is the mobility of charge carriers which depends on temperature, μ_p is the mobility of holes, μ_n is the mobility of electrons and e is electric charge. Given that

intrinsic concentration (n_i) is a function of the nature of a material (C), temperature (T in kelvin) and energy gap (E_g), hence,

$$n_i = \sqrt{CT^3 e^{(-Eg/KT)}} \tag{2.42}$$

where, k is the Boltzmann's constant, C is a constant which is different for different materials depending effective densities in the bands.

2.7.3.2 *Extrinsic semiconductor*

Extrinsic semiconductors are impure forms of semiconductor devices. Their conductivity is not only enhanced by thermal excitation but with the addition of foreign atoms called dopants to the crystal (Nada, 2017). In a general term, dopants are commonly known as impurities. The concentration of impurity atoms is about one part per million in the neighbourhood, which is very small compared to the parent atoms. These impurities may be implanted through a gaseous diffusion process, through ion implantation or photolithography (Neamen, 2003).

A dominant charge carrier in a semiconductor device is referred to as the majority carrier, while a charge carrier with lower concentration is referred to as the minority carrier.

Extrinsic semiconductors are of two types, namely: P-type and N-type semiconductors. The P stands for holes which represents positive charge, while the N stands for electrons which are negatively charged.

N-type semiconductor: An N-type semiconductor is formed by using a pentavalent impurity as dopant (Streetman, 2006). A pentavalent dopant has five electrons in its outmost shell. Some famous pentavalent elements are phosphorus, arsenic and antimony. Figure 2.10(a) describes a silicon crystal that is doped with a pentavalent impurity. While Figure 2.10(b) describes a pure silicon crystal. When this doped crystal is compared to a pure silicon crystal, it could be depicted that a pure silicon crystal has equal number of

electrons and holes, but for the doped silicon crystal, there are more electrons than holes, and so, the pentavalent impurity generates an extra electron (donor), thus having a net negative charge. A charge density will be left behind in the valence band. As a result, electric field is generated and occasionally a potential barrier is created inside the semiconductor (Sze and Kwok, 2007). Owing to the presence of ionized electrons, a new energy level will be established above the valence band. The energy gap between the new energy level of the donor electrons and the conduction band becomes very small. As a result of this, the donor electrons can easily mobilize into the conduction band. The presence of this free negative charge therefore improves the conductivity of the doped silicon crystal. Hence, conductivity of the material increases with increasing level of doping (James, 2019). For an N-type semiconductor, electrons are the majority carriers, while holes are the minority carriers.

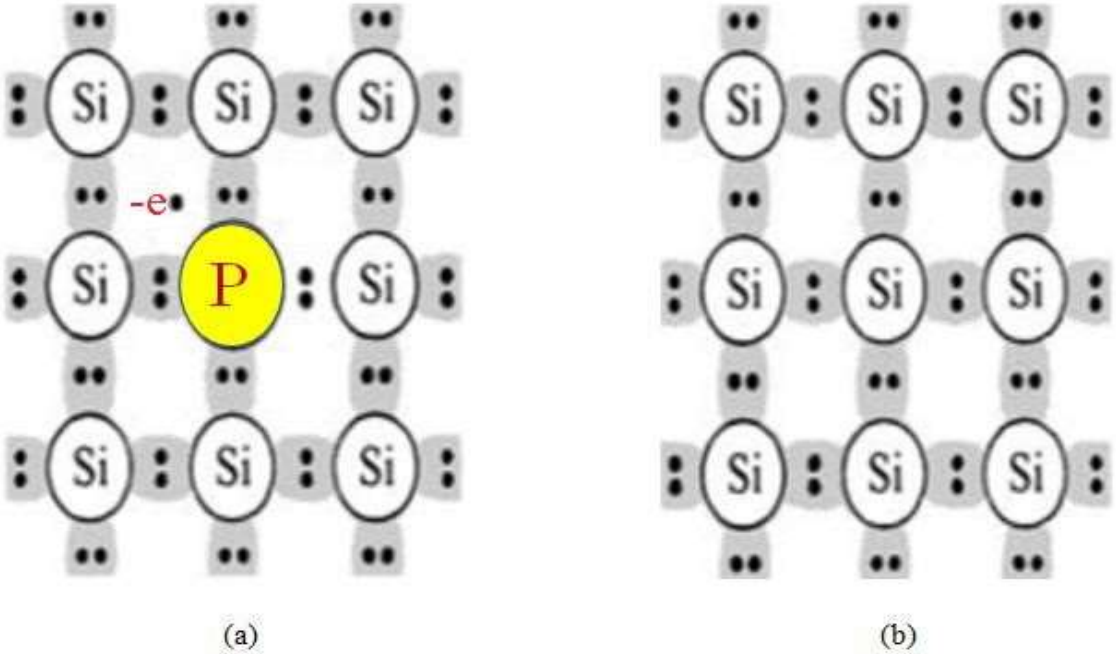

Figure 2.10: Pentavalent doped silicon crystal and pure silicon crystal (Source: Author).

P-type semiconductor: A P-type semiconductor is formed by using a trivalent impurity as dopant (Streetman, 2006). A trivalent dopant has three electrons in its outmost shell. Common examples include boron, gallium and indium. Figure 2.11 (a) and (b) describes

doped silicon crystal with trivalent impurity and pure silicon crystal respectively. By simple comparison, the pure silicon crystal has equal number of positive and negative charges, that is, equal number of holes and electrons. As for the doped crystal, the available three electrons from the trivalent dopant is unable to fill the available (four) holes, this makes it an acceptor because an electron is needed. Consequently, this empty hole resorts to a net positive charge in the crystal. Just as it is in the case of the N-type semiconductor, a charge density will be left behind in the valence band. This leads to the establishment of electric field and also, potential barrier is sometimes created inside the semiconductor (Sze and Kwok, 2007). The ionized hole attains new energy level above the valence band which therefore leads to a decrease of the energy gap. Owing to this decrease of the energy gap, holes are therefore more liable to jump into the conduction band. An increase in the concentration of the dopants will give room for availability of more holes, which in turn will improve the conductivity of the material. Hence, conductivity of the material increases with increasing concentration of dopants (James, 2019). For a P-type semiconductor, holes are the majority carrier, while electrons are the minority carrier.

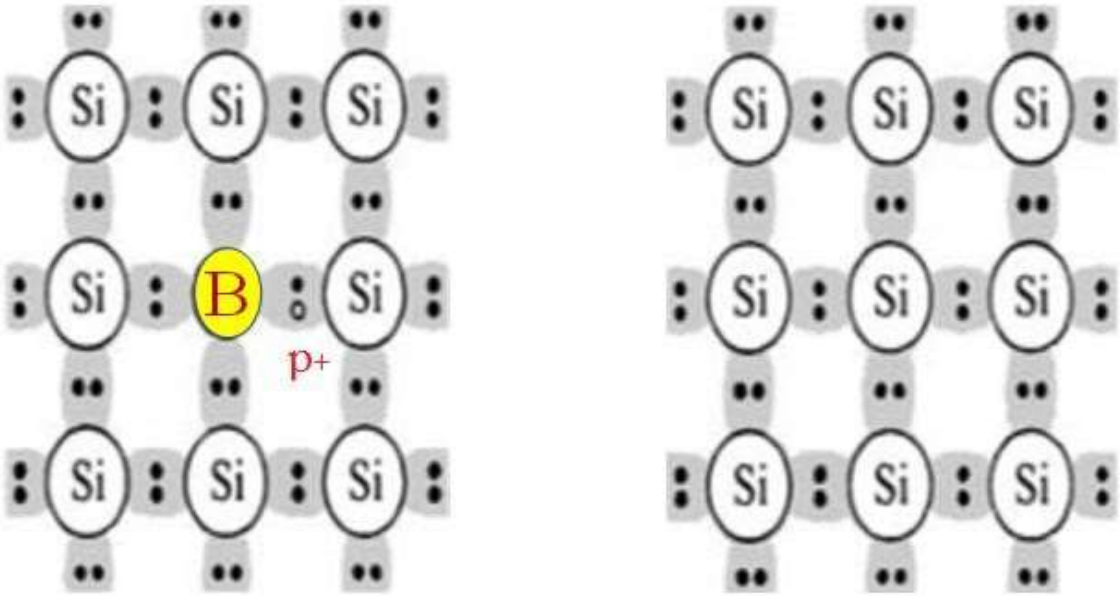

(a) (b)

Figure 2.11: Trivalent doped silicon crystal and pure silicon crystal (Source: Author).

Unlike the intrinsic semiconductor that possess zero conductivity at room temperature, the conductivity of an extrinsic semiconductor is not zero at room temperature. The product of charge carriers in a semiconductor is constant, depending on the energy gap and temperature. However, implantation of impurity leads to an increase in the charge density of a particular charge carrier and a decrease in the density of another charge carrier, hence, the concept of majority and minority carrier. From the condition of charge neutrality,

n_d + p = n_a + n (2.43) n = (n_d - n_a) + p (2.44) where, n_a is the impurity density of the acceptor, n_d is the impurity density of the donor, p and n are density of holes and electrons respectively. Recall that, carrier concentration

(n_i) = p = n then,

$$np = n_i^2 \tag{2.45}$$

Given that n_o is the electron concentration and p_o is the hole concentration, hence, at equilibrium,

$$n_o = n_d - n_a = {}^{n}p^{i}o^{2} \tag{2.46}$$

The equation is valid for (n_d - n_a) $\gg$ n_i

$$p_o = n_a - n_d = {}^{n}n^{i}o^{2} \tag{2.47}$$

The equation is valid for (n_a - n_d) $\gg$ n_i

Sometimes, in order to attain higher conductivity, P-type and N-type semiconductors are fused together to form a PN junction. A PN junction is an interface between a P-type and an N-type semiconductor. This combination gives room for electrical current to pass through the junction in one direction. Hence, the P side serves as anode while the N side

serves as cathode. It is the fundamental principle on which solid state semiconductor electronic devices are built. Such materials include diodes, transistors, integrated circuits, LEDs and PV cells. A typical structure of a PN semiconductor is presented in Figure 2.12.

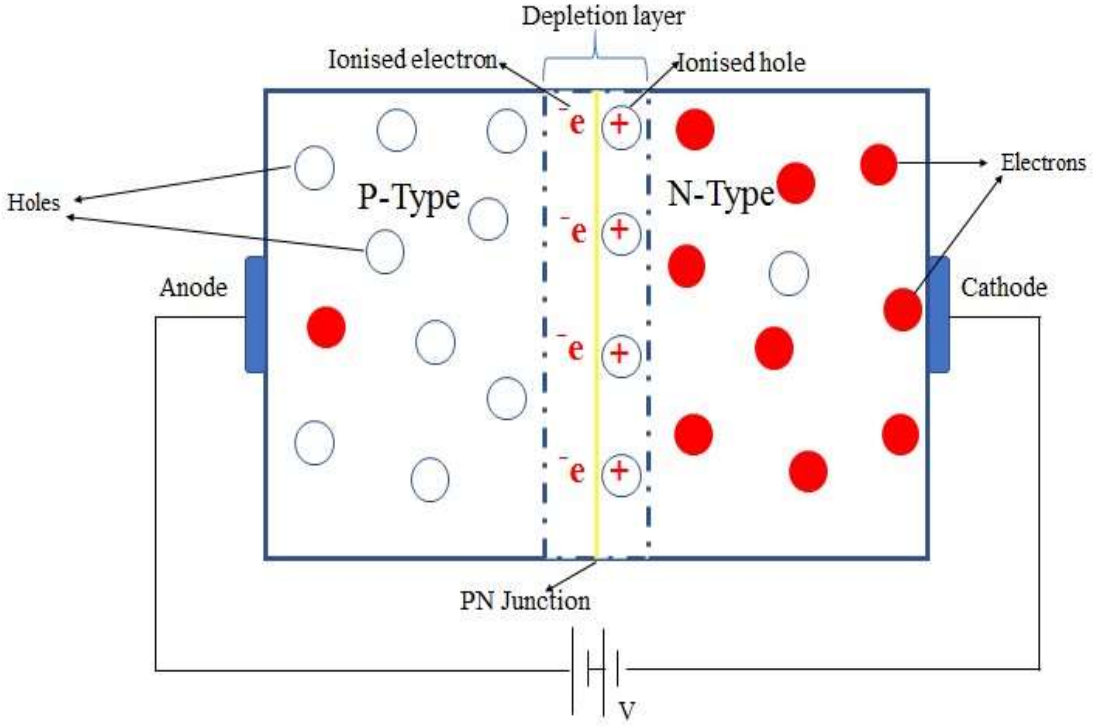

Figure 2.12: PN semiconductor crystal (Source: Author).

2.8 Application of Solar Energy

The main energy resources obtained from the sun are light and thermal energy. Utilisation of the two energy resources to generate power requires different technologies and designs. For the light energy resource, a PV technology is most suitable. And for the thermal energy resource, a well-designed thermal plant is most suitable. Notably, there are several other ways of harvesting solar energy as shown in Figure 2.13, but PV and thermal plant which are most famous will be discussed in the course of this research.

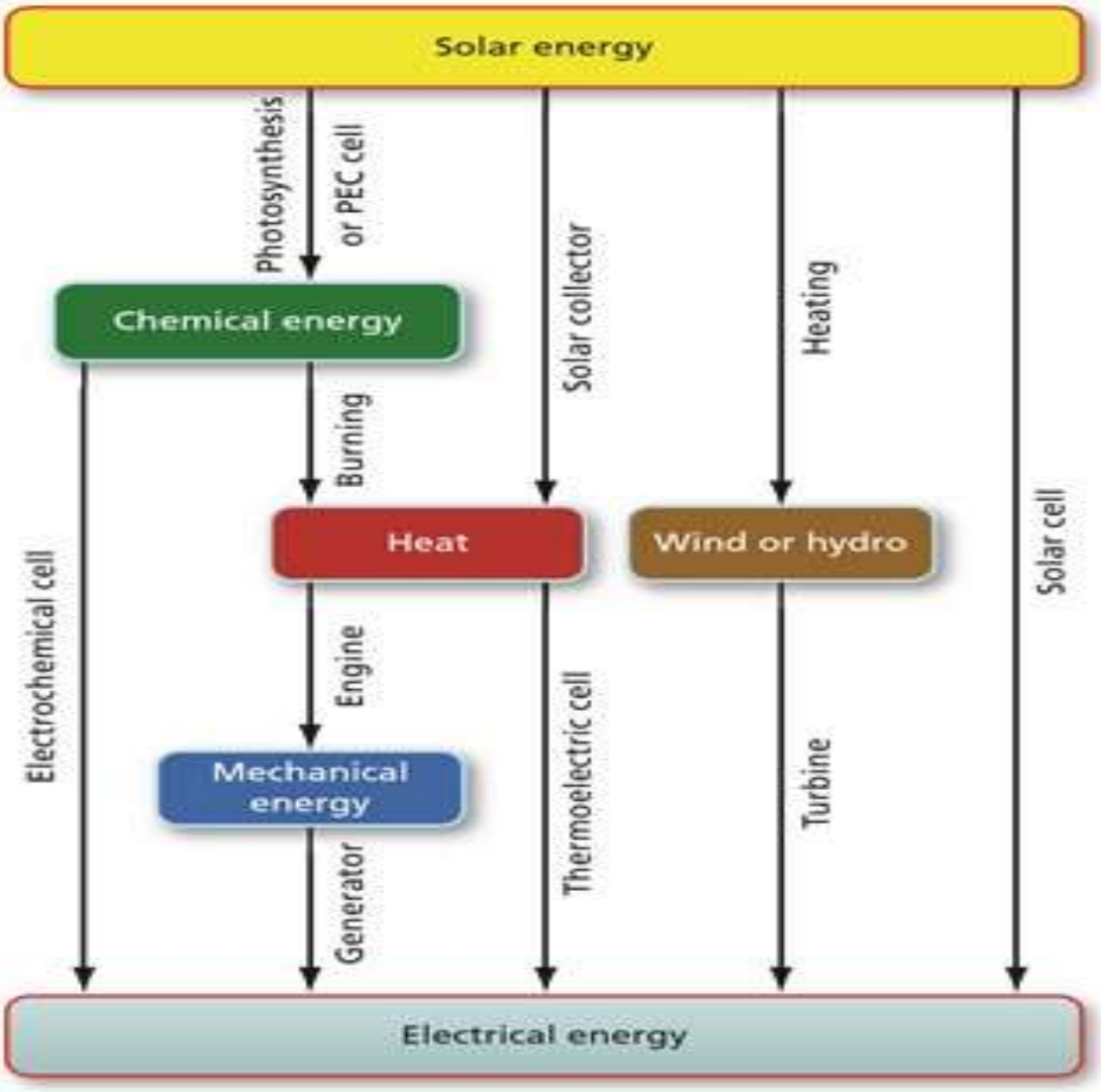

Figure 2.13: Conversion methods from solar to electrical energy (Liu *et al.*, 2012).

2.8.1 Solar PV technology

Photoelectric effect is a process through which electrons are liberated from a surface when exposed to photons of light (radiation). The intensity of the radiation determines the concentration of liberated electrons from the surface. PV cells are used to convert direct sunlight into electrical energy without the use of any chemical or mechanical device. PV effect was first discovered in the year 1839 by Edmund Becquerel, a French Physicist. He obtained a potential difference by illuminating some identical electrodes that was present in a weak conducting solution. The operation of a PV cell is based on the principle of operation of semiconductor.

When photons of light from the sun are imparted on solar cells, charge carriers from the P-type and N-type semiconductor materials become mobile. Charge opposition between the semiconductor materials result in the creation of electric field. This gives momentum and direction to the free charge carriers which result in the flow of electrical current. Silicon is the most excellently used material, which could exist as monocrystalline, polycrystalline or amorphous. The conversion efficiency (E_{ff}) of a solar cell is described as the ratio of electricity produced to incident solar radiation.

$$E^{ff} = Energy Incident\ ge\ neratedradiation\ (E\ (^{gen}S)\ )$$

(2.48) **Table 2.1: Solar panels, material types and efficiency**

Type of Solar Panel	PV Cell Material	Conversion Efficiency	Panel Efficiency	Area (1 KWp)
Copper Indium Gallium Selenide	Monocrystalline Silicon	10-13%	13-16%	7 m^2 (75 sq ft)
		9-12%	12-14%	8 m^2 (86 sq ft)
Cadmium Telluride	Polycrystalline Silicon			
Organic PV cell	Amorphous Silicon	7-12%	6-7%	15 m^2 (161 sq ft)

(Source: Mallikarjun *et al.*, 2017).

Monocrystalline silicon offers the highest conversion efficiency coupled with excellent heat tolerance, but expensive. Polycrystalline Silicon is less efficient when compared to the monocrystalline silicon, it is less expensive, easier to manufacture and has less heat tolerance. Amorphous silicon is also known as thin film. It has the least conversion efficiency and heat tolerance. Its price is lower than that of the monocrystalline silicon and slightly higher than that of the polycrystalline silicon. The various types of solar modules (panels) are shown in Figure 1.14.

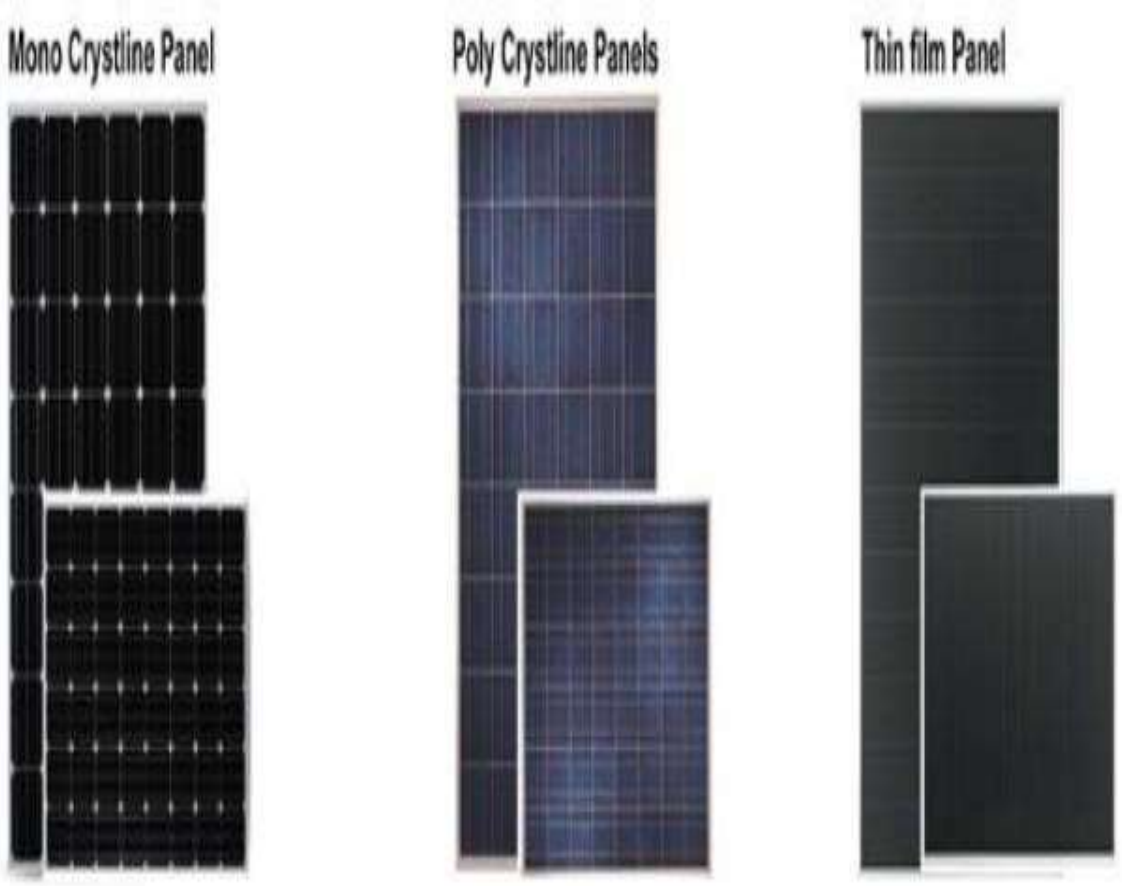

Figure 2.14: Types of solar module (Source: Noor, 2018).

In order to obtain maximum efficiency from a solar cell, the following conditions must be adhered to:

i. Shading of the solar cells or modules must be avoided. This is to ensure that the panel receives enough insolation from the sun. Shading of any kind diminishes the maximum output of a solar system. Shading of solar modules are often caused by neighbouring structures like buildings, trees, severe cloudy weather, even neighbouring solar modules can be a shading factor (Solar Choice, 2016). Shading of the solar modules must therefore be avoided in order to ensure that the panel receives enough radiation from the sun. ii. The surface of the solar panel must be free from dust or other forms of dirt.

When the surface of a solar panel is covered with dust, the dust can act as a

shade, or an unwanted reflector or absorber of solar insolation, thereby altering the expected behaviour and performance of the solar panel.

iii. Overheating of the solar cells should also be avoided in order to sustain its life span and proper working conditions. Before a solar module can be installed for any application, it is imperative to know its heat resistance ability. It is quite good to note that some solar modules deviate from the factory's performance specifications when installed in different climatic regions. This can sometimes be attributed to change in climatic conditions, which varies across regions of the world. The knowledge of incident solar radiation is very crucial at every point of application.

iv. An appropriate installation architecture must be ensured. Installation architecture include taking some factors like geographical location, tilt angle and the area required to accommodate the solar array into consideration. Tilt angle has to do with the setting of the panels to obtain maximum solar insolation. It is good to note that the tilt angle corresponds to the latitude of the geographic location. It is therefore of great importance to have an adjustable panel frame. An inclinometer is a device used for determining tilt angle (Franklin, 2017).

For maximum efficiency and durability, solar cells are fashioned into modules and arrays. The solar cell as a unit is fragile and cannot be taken to the field for use. Solar cells are coupled together to form solar modules which is the most crucial part of a solar PV system. For better resilience and efficacy, the solar module is the installable unit that can be used on a site. Solar modules are further combined either in parallel or series in the form of string to form solar arrays. This combination is dependent on current or voltage requirements for the application on purpose (Washington State University, 2009).

Connection of solar modules in series gives an enhanced voltage output, while parallel combination of solar modules produces larger current. A typical structure of a silicon solar cell is presented in Figure 2.15, while Figure 2.16 describes solar cell, solar module and solar array.

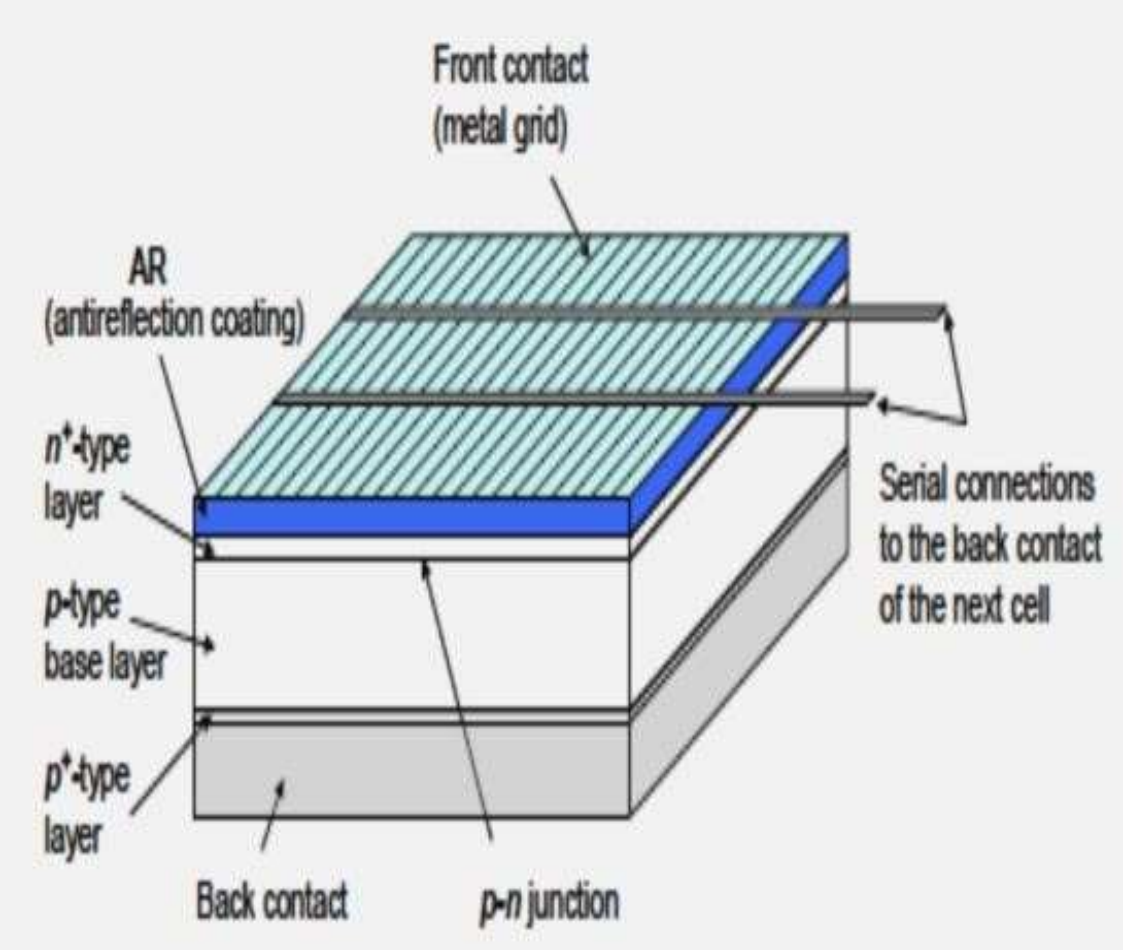

Figure 2.15: Structure of a crystalline silicon solar cell (Source: Mallikarjun, *et al*., 2017).

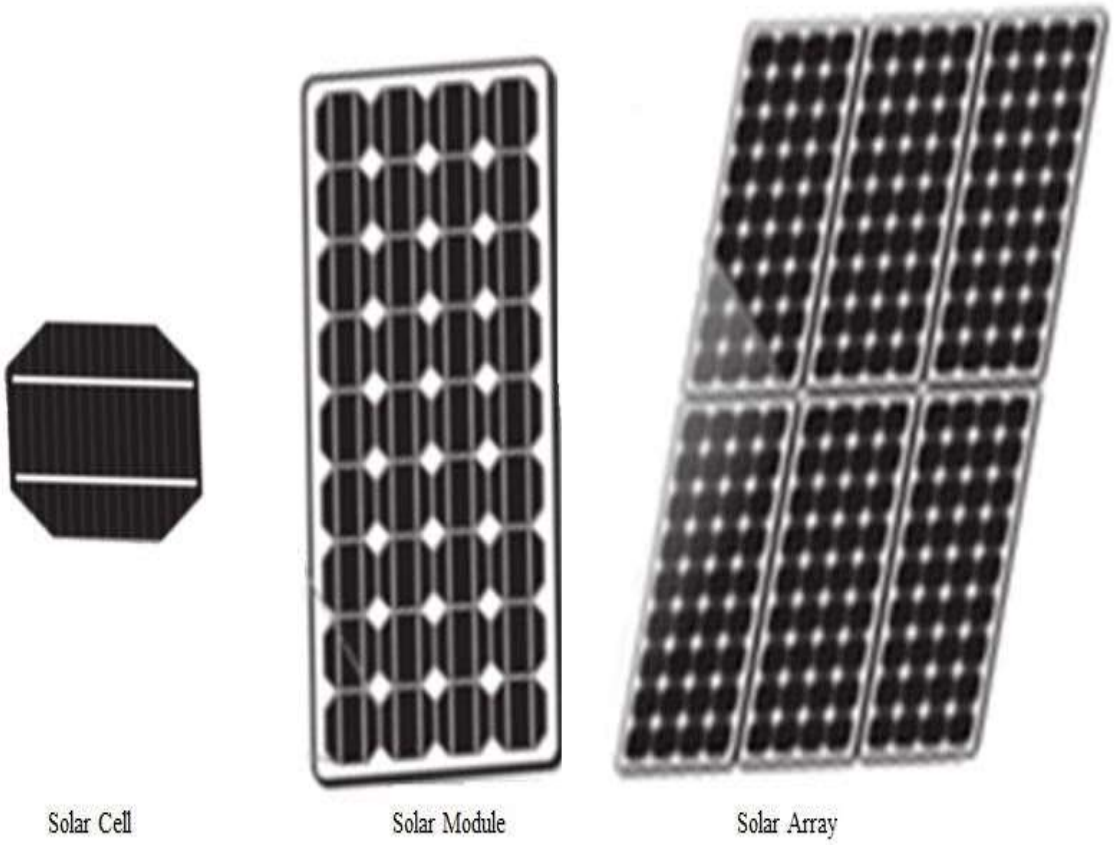

Figure 2.16: Solar cell, solar module and solar array (Source: Author).

2.8.1.1 *Categories of solar PV technology*

Solar PV technology is in two broad categories which include, the stand alone (off-grid) system and the grid (integrated) system (Ayaz, 2018).

Standalone or off-grid systems: The term grid describes the network or interconnection of electricity distribution from a generator point through to the end point users. Off-grid simply describe a PV system that is not connected to the electrical grid (Weis, 2013). It is also referred to as a standalone PV system because of its ability to generate the required energy and serve an anticipated purpose. Standalone PV systems are suitable for small communities, street lightening, small scale electrification, residential purpose and for electrifying remote locations that has no access to the national electricity grid. It is essentially important as a backup energy source in regions that experience epileptic electricity supply. However, since the solar insolation is not available throughout the day,

there is need to store the energy in order to sustain its availability. On this note, it is designed to store energy when production exceed consumption and release the stored energy when consumption exceeds production. The energy is stored in a battery in the form of chemical energy. A schematic diagram of a standalone PV system is shown in Figure 2.17.

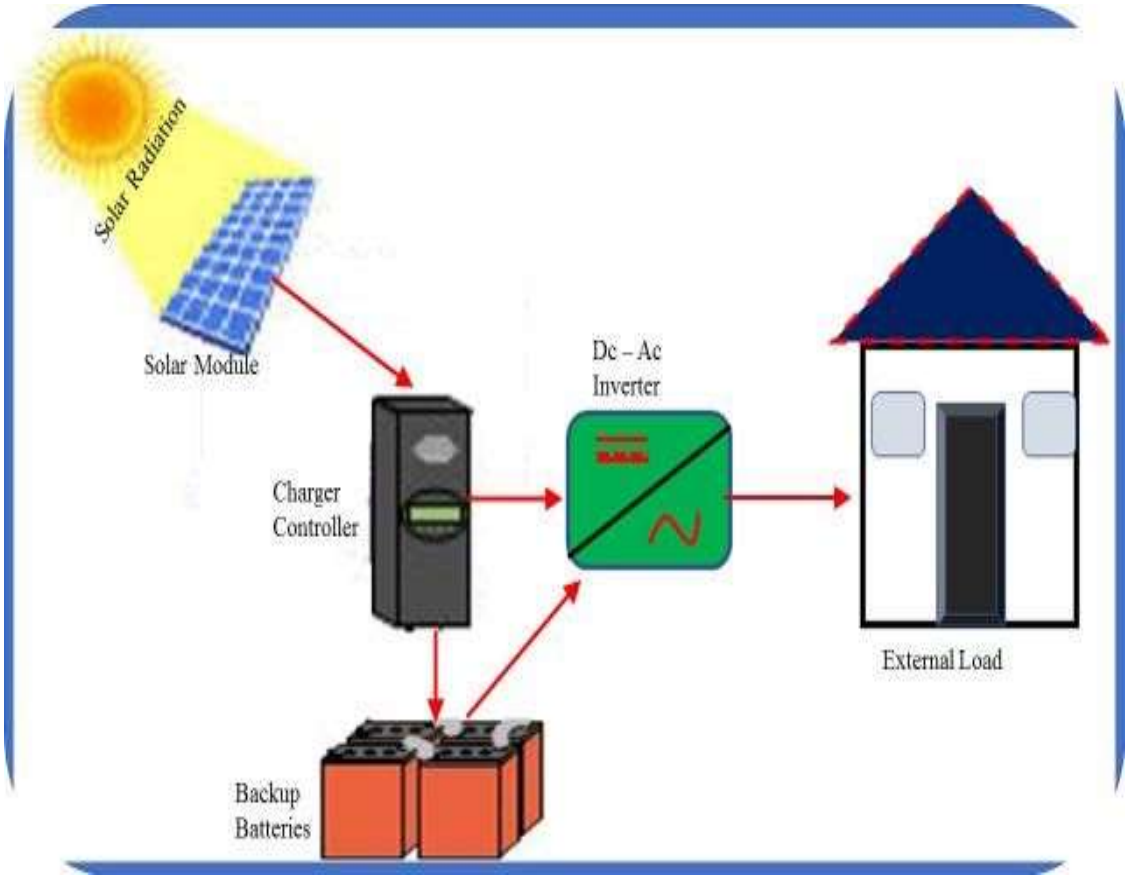

Figure 2.17: Standalone PV system (Source: Author).

Grid system: Generally, grid system is an overhead network of wires or underground cables by which electricity is distributed from power generating stations to end users. The system usually comprises of combination of solar modules (solar array), feedback meter, inverter and other materials needed to connect to the grid. Unlike the standalone system that are mainly designed for small scale applications, the grid systems are viable for different applications be it on a large-scale solar application or on a small-scale solar

application. Battery backups are not needed for grid PV systems. They are designed basically as additive source of energy which needed backup from other source when the solar insolation is not available, as presented in Figure 2.18.

On some occasions when production exceed consumption, the excess energy is automatically sent as feedback to the grid, which can be used by other consumers that are in connection to the grid at that time. The excess energy sent to the grid is however recorded by a meter for adequate compensation. In a situation when consumption exceed production or when solar insolation is not available, the grid will then serve as a backup.

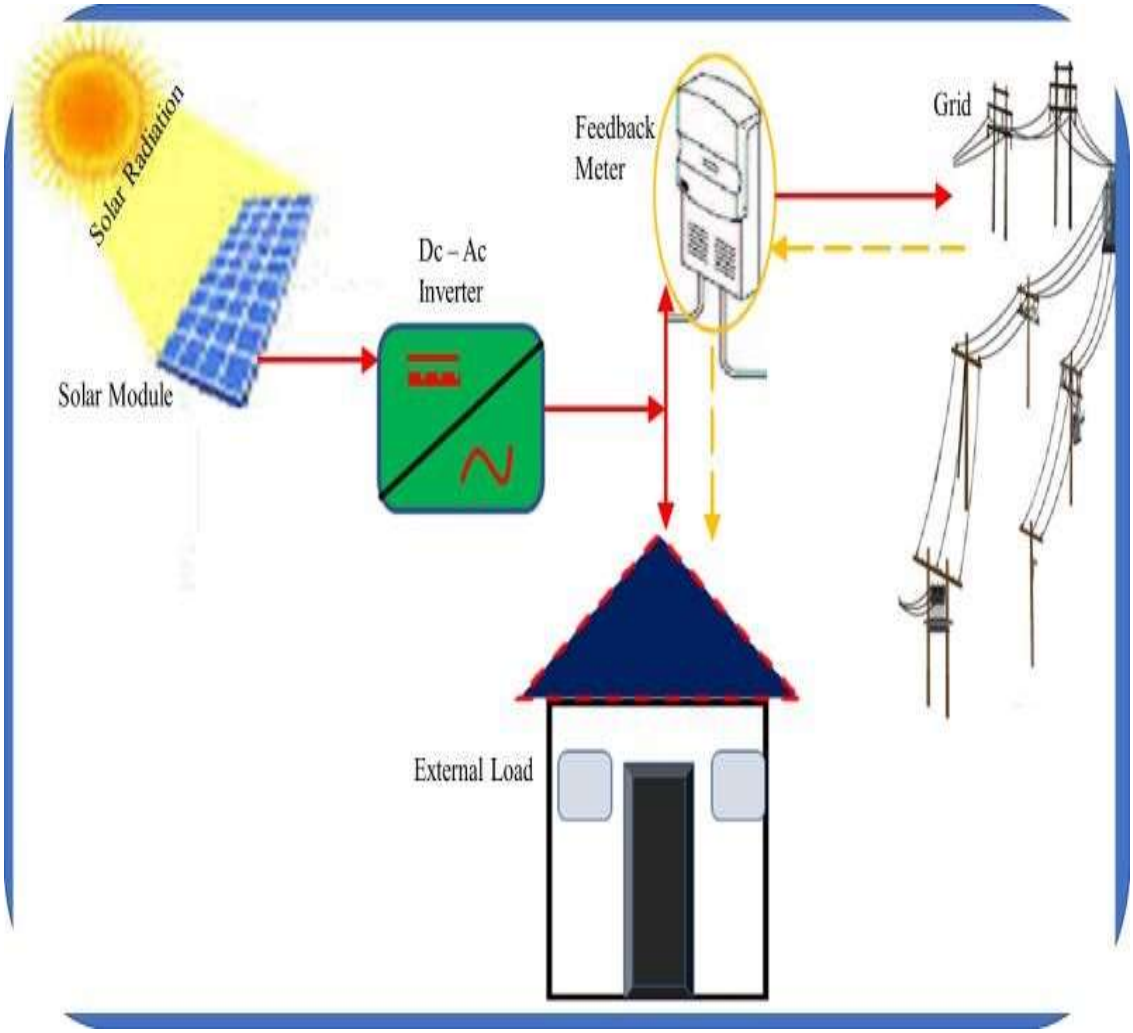

Figure 2.18: Grid PV system (Source: Author).

Hence, the energy generated in kilowatt hour is given by;

$$E = P_r \times P_{pv} \times S \quad (2.49)$$ where,

E is the amount of electricity produced (kWh), P_r is the performance ratio, P_{pv} is the nominal power of the PV system (kWp) and S is the incident insolation ($kWhm^{-2}$).

2.8.2 Solar thermal application

Solar thermal converts incident solar insolation directly into heat through solar collectors. Heat is a measure of the total internal energy of a body. Solar thermal has many applications which include solar thermal plant, solar cooker, solar air-conditioning systems, solar drier, solar stills, solar incubator, solar evaporator, solar desalination, solar heater and industrial heating applications. The principle of operation of any of the applications is based on the various modes of heat transfer which include radiation, convection, conduction or a combination of two or the three modes as the case may be. The modes of heat transfer in any of the applications depends on the materials in use. The three known collectors include the flat plate collector, the evacuated collector and the concentrating collector (Kalogirou, 2004; Rawlings, 2009; Sabonnadiere, 2009; Zambolin, 2009; Solar Server, 2011; Darling, 2012). The choice of collector to be used depends on application and the intended temperature.

For optimum efficiency of collectors, the following factors must be put into consideration.

a. The average operating temperature needed
b. The solar insolation at the site of operation
c. The nature or quality of construction materials used
d. The optical transmittance of the glass used
e. The absorption coefficient of the plate used
f. The total heat loss coefficient of the materials used and
g. The external air temperature

Heat energy results from the kinetic energy of a system, which leads to a change in its temperature. When a mass absorbs heat from the sun, the mass experiences a change in temperature which is directly proportional to its specific heat capacity. Materials generally absorb heat in two ways. This can be in the form of sensible heat or latent heat, depending on the temperature and the physical property of the material.

Sensible heat involves a change in temperature of system. For instance, if ΔT is the change in temperature and C is the specific heat capacity of the thermal mass, then, the quantity of heat absorbed by a unit mass of the thermal mass (1 kg) is given by:

$$Q = C\Delta T \tag{2.50}$$

while, the total heat absorbed by a thermal mass of variable mass (> 1 kg) is given by:

$$Q = mC\Delta T \tag{2.51}$$

where, Q and m are the total heat absorbed and total mass of the thermal mass respectively. On the other hand, if P is power in watt and t is time in second, then the equation becomes:

$$P = \frac{mC\Delta T}{t} \tag{2.52}$$

Furthermore, the heat absorbing capability of a body is largely dependent on its volume (V) and density (ρ). Hence,

$$Q = \rho VC\Delta T \tag{2.53}$$

Latent heat is the heat absorbed or emitted by a system which results in its phase change without a change in its physical temperature.

$$L = \Delta U + p\Delta V \tag{2.54}$$

$$Q = mL \tag{2.55}$$

$$Q = \rho VL \tag{2.56}$$

$$Q = m(\Delta U + p\Delta V) = \rho V(\Delta U + p\Delta V) \tag{2.57}$$ where, L is the specific latent heat, ΔU is change in internal energy of the system, p is pressure, m is mass and ΔV is the change in volume of the system. Hence, power (P) is given by:

$$P = \frac{m}{t}(\Delta U + p\Delta V) \tag{2.58}$$

2.8.2.1 *Thermal mass*

The ability of a material to absorb and retain heat for later use is referred to as thermal mass. A thermal mass is also referred to as a thermal energy battery. It is a material that can be used to store and distribute thermal energy. Examples include concrete, water, bricks, tiles, mud, stone, rock and kiln, to mention a few. They aid temporary storage of thermal energy till the time it will be needed. The primary process of a thermal mass occurs at atomic level of matter, which is accompanied by an addition or withdrawal of energy from a mass of solid or a volume of liquid which consequently result to a change in temperature (Sharston and Murray, 2019). On the other hand, some thermal batteries undergo phase transition through thermal application which allows the storage and release of more energy, due to high temperature gradient (Hledic *et al*., 2016). The amount of heat that each material can absorb relies largely on its density (Reardon *et al.*, 2013).

2.8.2.2 *Basic characteristics of thermal battery*

i. **Density:** Much heat is required to change the temperature of materials with high densities. This implies that such materials can absorb much heat as well as release the absorbed heat just like a black body. For instance, concretes have low air space compared to a brick, and because of this, concretes have higher thermal mass (Reardon *et al*., 2013).

ii. **Conductivity:** The efficiency of a thermal battery depends on its ability to conduct heat energy. That is, a thermal battery should be a good absorber and emitter of heat, comparatively to its maximum thermal absorbent capacity. High resistivity will lead to low conductivity (poor absorber) and consequently to high heat loss. Mathematically, resistivity (ρ) and conductivity (σ) are related by:

$$\sigma = \rho^{-1} \tag{2.59}$$

iii. **Thermal lag:** A thermal lag describes the time rate at which an uninsulated thermal mass absorbs and gives off its heat. The efficiency of a thermal lag is coordinated by its thickness, conductivity, insulation level and the temperature of its surrounding matter (Reardon *et al*., 2013). A precise knowledge of thermal mass is essential in order to choose the most appropriate material for the desired thermal application.

This describes the length of time a material can hold / store heat before finally reradiating.

iv. **Reflectivity:** Shiny and smooth surfaces absorb and re-radiate little heat, while matt and rough surfaces absorb and re-radiate more heat. Therefore, in the selection of a suitable material for thermal mass, colour, structure and texture are important factors to consider.

Phase change thermal battery: Phase change materials are lightweight materials that are capable of absorbing and releasing thermal energy. They function on the basis that matter generally require huge magnitude of energy input to change from one state to another, say from solid to liquid or from liquid to gas. The molecules in a material will continue to absorb more energy from its environment until a phase transformation (change

of state) is attained. The heat absorbed in this process is latent, which could be latent heat of melting or vaporisation.

Materials like water, salts and waxes are good for phase change thermal application (Reardon *et al*., 2013). Their phase transformation can easily be achieved with little energy input. When these materials absorb heat as a result of temperature gradient, they hold the heat until there is a shift in the temperature gradient. For instance, when wax absorbs sufficient heat, it melts and remains in the molten form until it gives off the heat and solidify. Phase change thermal materials are selected based on the purpose and the application they are meant to serve (Hledic *et al*., 2016).

2.8.2.3 *Solar collectors*

Solar thermal system concentrates sunlight to a desired high temperature with the use of mirrors or other reflecting surfaces to heat a fluid (Sen, 2008). Through heat exchangers, the hot fluid is used to generate high-pressure steam, which propels a steam engine mechanically and drives turbine generators in order to produce electrical energy. A solar thermal system also has the ability to store solar energy as heat in materials. This ability of solar thermal system to store energy as heat makes it a worthwhile means of electricity production both in the day time and at night when the sunshine is not available. The two types of solar collectors include the concentrating collectors and nonconcentrating collectors (Dagim, 2016). Solar concentrating collectors employs curved reflecting surfaces to converge sunlight on a receiving surface. In order to ensure a constant focus of the sunlight on the absorber, the concentrators can be designed to rotate automatically in accordance with the movement of the sun's position throughout the day (Sambeet and Tripathy, 2012). Concentrating collectors are automatically controlled to keep the track of the sun from its rising to its setting. On the other hand, non-concentrating collectors are stationary. They are installed at a fixed position in such a way that they can function

even with the constant change in the position of the sun. To obtain an optimum system throughput, calculations are carried out to determine optimum inclination or tilt angle of the module (Kalogirou, 2004).

Parabolic concentrating collector: A Parabolic Concentrating Collector or a Parabolic trough linearly focuses sunlight onto receiver tubes, thereby heating a fluid which is then used to produce superheated steam to power a generator (Ruiz, 2004). The parabolic trough employs a large assembly of mirrors or reflectors to track and converge multiple beams of the sunlight on a receiver tube which is placed at the focus of the parabolic mirror (Mark, 2012; Sambeet and Tripathy, 2012). A typical parabolic concentrating collector is presented in Figure 2.19.

Figure. 2.19: Parabolic concentrating collectors (Source: Solar Thermal, 2012).

Concentrating dish: A concentrating dish is also referred to as a Stirling system. It is made up of a solar dish and a Stirling system. The solar dish is a parabolic reflector, while the Stirling system is a silent closed-cycled machine that is designed to operate using any heat source. The concentrating dish is effectively designed to concentrate sunlight in two different dimensions onto a focal point (Solar Thermal, 2012). At the focal point, enormous heat is unleashed on a focal receiver which heats a gas chamber that produce pressure to power a generator, which produce electricity (Sambeet and Tripathy, 2012). A solar concentrating dish is shown in Figure 2.20.

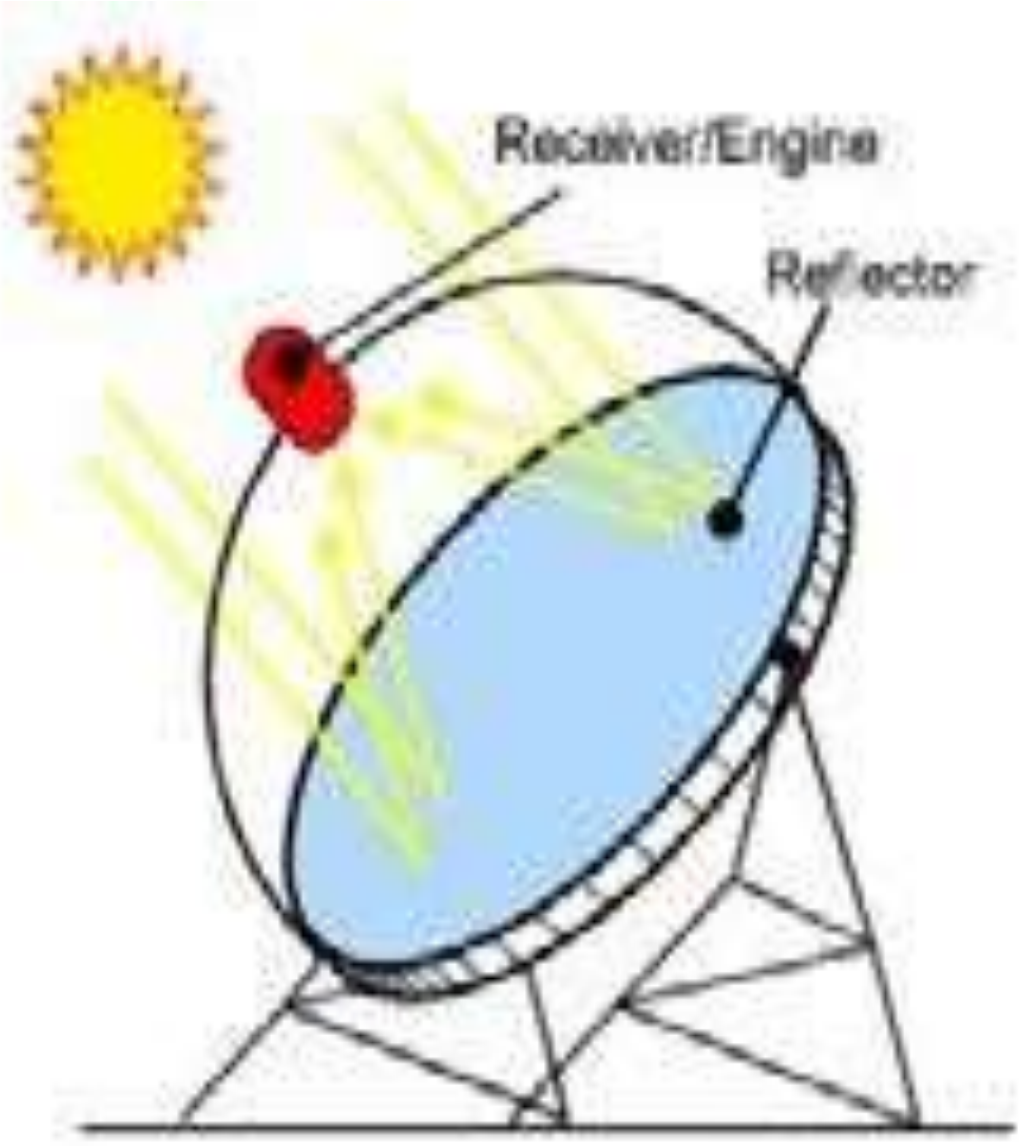

Figure. 2.20 Concentrating dish (Source: Dagim, 2016).

Concentrating tower: A concentrating tower is a solar technology device that employs a field of two-axis tracking mirrors known as heliostats (Sambeet and Tripathy, 2012). Each heliostat exists independently and are controlled by computer to track the movement of the sun and to reflect the concentrated beam to a receiving tower. A diagrammatic presentation of this is shown in Figure 2.21. Multiple reflections from different heliostats onto a common receiver result in an enhanced heat generation that is used to produce steam, which is therefore used to power a turbine to generate electricity (Philibert, 2005).

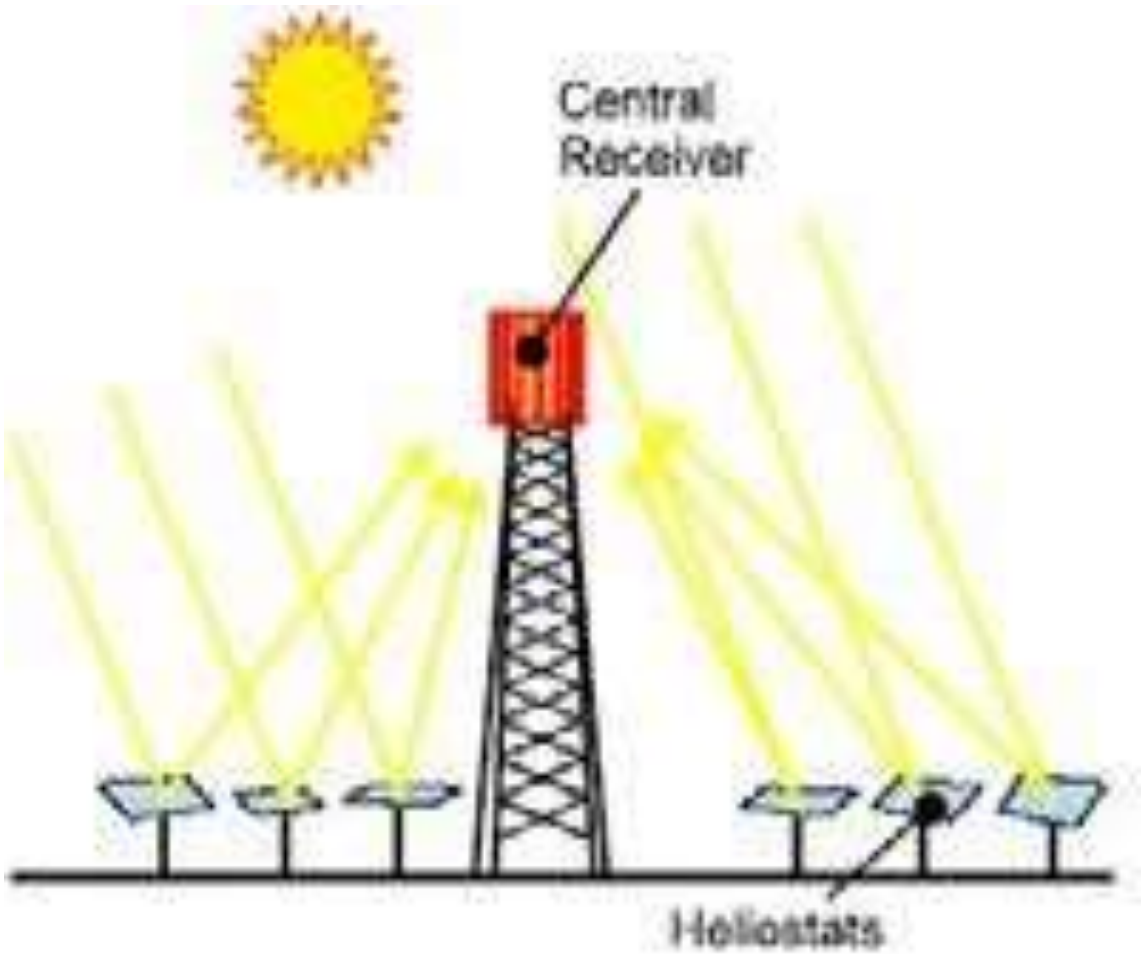

Figure. 2.21 Concentrating tower (Source: Dagim, 2016).

2.9 Electricity Production, Transmission and Distribution Status in Nigeria Human population growth in any country is highly dynamic which consequently leads to an increase in energy demand. For a country to meet her energy need, power generation, transmission and distribution musts be treated in a dynamic manner. Nigeria has a total land mass of about 910,771kilometre square with about 200 million citizens. The production and distribution of adequate power supply to all customers across all corners of the country are the bedrock of socio-economic development. Social development entails the transformation of the social institutions in a manner that improves the capacity of the society to meet her aspired goals. Economic development describes the growth of economic wealth (money, trade and industry) and resources. Socioeconomic status is therefore the measure of one's economic and social status. Furthermore, electricity is keen among other social amenities and it is a responsibility the government owes the citizens. The Electricity Corporation of Nigeria (ECN) and the Niger Dams Authority (NDA) were merged in the year 1972, to be called National Electric Power Authority (NEPA). NEPA as it is popularly called by Nigerians was in charge of electricity production, transmission and distribution till the year 2005, which as a result of power reform strategy was renamed Power Holding Company of Nigeria (PHCN) by the former President Olusegun Obasanjo (Udo, 2013). The power sector reform bill was passed into law in order to involve private companies in power production, transmission and distribution. In addition to this development, it was envisaged that the privatisation of the power sector would help the country meet her desired energy requirements and to improve quality service to the citizens, but on a contrary note, these objectives were not met. As identified by the citizens, some of the major lapses the distribution company experienced are:

i. Poor user-agency relationship ii. Poor distribution network iii. Inaccurate billing system, which is often over estimated iv. Unruly behaviour of staff

v. Weak and limited network coverage
vi. Overloaded transformers and bad feeder pillars vii. Poor maintenance culture viii. Inadequate logistic facilities such as tools and vehicles for mobility ix. Lack of regular training for staff

x. Staff poorly motivated

Over decades, the production of electricity in Nigeria has been achieved through oil-fired technology system, hydroelectric power technology system, coal-fired technology system and gas-fired technology system. However, the use of hydroelectric power and gas-fired technology systems have taken precedence over other methods (Sambo *et al*., 2014). The precedence can be linked to the huge availability of oil and water resources in the country. According to Sambo *et al*., 2014, a good percentage of the local oil and gas reserves are used to operate electricity generating plants (Sambo *et al*., 2014). An overview of some of the functioning power stations in Nigeria is presented in Table 2.2.

As at today, there are about 38 power generating stations in Nigeria, but only about 23 power stations are linked with the national grid with an expected total output of about 12,500 MW (Infoguide, 2020; Utuk, 2017). However, some of the stations are no longer functioning due to old age, most of the stations do not deliver up to their installed capacity, while some others are not in operation owing to fuel shortage or scarcity. Thereby bringing the total generated power to about 7,000 MW, which also experience about 25% loss (Gerretsen, 2018).

Power Station	Location (State)	Source	Year Completed	Installed Capacity (MW)
AES Barge (IPP)	Lagos	Gas	2001	270
Afam IV-V	Rivers	Gas	1982	580
Afam VI	Rivers	Gas	2009	980
Alaoji (NIPP)	Abia	Gas	2015	335
Delta	Delta	Gas	1990	740
Egbin	Lagos	Gas	1985	1320
Egbema	Imo	Gas	2013	338
Geregu	Kogi	Gas	2007	414
Ibom	Akwa Ibom	Gas	2009	142
Ihovbor (NIPP)	Benin	Gas	2012	450
Jebba	Niger	Hydro	1986	570
Kainji	Niger	Hydro	1968	760
Okpai (IPP)	Delta	Gas	2005	480
Olorunsogo Papalanto	Ogun	Gas	2007	335
Olorunsogo (NIPP)	Ogun	Gas	2012	675
Omoku	Rivers	Gas	2005	150
Omotosho	Ondo	Gas	2005	335
Rivers (IPP)	Rivers	Gas	2009	136
Sapele	Delta	Gas	1978	1020
Transcorp Ughelli	River	Gas	1966	972
Shiroro	Niger	Hydro	1989	600

Table 2.2 Some power stations in Nigeria, their locations and capacities

(Source: Energypedia, 2020; Uchegbulam *et al*., 2014).

From Table 2.2, it is clear that about 87.5% of the electricity generated in Nigeria is from thermal source, while the remaining portion is from hydro source (Infoguide, 2020). The human population is on a daily increase, while the supply of electricity to meet the demand of the growing population has remained stagnant for more than two decades, which is the main limiting factor to business and economic activities in the country (USAID, 2020). It is also regrettable to know that only about 4,000 megawatts out of the total installed capacity of 12,522 megawatts is realisable (Gerretsen, 2018; USAID, 2020). The losses are attributed to the following militating factors;

i. Poor or insufficient funding (revenue) ii. System's old age and poor infrastructure

iii. Inadequate equipment, tools, facilities and spare parts for prompt maintenance iv. Out-dated equipment, tools, facilities and technology

v. Poor transmission infrastructure (grid) vi. Poor maintenance culture vii. Poor communication network between agency and the end users viii. Poor incentive for staffs (welfare) ix. Corruption / misuse of fund

x. Heavy reliance on gas and oil xi. Poor security to pipelines and power stations (vandalization) xii. Overloading of transformers xiii. Inadequate professional staffs (technical skills)

xiv. Futile energy reform regulations

Full time access to electricity today is an afterthought in most parts of the world. Having known the benefits of electricity in a dynamic society, it is appalling to note that about

16% of the total world's population (1.2 billion) have no access to electricity (Energypedia, 2020). The World Bank rated Nigeria as the poorest in Sub-Saharan Africa and the second poorest in the world in terms of electricity generation and distribution (Odin, 2018). The rating is owing to the fact that Nigeria has not been able to provide electricity to more than 80 million people out of its entire population. Worse still, the people who had access to the grid often experience unstable and insufficient electricity supply, which on the other hand has led to the high purchase of stabilizers or voltage regulators by consumers to protect their properties from power surge. As a result of this, the World Bank projected that Nigeria would need to supply electricity to about 500,000 to 800,000 new households annually, from now in order to meet up with her power agenda in 2030 (Energypedia, 2020; Odin, 2018).

Energy poverty is a brick-wall between man and modern-time advancement in all spheres of life. In the quest to make energy available for different daily activities, citizens and business owners have resorted to the use of standby generators of different serving capacities. A rough estimate revealed that about 14 – 20 GW is generated daily from the use of petrol and diesel generators in Nigeria which is highly dangerous to the global world. According to the Nigerian minister for power in a speech delivered in London, Babatunde Fashola iterated that the country aims to generate about 30 percent of her total energy from renewable sources by 2030 (Gerretsen, 2018). Citizens and supporters welcomed the development to explore the renewable energy sources as an efficient way to bring power to rural communities and help clean up a country with some of the world's worst urban pollution rates. They further stated that access to this energy source will mitigate unemployment among the youths and encourage productivity. This will further

help in decongesting the highly populated cities in the country which arose from outward migration of people from the rural areas (Gerretsen, 2018).

According to the research conducted by Njoku (Njoku, 2014), results showed that solar PV applications is viable anywhere in Nigeria. The researcher further stated that solar PV applications are more suitable for installation in the Northern part of Nigeria where there are many large expanses of uninhabited lands with sparse vegetations, low human population density and higher solar insolation.

2.10 Models for Estimating GSR

The potential of the sun to sustain life and other activities on Earth cannot be underestimated. This is implying that the existence of the planet 'Earth' and all its constituents is directly linked to solar energy resources. For every application, a precise knowledge of the total insolation at the point of application is crucial (Suckling, 1983; Otkin *et al*., 2005; Osinowo *et al*., 2015; Olubusade *et al*., 2022).

Over the years, researchers from many parts of the world have developed models for the estimation of GSR using different methods and input parameters that vary with varying solar intensity (Ojosu and Komolafe, 1987; Vernay *et al*., 2013; Torres *et al*., 2013; Nwokolo and Ogbulezie, 2018). The developed models are though at different degrees of accuracy (Pandey and Katiya, 2013). Furthermore, many of the existing models are modification and amalgamation of pre-existing models, this therefore brings about much structural and functional similarities between the models. Some models were developed using single parameter as input, while some others were developed from the combination of two or more parameters as inputs (Almorox, 2011). Commonly used parameters include meteorological parameters, physical parameters, astronomical parameters, geographical parameters and geometrical parameters.

Unfortunately, most of these parameters are not available in many stations around the globe, more especially in the developing countries owing to low budgetary allocations to the vital sectors and inadequate or lack of technical skills involved in operation and maintenance (Gueymard and Myers, 2009; Antonanzas *et al.*, 2013). Precipitation, cloud cover, atmospheric pressure, relative humidity, wind speed, longitude, latitude, altitude, minimum and maximum temperature are familiar elementary data that can easily be assessed daily globally (Bojanowski *et al.*, 2013). As a result, models are developed on the basis of data availability (Veeraboina and Guduri, 2014).

Common meteorological parameters include minimum and maximum temperature, sunshine duration, atmospheric pressure, relative humidity, cloud cover and precipitation. Common Physical parameters are albedo, water vapor content and scattering by atmospheric particles. Prominent astronomical parameters are Sun-Earth distance, solar constant, extra-terrestrial radiation, solar declination angle and solar hour angle. Geographical parameters include longitude, latitude, and altitude; while tilt angle, surface azimuth, solar altitude and solar azimuth are the common geometrical parameters (Menges *et al.*, 2006).

Most of the existing models are empirical models, which are acknowledged as the simplest models for employing common atmospheric parameters. They correlate regression coefficients and atmospheric parameters with clearness index. It is therefore good to note that the regression coefficients are different for different datasets (Teke *et al*., 2015). Nevertheless, physical models are well known for their precision and generality. Input parameters for the physical models include atmospheric transmittances, aerosol optical depth, column ozone and column precipitable water to mention a few (Dazhia *et al.*, 2011). But its drawback lies in data unavailability. Another means of predicting global irradiation is by using the SCMs. SCMs are designed on the basis of

computer Artificial Intelligence (AI). The SCMs are identified as the best predictor when comparing complex situations (Maqsood *et al*., 2002). ANN, which imitates the method of information processing of the human brain is the most prominent among the SCMs (Fadare *et al*., 2010).

Common parameters for empirical models: Common features of empirical models are H which is the GSR on horizontal surface and H_o which is the extra-terrestrial solar radiation. H_o may be given by the expression (Olomiyesan and Oyedum, 2016a):

$$H_o = \frac{24}{\pi} I_{sc}\left[1 + 0.033\cos\frac{360}{365}dn\right] \times \left[cos\varphi.cos\delta.sin\omega_s + \frac{180}{\pi}\omega_s.sin\varphi.sin\delta\right] \quad (2.60a)$$

$$H_o = \frac{24}{\pi} I_{sc} \times \Gamma \times K \quad (2.60b)$$

$$\Gamma = \left[1 + 0.033\cos\frac{360}{365}dn\right] \quad (2.61a)$$

$$I_{rr} = I_{sc}\left[1 + 0.033\cos\left(\frac{72dn}{73}\right)\right] \quad (2.61b)$$

$$K = \left[cos\varphi.cos\delta.sin\omega_s + \frac{180}{\pi}\omega_s.sin\varphi.sin\delta\right] \quad (2.62)$$

$$\delta = 23.45\sin\left[\frac{360}{365}(284 + dn)\right] \quad (2.63)$$

$$\omega_s = cos^{-1}(-tan\varphi.tan\delta) \quad (2.64)$$

$$s_o = \frac{15}{2}\omega_s \quad (2.65)$$

where;

ω_s is the sunset hour angle

I_{sc} is the solar constant = 1,367 Wm^{-2}

I_{rr} is the intermittent variation of the extra-terrestrial solar radiation (solar flux)

φ is the latitude of the site δ is

the solar declination dn is the

day number of the year

s_o is the average day length

K is the combination of latitude, solar declination and the mean sunrise hour angle

Γ is a factor of monthly variation of extra-terrestrial solar radiation

Other common features are: T_{max} which is the maximum temperature, T_{min} is the minimum temperature and ΔT is the temperature range ($T_{max} - T_{min}$).

2.10.1 Temperature-based empirical model

Temperature based models employ minimum and maximum air temperature in correlation with extra-terrestrial solar irradiation to estimate global solar irradiation. Models in this category are developed on the basis of atmospheric transmissivity. This implies that, a cloudy atmosphere will decrease transmissivity which also will decrease maximum temperature. On the other note, a clear sky will increase atmospheric transmissivity which will in turn increase the maximum air temperature and consequently decrease the minimum temperature.

Hargreaves and Samani model

Hargreaves and Samani employed minimum and maximum air temperature to predict solar insolation (Hargreaves and Samani, 1982; Almorox, 2011). The researchers were the pioneer scientists that correlated extra-terrestrial radiation with temperature difference to estimate GSR. The proposed equation is of the form:

$$H = \left[a.\left(\sqrt{T_{max} - T_{min}}\right)\right] H_o \quad (2.66)$$

where the empirical coefficient 'a' is location-dependent and must be derived from the datasets of the site under study. For simplicity and easy adoption of the model, suggested

values for coefficient 'a' are 0.16 and 0.19 for interior and coastal regions respectively (Brkic and Tuka, 2019).

Bristow and Campbell model

Bristow and Campbell developed an exponential function using the difference between minimum and maximum air temperature to estimate daily GSR (Bristow and Campbell, 1984). The model is developed based on a theoretical notion for energy exchange in the surface boundary layer (Goodin *et al*., 1999). Bristow and Campbell model is adopted by many researchers, because of its ease and basic requirements which are latitude and air temperature range. It is of the form;

$$H = [a.\langle 1 - \exp(-b\Delta T^{c})\rangle]\, H_o \qquad (2.67)$$

where, a, b and c are empirical coefficients. The major limitation to the model is the assumption that solar irradiance has high influence on air temperature range. Whereas in some regions, air temperature range is more attributed to regional advection and frontal activities (Goodin *et al*., 1999).

Annandale model

Annandale developed a solar radiation model which is a modification of Hargreaves and Samani solar radiation model (Annandale *et al*., 2002). The model considers the role of altitude and atmospheric thickness as factors of GSR variation. Parameters necessary for the model include temperature difference and the altitude of location above sea level (Prieto and García 2022). The model is of the form;

$$H = \left[a.\,(1 + 2.7 \times 10^{-5}\, z)\left(\sqrt{T_{max} - T_{min}}\right)\right] H_o \qquad (2.68)$$

where, a is a empirical coefficient = 0.15, and z is the altitude of location above sea level (m).

Allen model

Richard Allen, back in the year 1997 (Allen, 1997) presented a self-calibrating solar radiation model (Brkic *et al*., 2019). The model correlates maximum and minimum air temperature with extra-terrestrial solar radiation as a function of GSR. It is a modification of Hargreaves and Samani model, where the empirical coefficient is given as a function of elevation. The model is of the form:

$$H = \left[a_\alpha \left(\sqrt{T_{max} - T_{min}}\right)\right] H_o \tag{2.69}$$

$$a_\alpha = b\left(\sqrt{\frac{P}{P_o}}\right) \tag{2.70}$$

where, P is the mean atmospheric pressure of the site (kPa), P_o is the mean atmospheric pressure at sea level (101.3 kPa), a_α and b are empirical coefficients. The values of b are 0.17 and 0.20 for interior and coastal regions respectively (Allen, 1997). The expression for the coefficient a_α was introduced in order to put the effects of elevation on the volumetric heat capacity of the atmosphere into consideration. Despite this consideration, the model is said to be unreliable at elevations above 1,500 m.

2.10.2 Cloud-based empirical models

Cloud data is another weather parameter that is extensively employed for the estimation of GSR (Muneer and Gul, 1999). Clouds are strong modulators of GSR, as they affect different components of the solar irradiation differently (Younes and Muneer, 2006; Sanchez *et al.*, 2012). However, huge uncertainty often arises from the correlation of cloud type with GSR which is liable to continuous changes. Among the factors that are responsible for solar radiation balance on the surface of the Earth, clouds display huge uncertainty in their characterisation and quantification (Norris, 1968). The presence of cloud in the sky could either reflect, scatter or absorb the incoming solar beam. Cloud cover is usually estimated by eye in most meteorological stations by trained personnel

(Badescu, 2015). The unit is in tenths of Okta. 0 Okta is recorded for a clear sky while 8 to 10 Okta are assigned to a cloudy sky.

Kasten and Czeplak model

Kasten and Czeplak (1980) developed a cloud-based regression model for estimating GSR. The researchers achieved this by using a ten-year continuous record of hourly upward and downward radiation flux densities, in correlation with hourly cloud records from Hamburg (Kasten and Czeplak, 1980). Results revealed that the ratio of GSR under cloudy atmosphere to global radiation under clear sky does not depend on their solar elevation when considered at the same solar elevation and was validated in five different locations in the United Kingdom. The model equation is of the form:

$$H = [1 - c\left(\frac{C_{ld}}{8}\right)^{d}]\, H_o \tag{2.71}$$

$$H_o = (a.\sin\delta - b) \tag{2.72}$$

where, a, b, c and d are empirical coefficients, which are location dependent, C_{ld} is the amount of cloud (Okta).

Badescu model

Badescu developed a model which estimates GSR from ground based hourly cloud fraction data (Badescu, 2015). The model equation is of the form:

$$H = [a + b(C_{ld})]H_o \tag{2.73}$$

where, a and b are regression coefficients, and C_{ld} is the amount of cloud (Okta).

Lumb model

Lumb (1964) presented a mathematical model to estimate solar radiation using cloudbased data. The researcher classified clouds into nine arbitrary groups through

which the regression between the intensity of solar radiation and the sine of solar elevation were determined for each group (Norris, 1968). The model is of the form:

$$H = AS + BS^2 = 135FS \quad (2.74)$$

$$F = a + bS \quad (2.75)$$

$$H = (aS + bS^2)135 \quad (2.76)$$

where, 135 ($MWcm^{-2}$) is the solar constant, a, b, A and B are constants. a and b can be deduced by least squares data analysis. S is the mean of the sines of the solar altitude, and H is the solar irradiation ($Mwhrcm^{-2}$).

Black model

Black in the year 1956 presented a quadratic expression which correlates GSR with extraterrestrial solar radiation and average total cloud cover by employing atmospheric data from some parts of the world (Black, 1956). Majority of the examined parts are found in North America and Europe. As a result, the model cannot be precise in all parts of the world. The proposed model is of the form:

$$H = [a + bC_{ld} + c(C_{ld})^2]H_o \quad (2.77)$$

where C_{ld} is the mean cloud amount (Okta).

a = 0.803

b = -0.340

c = -0.458

2.10.3 Sunshine-based empirical models

Sunshine models is famous among the GSR models. This category of GSR models assumed that the intensity and the duration of sunshine are good predictors of GSR. This is achieved by correlating the fraction of the available sunshine hour and the possible hours of sunshine (day length) with clearness index.

Angstrom-Prescott model

Angstrom in the year 1924 developed the first mathematical relationship between GSR and sunshine duration (Angstrom, 1924). The relationship is linear and it is of the form:

$$H = [\propto + s\_^{S_o}(1-\propto)]\, H_c \tag{2.78}$$

where $\propto$ is coefficient of transmittance for shortwave solar radiation, S is the available measured sun hour, S_o is the possible hours of sunshine (day length) and H_c is the daily amount of global radiation on a perfectly clear day. Owing to the complexity involved in determining the precise value of H_c, Prescott in the year 1940 modified the proposed linear equation of Angstrom by replacing H_c with H_o (Prescott, 1940). The modified version of the equation is given as:

$$H = [a + b\,(s^{S_o})]\, H_o \tag{2.79}$$

where H_o is the shortwave radiation received at the top of the atmosphere (Angot-value), a is the percentage of H_o that reach the surface of the Earth on a cloudy day, b is the percentage of H_o that is absorbed by the cloud on a cloudy day.

$$a = -0.110 + 0.235\cos\varphi + 0.323\left(\frac{S}{S_o}\right) \tag{2.79a}$$

$$b = 1.449 - 0.553\cos\varphi - 0.694\left(\frac{S}{S_o}\right) \tag{2.79b}$$

Hence, Angstrom-Prescott equation became widely known and most of the existing empirical models originated from it. The accuracy of the model therefore depends on the precision in the determination of coefficients a and b (Rietveld, 1978).

Glover and McCulloch model

Glover and McCulloch developed a latitude and sunshine-dependent model, which is valid for latitudes between 0^o to 60^o. The model is a modification of Angstrom-Prescott

model, which was achieved by the introduction of latitude into the equation (Glover and McCulloch, 1958). The model is of the form:

$$H = [a.\cos\varphi + b\ (s^{S}{}_{o})]\ H_{o} \quad (2.80)$$

where coefficients a, and b are given as 0.29 and 0.52 respectively. The researchers stated that the slope of b shows an effective constant relationship, while the minimum value of a is a function of latitude.

Ogleman model

Ogleman *et al.* (Ogleman *et al.,* 1984) developed a new means through which the estimation of solar radiation can be made from sunshine data. The model correlates GSR with extra-terrestrial radiation and bright sunshine as a ratio of daylength in Turkey (Ogleman *et al.,* 1984). By using maximum possible quadratic fit, Ogleman *et al.* (1984) were able to deduce the fact that monthly averages of sunshine ratio and its standard deviation are sufficient to estimate monthly average clearness index. The model equation is of the form:

$$H = [a + b\ (s^{S}{}_{o}) + c\ (s^{S}{}_{o})^{2}]\ H_{o} \quad (2.81)$$

Coefficients a, b, and c are given as 0.195, 0.675 and -0.142 respectively (Namrata *et al.,* 2013).

Newland model

Newland developed a logarithmic non-linear model from the correlation studies which aimed at separating global solar irradiation into its components (Newland, 1989). The model establishes a mathematical relationship between solar radiation and sunshine duration. The model equation is of the form:

$$H = [a + b\ (s^{S}{}_{o}) + c.\log\ (s^{S}{}_{o})]\ H_{o} \quad (2.82)$$

The model is a modification of Page and Rietveld models, in which the regression coefficients a, b and c are given as 0.34, 0.40 and 0.17 respectively (Newland, 1989). According to the researcher, the model is adjudged to be preferable for regions with prolonged severe cloudy conditions, that is, regions with low sunshine duration.

2.10.4 Multiple parameter-based empirical models

The multiple parameter-based models are often referred to as hybrid parameter-based models (Olomiyesan, 2016b). The model combines two or more atmospheric parameters to predict GSR. Some of the commonly combined parameters include air temperature, sunshine duration, relative humidity, cloud cover, amount of rainfall, atmospheric pressure, soil temperature and dew point temperature. Unlike the single parameter-based models, multiple parameter-based models are developed on the basis that the balance of solar radiation is determined by many factors in the atmosphere. According to Quej *et al.* (2016), multiple parameter-based models are more reliable than the single parameterbased models.

Abdalla model

Abdalla developed an empirical multiple parameter-based GSR model by correlating maximum temperature, relative humidity and hours of bright sunshine with extraterrestrial solar radiation (Abdalla, 1994). The model is said to be a modification of the

Gopinathan model, which is highly dependent on meteorological parameters (Gopinathan, 1988; Ouali and Alkama, 2014). Given that RH is relative humidity, T_{max} is maximum temperature, while a, b, c and d are constants, the model equation is of the form (Abdalla, 1994):

$$H = [a + b\,(s^{S_o}) + cT_{max} + d(RH)]\,H_o \qquad (2.83)$$

where a = 0.5289

b = 0.459 c

= 4.073×10^{-3}

d = -6.481×10^{-3}

Swartman and Ogunlade model

Swartman and Ogunlade (1967) established a multiple parameter-based model for estimating GSR from the ratio of bright sunshine hour and relative humidity. According to Swartman *et al.* (1967) the amount of precipitation has little influence on solar radiation and therefore not suitable for its prediction. On the other hand, relative humidity, which is the volume of H_2O vapour present in the atmosphere is highly influenced by solar radiation (Fritz, 1957) and it is as a result of that it is selected as a crucial parameter for predicting GSR. The model is of the form:

$$H = [a + b\ (s^S_o) + c(RH)]\ H_o \quad (2.84)$$

where a, b and c are empirical coefficients, RH is the monthly average daily relative humidity (%). On application, the model is said to have shown remarkable agreement with measured data (Chegaar and Guechi, 2009).

Okundamiya model

Okundamiya developed a multiple parameter-based model which correlates GSR with the ratio of bright sunshine hour, ratio of air temperature, maximum air temperature, cloud cover and extra-terrestrial solar radiation. The model employs a set of monthly average daily data, which was obtained from different data stations in Nigeria (Okundamiya *et al.*, 2015; Olomiyesan, *et al.,* 2015). The model is adjudged to have good performance in the

various places of application, with the least RMSE and MABE when compared with other solar radiation models. The model is of the form:

$H = [a + b\ (^{S}/_{S_o}) + c\ (^{T_{max}}/_{T_{max}^{min}}) + d.\ T_{max} + e(C_{ld})]\ H_o$ (2.85) where a, b, c, d and e are regression coeffients.

Olomiyesan and Oyedum model

Olomiyesan and Oyedum (2016a) developed a two parameter-based regression model for predicting GSR on the horizontal surface. The model is a modification of AngstromPrescott and Garcia solar radiation models. The model is a correlation between sunshine duration ratio, air temperature range, extra-terrestrial solar radiation and GSR. The model is given by:

$$H = [a + b\ (^{S}/_{S_o}) + c\ (^{\Delta T}/_{S_o})]\ H_o \quad (2.86)$$

where a, b and c are regression coefficients, ΔT is air temperature range.

2.11 Soft Computing Method (SCM)

The estimation of GSR can also be achieved using SCMs. SCMs involves the use of Artificial intelligence (AI). The method includes ANN, Recurrent Neural Network, Radial Basis Function Network, Support Vector Machine, Genetic Algorithm, and Artificial Neuro-Fuzzy Inference System to mention a few (Mohanty *et al.*, 2016; Xinhua and Hongwei, 2019).

2.11.0 Artificial neural network

ANN is a set of computing components that is characterised by artificial neurons which are connected by artificial synapses to perform parallel distributed processes that are controlled by vectors and matrices of synaptic weights (Eichie *et al*., 2016; Shepherd,

2004). ANN imitates the neural process of the human brain (Hodgkin and Huxley, 1952). Human brain is made up of about 100 billion neurons, with each neuron connected to about 1,000 to 10,000 other neurons (Kandel *et al*., 2000). Nevertheless, ANN is not as complex as the biological neural network (BNN), but both are similar owing to the fact that they are built from the interconnection of neurons.

ANN is a powerful and versatile tool (Suzuki, 2013). It is applicable in copious sectors which include educational, industrial, medical, economic, environmental, engineering, biological, security, research and social sectors to mention a few. ANN can be used for classification, clustering, vector quantisation, pattern association, function approximation, forecasting, control applications, optimisation and search. As a result of numerous uses and applications, ANN may be regarded as the single most successful technology of the 21st century (Suzuki, 2013). However, there are many types of ANN which are distinguishable by the underlying problem they are meant to solve (Folorunso *et al.*, 2019). A typical biological neuron is shown in Figure 2.22, while Figure 2.23 shows an artificial neuron. The features of BNN are described below.

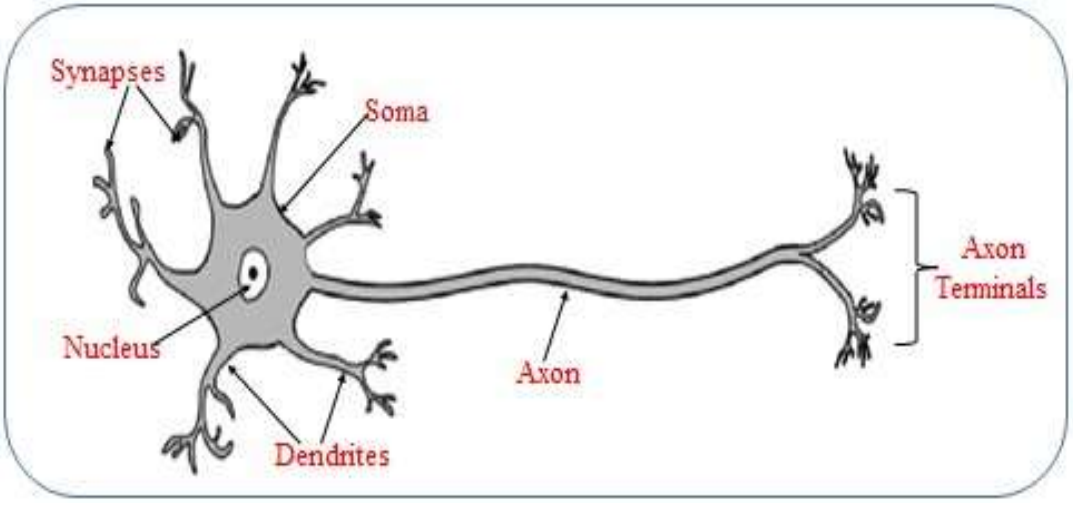

Figure 2.22: Biological neuron (Source: Author).

Axons: axon is the long connecting substance which extends from the soma to other parts.

It transmits signals from the neurons to cells or effectors as output. The output layer of ANN serves the same purpose as the axon of BNN.

Dendrites: dendrites are tree-like structures on the biological neurons which are composed of nerve fibres and connected to the cell body. The dendrites are responsible for the reception of incoming signals into the cell body.

Soma: soma is also known as the cell body. It is the main structural part of the neuron where the nucleus is found. Incoming signals from the dendrites are integrated and processed by the soma before being sent as output through the axons.

Synapses: synapses are structures that function as the connecting regions between axons and dendrites (Jeon and Kim, 2023). They enable interconnections between neurons and exchange of signals. When signals or impulses are sent or received between structures with the aid of the synapses, the synapses determine the potential of such signals so as to either increase or decrease such potential. As for the artificial network, the neurons contain processing units which are connected by weights as shown in Figure 2.23 and in the same vein, Figure 2.24 shows the relationship between biological and artificial neurons.

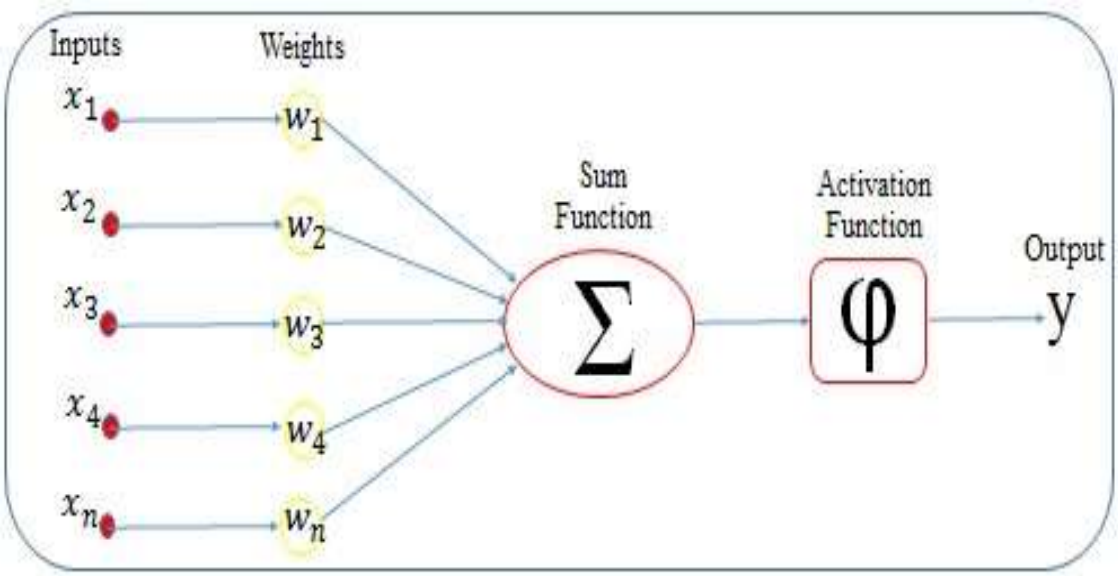

Figure 2.23: Artificial neuron (Source: Author).

If w is the weight of the corresponding variables, φ is the activation function, b is bias value, x and y are the respective input and output variables. Then,

$$y = \sum_{i=1}^{n}(w_i x_i + \ldots\ldots + w_n x_n) \tag{2.87}$$

$$y = (w^T x) \tag{2.88}$$

where, $$w^T = (w_1, w_2, w_3, \ldots\ldots w_n)^T \tag{2.89}$$

that is the transpose of the weight and

$$x = (x_1, x_2, x, \ldots\ldots x_n) \tag{2.90}$$

By introducing a bias value and activation function, the equation becomes;

$$y = \varphi\left(\sum_{i=1}^{n}(w_i x_i + \ldots\ldots + w_n x_n + b_1)\right) \tag{2.91}$$

$$y = \varphi\left(\sum_{i=1}^{n}(w^T x + b_1)\right) \tag{2.92}$$

$$y = \gamma\left[\sum_{i}^{n}(w_j y + b_2)\right] \tag{2.93}$$

$$y = \gamma\left[\sum_{i}^{n}\left(w_j \varphi\langle\sum_{i}^{m}((w_i x_i + \ldots\ldots + w_n x_n + b_1)\rangle + b_2\right)\right] \tag{2.94}$$

$$y = \gamma\left[\sum_{i}^{n}\left(w_j \varphi\langle\sum_{i}^{m}(w^T x + b_1)\rangle + b_2\right)\right] \tag{2.95}$$

A well-designed ANN should therefore have the following basic elements: Input signal, Synaptic weight, Linear aggregator, Activation bias, Activation potential, Activation function and Output signal.

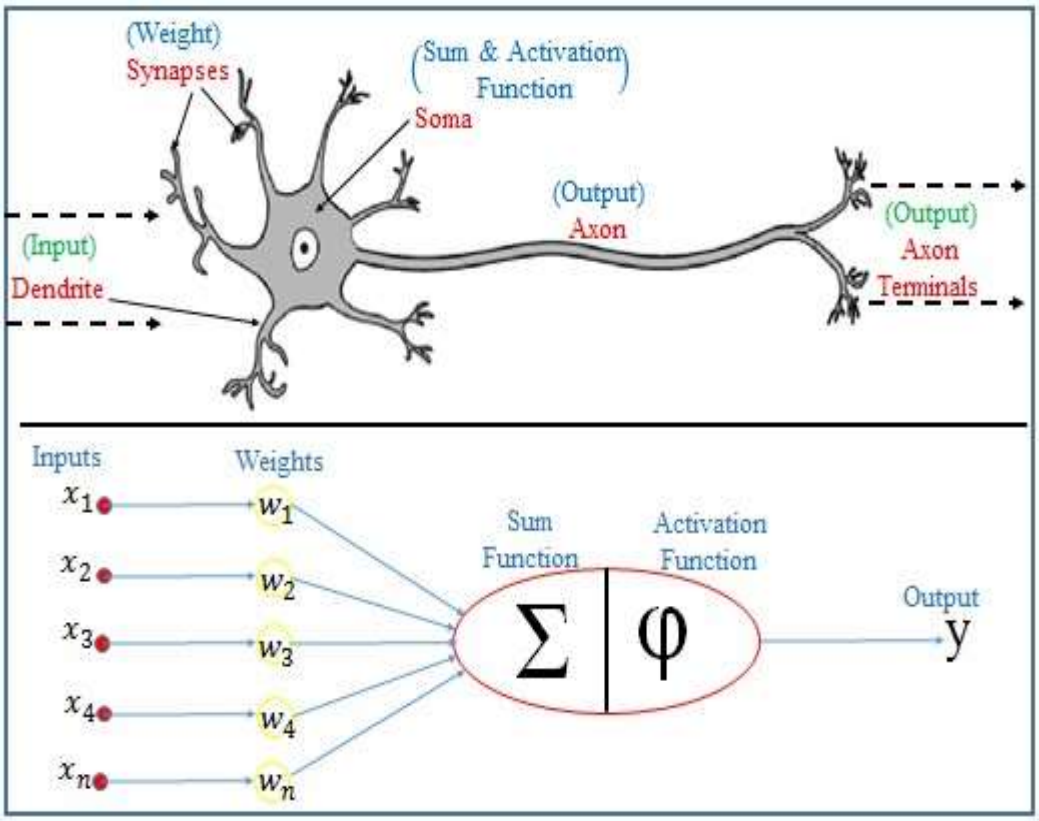

Figure 2.24: Relationship between biological neuron artificial neuron (Source: Author).

2.11.1 Architecture of neural network

The architecture of an ANN is mainly distinguished by the numbers of computational layers employed for the underlying task. The two architectures of ANN are the singlelayer neural network and the multi-layer neural network.

2.11.1.1 *The single-layer neural network (SNN)*

This is the simplest form of ANN. It contains one input and one output layer. SNN is a neural network with one computational layer. Though, it is built up of a single input and output layer, the input layer only transmits feature values to the output layer and no computation is carried out within the input layer. As a result, only the output layer is counted as computational layer. In a SNN, all computations are completely visible to users. However, SNN can only provide solutions to features that are linearly separable.

The structure of a single perceptron is shown in Figure 2.25.

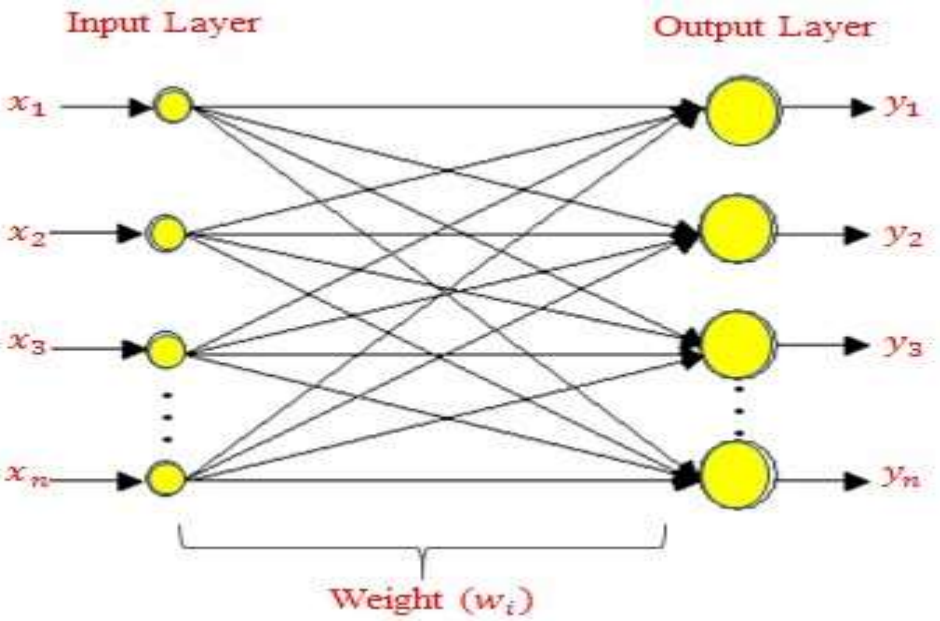

Figure 2.25: A Single-layered neural network (Source: Author).

Linearly-separable and non-linearly-separable features: Linearly-separable feature describes the feature in which the boundary between constituting variables can easily be mapped out by a linear function. While non-linearly-separable feature describes the feature in which the boundary between constituting variables cannot be mapped out by a linear function. Non-linearly-separable features are complex and the boundaries between variables can be mapped out by curve fitting functions, such as sigmoid, hyperbolic tangent, and rectified linear unit to mention a few.

From Figure 2.26 (a), the boundary between the two variables is mapped out by a straight line which represents a linear function. In Figure 2.26 (b), mapping out of the variables is better achieved using a curve which ordinarily a linear function will not be able to achieve. Hence, the need for activation functions to identify, classify and scale a neuron's response to incoming signals.

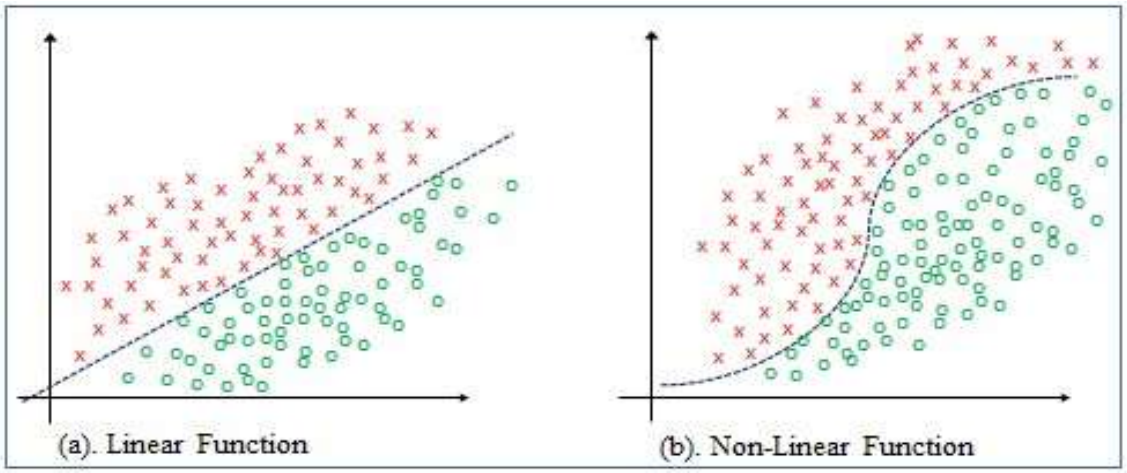

Figure 2.26: Separable functions (Source: Author).

2.11.1.2 *The multi-layer neural network (MNN)*

MNN is famous among the network architectures in ANN. ANN architecture of two or more computational layers is referred to as MNN and can be seen in Figure 2.27. The network is comprising of the input layer, output layer and an intermediate layer between the input and the output layers called the "hidden layer". Computations within the hidden layer are invisible to users, thus depicting its meaning. According to Folorunso *et al.* (2019), MNN is good for modelling linear problems. The significant difference between the SNN and the MNN is the presence of the hidden layer, thus, there is no direct link between the input and output layers of MNN. In addition, SNN can only be used for solving problems that are linearly separable.

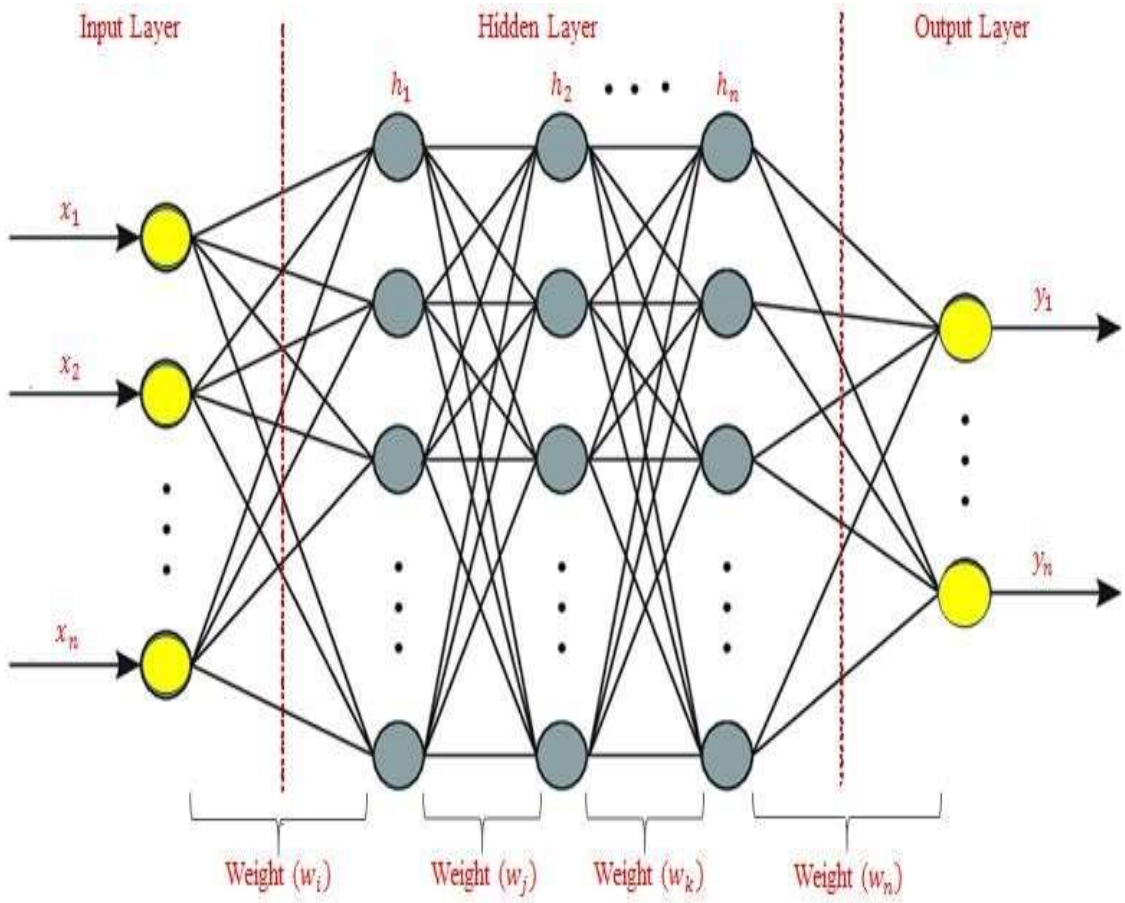

Figure 2.27: Multi-layer neural network (Source: Author).

Nevertheless, as a result of single threshold function, a perceptron is basically a feedforward network (Andreas, 1994). The simplex explanation for this is that all the arrows are coming from the input layer and directly pointing towards the output layer. A feedforward network contains neither cycles nor loops in the training process (Jurgen, 2015). The input nodes are passed directly to the output nodes through a series of synaptic weights in one direction. A feedforward network is simple to use, but it is not suitable for handling complex problems.

A backpropagation (backward-propagation) network is more suitable for use in MNN and in providing solutions to complex problems. Backpropagation is an algorithm that is developed to determine the gradient of the loss function with respect to each weight through chain rule (Rojas, 1996). It is divided into two stages which include the forward phase and the backward phase. In the forward phase, features are fed for computation

directly from the input layer to the output layer. In the backward phase, possible errors between the target value and the output values are propagated backwards to the network in order to modify the weight and bias values. In a simple term, backpropagation is a method which is aimed at determining the total error in a network, identifying the contribution of every node to the total error and as a result adjust the weights and biases in order to minimize the recorded error (Kostadinov, 2019). This process is attainable using a gradient descent and chain rule. Hence, the method is referred to as a dynamic programming.

2.11.2 Learning algorithms

Algorithms describe the various mechanisms through which a network learns from available sets of samples. The two most prominent algorithms are the supervised and the unsupervised learning algorithms. Other learning algorithms include reinforced, semisupervised, online and offline (Paluszek and Thomas, 2017).

Supervised learning algorithm: This learning method requires input and desired output / expected result to aid the learning process (Paluszek and Thomas, 2017). Provision of the desired result allows for comparison between the result given by the network and the desired result, thereby giving room for weight adjustment which will possibly help in minimising errors (Kriesel, 2005). The method is practicable and highly effective in providing solution to problems. But, because of possible adjustment of weights and biases, the supervised learning method is therefore not biologically credible when compared to biological neural network.

Unsupervised learning algorithm: This pattern of learning only involves sets of input data without the expected / desired output to aid the learning process (Paluszek and Thomas, 2017). Since there is no provision for the desired output, the network therefore identifies the relationship between the sets of sample data, assembles them and classifies

them on its own. Unsupervised learning method is biologically more credible than the other learning methods, but not suitable for providing solution to some specific problems (Kriesel, 2005).

Reinforced learning algorithm: Reinforced learning is built on observation in which the network decides on an output by observing its environment. In the method, feedback is given to the network irrespective of its performance. The provided feedback is used to establish a benchmark which helps in solving problems. Reinforced learning method only input data sets, and when the network gives output, a value is sent back to the network to determine whether the generated output is exact or not, and also to indicate the level of precision. Equally, if the network gives a desirable output, then there will be no need for further feedbacks. The reinforced learning algorithm is most suitable for system control.

In order to develop a reliable ANN-based model, parameters like system architecture, activation function, number of neurons in the layers and the learning rate are of utmost importance (Folorunso *et al*., 2019).

2.11.3 Activation functions

This describes the output of a neuron from given set of inputs. This is achieved by passing the weighted sum of the neuron through an activation function, which will then process the weighted sum to a number between some upper limits and lower limits.

Logistic sigmoid (logsig) activation function: For a sigmoid function, 1 is the upper limit while 0 is the lower limit as depicted in Figure 2.28 (Karlik and Vehbi, 2011). The function transforms every input data set to numbers between 0 and 1 (Han and Moraga, 2019). For instance, when a negative number is fed into sigmoid function as input, sigmoid will transform the input to a number that is close to zero (0). On the other hand, if the input data set is positive, then sigmoid will transform such input to a number that is

close to one (1). As a result of this, when the output is 1, this translates to the fact that a neuron will be activated and if it is 0, then the neuron will be deactivated. However, sigmoid is often faced with the problem of vanishing gradient and has slow convergence (Glorot and Bengio, 2010). It takes the form:

$$F(x) = \frac{1}{1 + \exp(-x)} \tag{2.96}$$

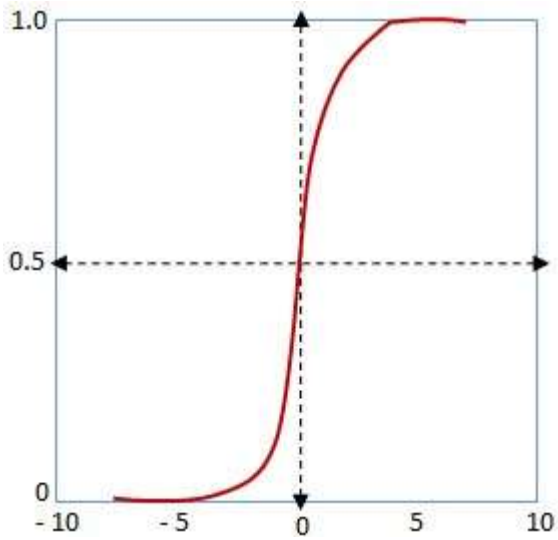

Figure 2.28: Sigmoid activation function (Source: Author).

Hyperbolic Tangent (tanh) Activation Function: This describes the ratio between the hyperbolic sine and the hyperbolic cosine functions of two exponential functions. It is achieved by computing the fraction of the half-difference and half-sum of two exponential functions (Karlik and Vehbi, 2011). Tanh has -1 as its lower limit and +1 as its upper limit as shown in Figure 2.29. The function crushes real number into a range between -1 and +1. Its output is centred on zero (0) which gives room for better optimisation. Tanh is similar to the sigmoid function and also suffers from vanishing gradient. The function takes the form:

$$F(x) = \frac{1 - \exp(-2x)}{1 + \exp(-2x)} \tag{2.97}$$

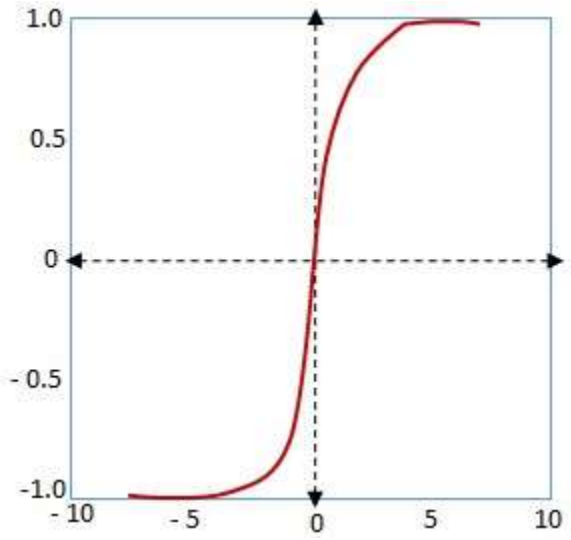

Figure 2.29: Tanh activation function (Source: Author).

Rectified linear unit (ReLU) activation function: In ReLU, inputs are transformed to maximum of the input and zero (0). When the input is equal to or less than 0, ReLU will give the output as 0, but if the input is greater than 0, then ReLU will give the output as the input (Nair and Hinton, 2010). In other words, more positive neurons are activated while more negative neurons are eliminated in ReLU as presented in Figure 2.30. In addition, ReLU has a good convergence and does not suffer from vanishing gradient (Ramachandran *et al*., 2017), but it often results to the death of weak neurons. It is more efficiently used for signal response and can only support forward propagation. ReLU takes the form:

$$F_{(x)} = \max(0, x) = [x0^{\prime}, {}^{if}{}_{if}\ {}_{x_{i}{}^{i}}{}^{\geq}{}_{<}{}^{0}0] \tag{2.98}$$

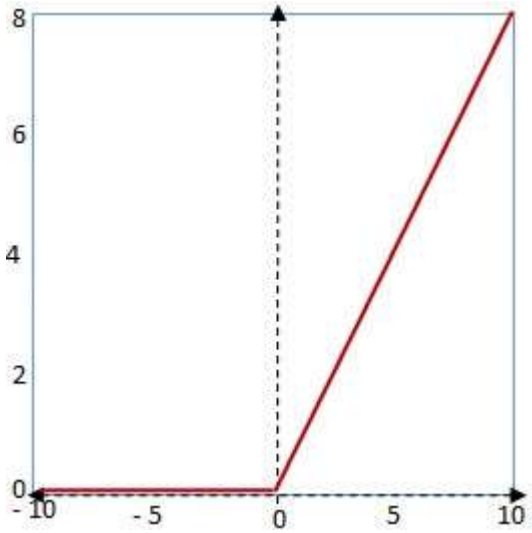

Figure 2.30: ReLU activation function (Source: Author).

Softmax activation function: Softmax activation function is better employed in probability distribution process from vector of real numbers (Nwankpa *et al*., 2018). It generates output between the range of 0 and 1, and giving the sum of the probabilities of the output to be 1 (Godfellow *et al*., 2016). This implies that it maps all the output and makes the summation of the total output to be 1 (Sutskever, 2013). For instance, if the input value is positive, negative, zero, or a value greater than one, softmax will automatically change the input value to that between 0 and 1, this is done in order to process the values as normalized probabilities distribution. Softmax activation function is employed in neural network to proffer solutions to problems that deal with multi-class logistic regression. It is designed to give feedback of the probabilities of each class and then assign the highest probability to the target class. It is more appropriate for use in the final layer of a neural network (Badrinarayanan *et al*., 2016). Unlike sigmoid that is more preferable for binary classifications, softmax is more preferable for multivariate classifications (Nwankpa *et al*., 2018). A typical softmax activation function is given by:

$$F^{(x_i)} = \frac{\exp(x_i)}{\sum_j \exp(x_j)} \tag{2.99}$$

Softplus activation function: A Softplus activation function is an improved version of ReLU and Sigmoid activation functions. It was developed by Dugas *et al.* (2001) with the aim to make-up for the short-comings of ReLU and sigmoid activation functions which cause death of neurons and vanishing gradients respectively (Zheng *et al*., 2015). By so doing, the performance and stability of deep learning is enhanced. Softplus activation function is adjudged to be continuous, smooth and applaud able in statistical applications (Chieng *et al*., 2018). The function is defined as:

$$F_{(x)} = \log\,(1 + exp^{x}) \tag{2.100}$$

Swish activation function: The swish activation function is a hybrid function. It is termed hybrid because it is a combination of a sigmoid function and a set of input functions (Ramachandran *et al*., 2017). The function was developed by Ramachandran *et al.* (2017). The researchers in their work proclaimed swish as the best-known activation function and further discovered from their numerous scientific experiences that swish is a better match for ReLU and that it outperforms ReLU in a couple of different applications. According to Nwankpa *et al*. (2018), swish activation function is smooth, simple, non-monotonic, precise and does not suffer vanishing gradients. It employs reinforced learning algorithm as its learning rule. The function is expressed as:

$$F_{(x)} = x\,.\ sigmoid(x) = \frac{1}{1 + \exp^{x}(-x)} \tag{2.101}$$

2.11.4 Weight and bias regulation

The relevance of weights and biases in training an ANN to accomplish maximum optimisation cannot be ignored. In order to obtain a good model for an ANN, there is need to adjust the weights and biases of the network. The weight of an ANN shows how steep the output is, in relation to the input, thereby determining the potential of neurons. On the

other hand, bias determines the neurons to be activated and achieves this by increasing the flexibility of the model in order to fit the given data.

Let us consider the equation of a straight line given below:

$$y = mx + c \tag{2.102}$$

where, y and x are variables, m is the slope and c is the intercept of the line. Figure 2.31 describes the effect of varying slope in a linear equation.

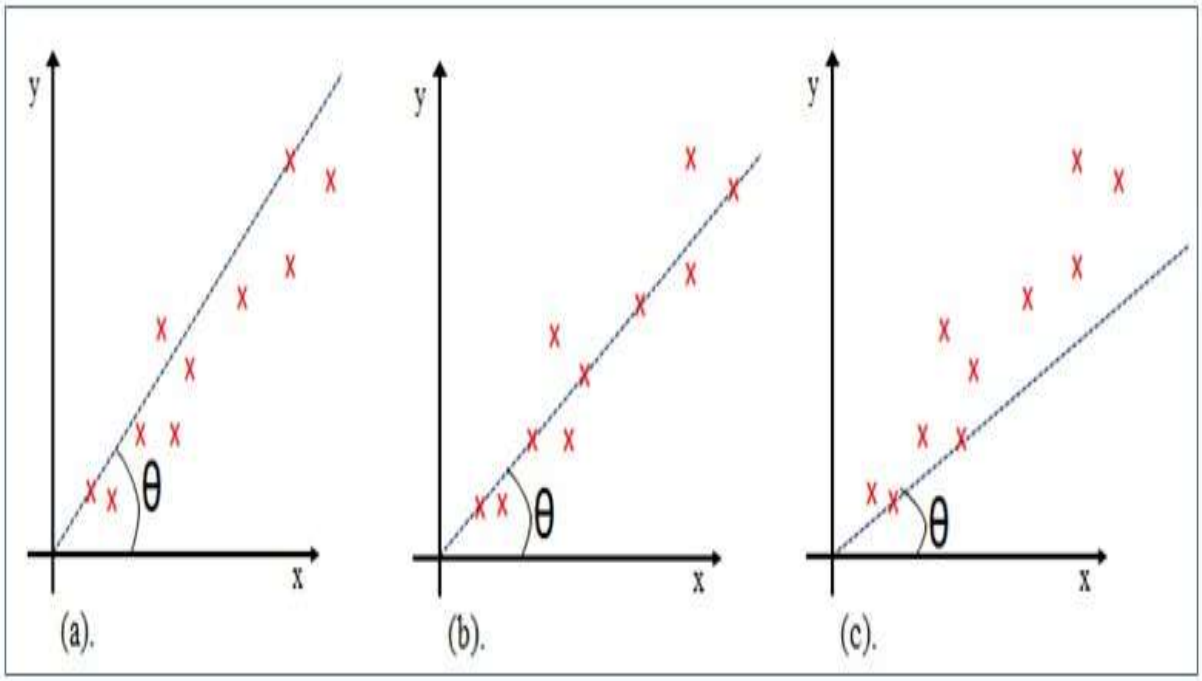

Figure 2.31: Varying gradient at fixed intercept (Source: Author).

As depicted from Figure 2.31, the slope or gradient (m) describes the steepness of the linear model and it is a function of the angle (θ). The slope decreases with a decrease in angle from (a) through (b) to (c). By comparing equations 2.92 and 2.102, the slope performs the same function as the weight of an ANN, which reveals the steepness of the activation function. In the same vein, Figure 2.32 explains the effect of varying intercept on a linear model.

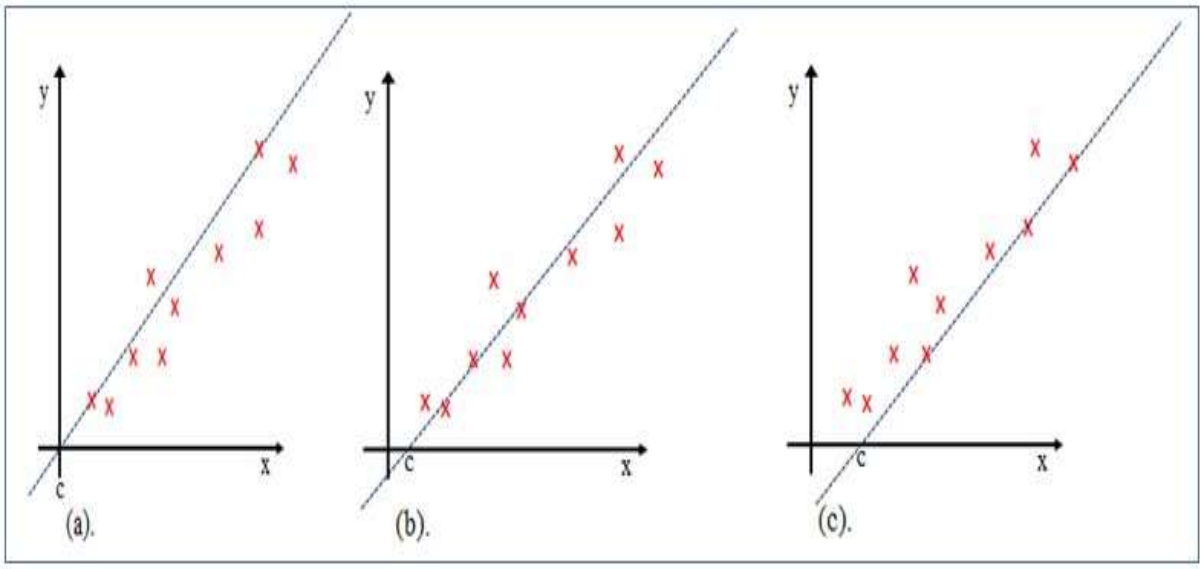

Figure 2.32: Varying intercept at fixed gradient (Source: Author).

According to the relationships between equations 2.92 and 88, the intercept ‘c’ of the straight line corresponds to the bias ‘b’ of the ANN as depicted in Figure2.32. The bias, just as the intercept, changes the alignment of a model. It can be shifted to the left or right positions in order to attain the best fit for the model. The movement of the bias via right or left positions also constitutes a change to the activation function, by controlling the threshold at which the activation function will trigger.

2.12 Renewable Energy Technology

Renewable energy technology is a means through which clean and sustainable energy sources are developed from sources like the sun, wind, plants and water (Ramli *et al*., 2017). They are developed in order to provide cheap energy to control incessant climate change and attain a level of energy independence and efficiency (Vigneswaran *et al*., 2008; Zhang *et al.*, 2017).

An off-grid renewable energy system is also referred to as a stand-alone system. As implied, “stand alone” not dependent. That is, a renewable energy system that is not connected to the grid. They are designed basically on specification and demand. A stand

- alone PV technology system provides a more economic opportunity to power consumers compared to the more expensive grid system (Givler and Lilienthal, 2005). International Resources Group carried out research in Sri Lanka and concluded that majority of the homes that utilise solar technology does not exceed 50 watts which were sufficient to light their homes and power other small home gadgets (International Resources Group, 2003).

An effective stand-alone PV power system, consists of solar panel, charge controller and rechargeable battery (Ramli *et al*., 2017). In order to ensure an uninterrupted power supply, the energy generated during the sunshine hours has to be stored in rechargeable batteries so as to make up for the dark hours. However, a major drawback of the off-grid solar system is power fluctuation which arises from the varying nature of the GSR (kumar *et al*., 2016). According to Turkay and Telli (2011) and Panhwar *et al*. (2017), the combination of a hybrid renewable energy system with the grid is more efficient than the use of solar energy system as the only source of energy.

2.13 Renewable Energy Tools

Over dependence on traditional sources of energy like coal and other fossil energy sources is a major limiting factor to the growth of the non- developed countries of the world (Jerabaj and Iniyan, 2006). Energy diversification is very important in order to live a wealthy and healthy life style. To achieve this, several vital information and tools are required to design, analyse and plan to make use of modern energy technologies effectively. In doing this, computer tools are required to provide the anticipated information by which the potentials of various energy resources can be assessed through modelling. There are many energy tools in literature as at present (Jerabaj and Iniyan, 2006). Making the right choice of tool is dependent on the types of required inputs system configuration and the load demand. The tools are categorised into five different groups according to their number of users in descending order. Group A comprises of tools with

very high number of users. Group B denotes high number of users. Group C represents medium number of users while Group D belongs to a category of low number of users and finally, Group E denotes unspecified number of users because the tools were not monitored (Connolly *et al.*, 2010).

Group A: This has users between 1,000 and 200,000. It includes RETScreen, HOMER, LEAP, BCHP Screening Tool and energy PRO (Connolly *et al*., 2010).

Group B: This has from 100 to 1000 users. It includes Energy PlAN, Invert, MARKAL / TIMES, MESSAGES, ORCED, TRNSYS16, and WASP (Connolly *et al*., 2010)

Group C: Users in this group are between 20 and 50. It includes EMCAS, EMPS, ENPEP - BALANCE, GYMNast (Connolly *et al.*, 2010).

Group D: This is from 0 to 20 users. It includes RAMSES, EMINENT, COMPOSE, IKARUS, Mesap plaNet, INFORSE, PERSEUS, NEMS, ProdRisk, SIVAEL, PRIMES, AEOLIUS (Connolly *et al.*, 2010).

Group E: This has an unspecified number of users and includes WILMAR planning Tool, BALMOREL, E4Cast, UniSyD3.0, MiniCAM, SimREM, H2RES, STREAM, HYDROGEMS (Connolly *et al.*, 2010).

2.13.1 HOMER

Hybrid Optimisation Model for Electric Renewable (HOMER) was developed in the year 1993 by Mistaya Engineering in Canada, U. S. A. for the National Renewable Energy Laboratory (NREL) (Kumar *et al.,* 2016). HOMER is a computer-based renewable energy micro-power optimisation tool (Lambert *et al.,* 2006). Its development was aimed at assisting users to attain prime micro power system designs and analysis (Nurunnabi and

Roy, 2015). Basically, HOMER is designed for stand-alone applications which are usually on small scales (Luvchik, 2015). Therefore, in designing a renewable power project for a single point, a building or a small community, HOMER is relatively good for such task.

HOMER is used globally by corporate bodies, academic institutions, governmental and non- governmental organisations. HOMER can model power systems for both electric and thermal applications by employing any combination of PV arrays, biomass power, wind turbines, micro-turbines, hydro power, combustion engine generators, fuel cells, batteries, and hydrogen storage (Connolly *et al.*, 2010). The flexibility of the model allows for comparison of different design options, with regards to their technical and economic values (Ramli *et al.*, 2017). Nevertheless, the model also provides information about uncertain conditions that might arise due to changes in input parameters (Lambert *et al.*, 2006).

HOMER performs three basic functions which include simulation, optimisation and sensitivity analysis (Connolly *et al.*, 2010).

Simulation: The simulation process attempts to present a workable system for all probable combinations of the desired equipment. This is done to obtain balance at every hour for every 8,760 hours in a year. However, there is no limit to the number of simulated systems. This is determined by the available materials set up and the load requirement.

Optimisation: The optimisation process entails the sorting and clarification of the simulated systems following a laid down criteria or load demand. This is done in order to select a system that will best fit the load demand by considering economic merits, technical practicability and energy resource availability. Economic optimisation is carried out in order to determine the best combination, quantities and efficiencies of battery bank, converter, solar panel, wind turbine and generator.

Sensitivity: The sensitivity analysis is done to carry out a probabilistic examination of the available models, as this will help to predict the effects of uncertainties or fluctuations of input variables. For instance, GSR, wind speed, and other atmospheric factors that are used as inputs are not controlled by the users and varies with time and season. Hence, the need for the sensitivity analysis to determine the peak system variations in the case of uncertainties in the non - developed parts of the world.

2.13.2 RETScreen

RETScreen is a renewable energy system tool which was developed in Canada with the aim of analysing, planning, implementing and monitoring of renewable energy projects (RETScreen, 2015). It was developed jointly by Canada Centre for Mineral and Energy Technology (CANMET) in conjunction with professionals from academic institutions, industry and government (EL-mohr and Anas, 2014). It uses Microsoft excel spreadsheets to model power systems (Ramli *et al*., 2017; Khan, 2019). The software comprises of different packages which include product, project, hydrology and climate databases. Not only that, it is user friendly and supports about 36 different languages (Diarra, 2018). RETScreen has data records with about 6,000 data logging stations which cut across the globe (Diarra, 2018; Chowdhury *et al*., 2020).

RETScreen has some intrinsic features that enable it to assess energy production, life-cycle cost and reduce the emission of greenhouse gases. Its fundamental value is to expedite pre-feasibility and feasibility study of renewable energy technology applications. RETScreen is suitable to model renewable energy projects both on small scales and on large scales for global applications (Luvchik, 2015). It is free and rated as the highest used renewable energy tool across the globe (Connolly *et al.*, 2010). The dynamic nature of RETScreen enables it to model all forms of thermal-energy applications with energy efficiency (Thevenard *et al.*, 2010).

In designing energy projects using RETScreen, some factors have to be taken into consideration. Foremost, there is need to ascertain the feasibility of the project. This is done by comparing the total load output of the system to the total load demand. When this is achieved, it is then good to know the total net cost of setting up the system. This could be achieved by estimating its initial setup cost, maintenance cost, and operational cost. The assessment is therefore completed by comparing the efficiency of the system and the total net cost with other forms of available energy system. However, the choice of the most favourable energy system does not only depend on technical efficiency or economic efficiency, but also on environmental management (Li *et al*., 2013).

CHAPTER THREE

3.0 METHODOLOGY

3.1 Data Collection

A 25year data of GSR, relative humidity (RH), amount of cloud (C_{ld}), precipitated rainfall, maximum and minimum temperature (T_{max} and T_{min}) were used for each of the following locations: Benue, Plateau, Abuja, Kwara, Nasarawa, Kogi and Niger States respectively. Grid point data were used for the study. The data is satellite-based (Vernay *et al*., 2014) which were downloaded from the National Aeronautics and Space Agency (NASA) on monthly average for 25 years (1993 to 2018). It is extrapolated to other places on assumption that it is homogenous. GSR was measured in kW-hr/m^2/day, RH was measured in percentage (%), while minimum and maximum temperatures were measured in ^oC.

3.2 Estimation of GSR

In the course of this study, GSR was estimated using empirical and soft-computing models. For the empirical model, single-parameter-based models was used as well as multiple-parameter based models. The single-parameter based models include:

Hargreaves and Samani Model (Md 1), Bristow and Campbell Model (Md 2), Annadale Model (Md 3), Allen Model (Md 4), Angstrom-Prescott Model (Md 5), Glover and McCulloch Model (Md 6), Ogleman Model (Md 7), and Newland Model (Md 8). For the multiple parameter-based models, Swartman and Ogunlade Model (Md 9), Abdalla Model (Md 10), Okundamiya Model (Md 11), Olomiyesan and Oyedum (Md 12), and Badescu Model (Md 13). In the same vein, the proposed model was used as the SoftComputing Model (SCM).

Table 3.1: Categorisation of models

Model name	Abbreviation	Parameter(s)	Model type (Parameter)
Hargreaves and Samani	Md 1	temperature	single
Bristow and Campbell	Md 2	temperature	single
Annadale	Md 3	temperature	single
Allen	Md 4	temperature	single
Angstrom-Prescott	Md 5	sunshine	single
Glover and McCulloch	Md 6	sunshine	single
Ogleman	Md 7	sunshine	single
Newland	Md 8	sunshine	single
Swartman & Ogunlade	Md 9	sunshine, relative humidity	multiple
Abdalla	Md 10	temperature, sunshine, relative humidity	multiple
Okundamiya	Md 11	temperature, sunshine, cloud	multiple
Olomiyesan & Oyedum	Md 12	temperature, sunshine	multiple
Badescu	Md 13	cloud	Single
Soft-Computing	SCM	temperature, solar flux, relative humidity	multiple

3.3 Model Design and Development

In order to design a mathematical model that will take the form of ANN, a neural network was trained for each of the stations under study for optimum result. To attain this objective, the process is further divided into three phases namely: data processing, ANN design and model validation.

Data processing: After data acquisition, the data were examined to ascertain the validity. After the validity check, the datasets were filtered in order to eliminate periods of no records. The filtered dataset is then normalised to ensure even distribution (Folorunso *et al*., 2018). Normalising the dataset is achieved using the 'minmax' method. This is done

in order to establish a dimensional consistency of the dataset and to ensure data conformity with the transfer functions. The 'minmax' method is given by:

$$\text{Minmax}\,(x) = \frac{x - x_{min}}{x_{\max} - x_{min}} \tag{3.1}$$

where x represents the sampled value of the dataset, x_{min} and $x_{\max}$ represent the minimum and maximum values of x respectively. Seventy percent (70%) of the dataset is specified to train the network, while the remaining thirty percent (30%) is specified for testing and validation.

ANN design: Relative humidity (RH), Temperature change ($T_{max} - T_{min}$) and the solar flux ($I_{rr} = I_{sc}\,[1 + 0.033cos\,(\frac{dn}{73} \times 72)]$) are the three inputs to the ANN network, where I_{sc} is solar constant and dn is day number of the year. Measured GSR is the target of the network while the network-predicted GSR is the output. The proposed SCM is developed using a MNN consisting of four nodes at the input layer, multiple neurons at the hidden layer (which depends on the training performance) and one node at the output layer (Herculano-Houzel, 2017). The network training process employed the feedforward back-propagation network, which has gained popularity for its great performances in providing solutions to several complex linear and non-linear problems (Shahin *et al*., 2008; Al Shamisi *et al*., 2011; Nguyen *et al*., 2019) and it is a supervised learning process that adopts the Levenberg-Marquard training algorithm (TRAINLM). In addition to this, the three most famous activation functions were used. These include the logsig, tansig and purelin activation functions (Eichie *et al*., 2016). Either of the logsig or the tansig activation functions were employed at the first layer of the network, while the purelin was employed at the second layer of the network. The structure of the proposed model is presented in Figure 3.1.

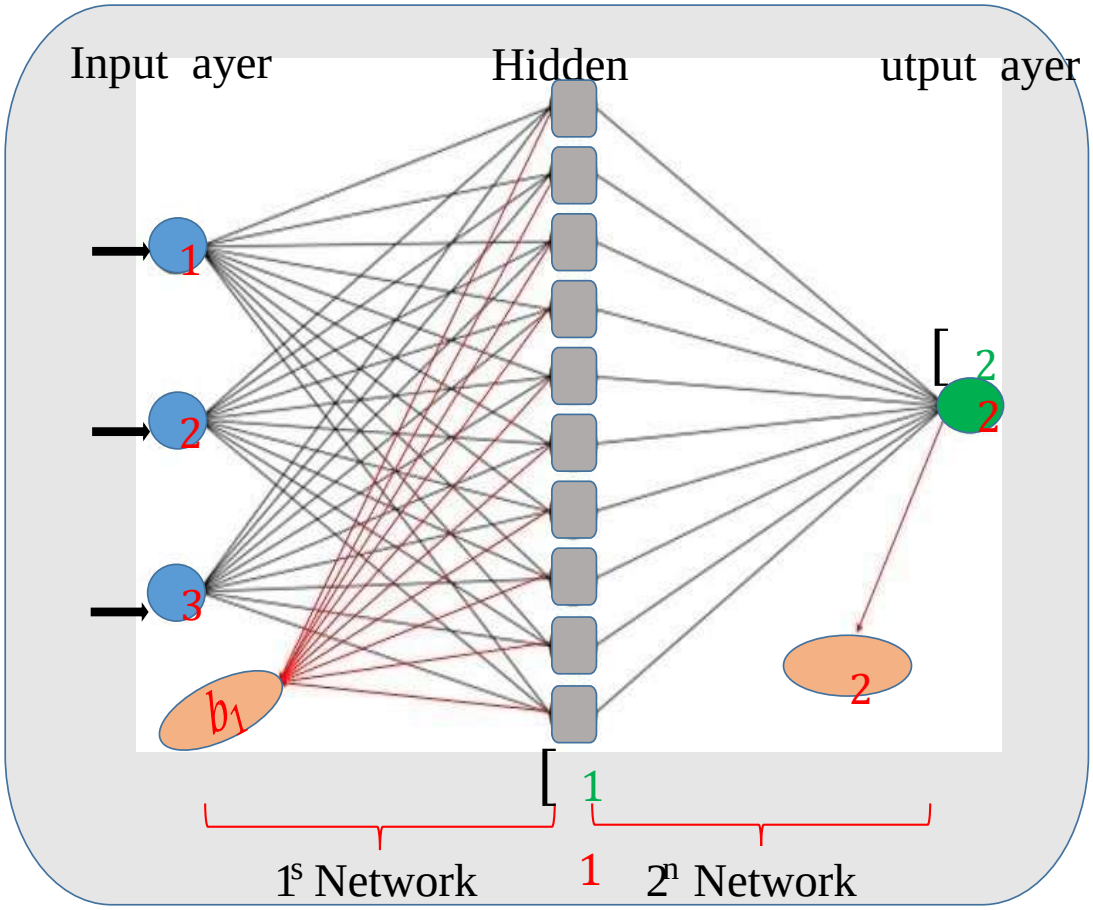

Figure 3.1: ANN Structure for the proposed GSR model (Source: Author).

The mathematical representation of Figure 3.1 is given by:

$$y_1 = \varphi_1[\Sigma_i^n(w_{ij}x_i + b_j)] \tag{3.2}$$

where y_1 is the output of the first layer, φ_1 is a linear activation function (logsig) of the first layer, w_{ij} is the adjustable weight that connects the input layer to the hidden layer, b_j is the input bias that is associated with the jth neuron of the first layer and x_i is the set of input data to the ANN for which ($1 \leq \quad \leq i\ n$ and n = 3). Hence,

$$y^2 = \varphi_2[\Sigma_j^m(w_{jk}y_1 + b_k)] \tag{3.3}$$

where y_2 is the output of the second ANN layer, φ_2 is a non-linear activation function (tansig) of the second layer, b_k is the output bias that is related to the kth neuron of the second layer and w_{jk} is the adjustable weight that connects the hidden layer to the output

layer, for which ($1 \leq j \leq m$ and m = 49, that is, number of neurons). Thus, the combination of equations 3.2 and 3.3 gives:

$$y^2 = \varphi_2\left[\sum_j^m (w_{jk}\langle\varphi^1\left(\sum_i^n (w_{ij}x_i + b_j)\right)\rangle + b_k)\right] \quad (3.4)$$

where all parameters have retained their initial properties and identities.

3.4 Evaluation Metrics

Evaluation of scientific model performances are often carried out using some famous statistical evaluators which include:

Error (E): This refers to the magnitude of the deviation recorded in the course of representing a measurable quantity differently from its actual value.

Mathematically, it is calculated as:

$$\text{Error} = \text{Actual Value} - \text{Estimated Value} \quad (3.5)$$

Absolute error (AE): This describes the absolute magnitude of the difference between the definite value and the estimated value of a quantity. In relation to this study, absolute error of GSR is given as the absolute difference between measured GSR and estimated GSR.

$$\text{AE} = |H_M - H_E| \quad (3.6)$$

where H_M is the ground-assessed GSR and H_E is the estimated GSR.

Mean absolute error (MAE): Simply implies the statistical average of all the observed AE (Chai and Draxler, 2014). It is a scale dependent accuracy measure of errors between two quantities that express the same phenomenon (Pontius *et al*., 2008). The accuracy of a model increases as the magnitude of the MAE decreases to zero (Willmott *et al*., 2009). Mathematically,

$$\text{MAE} = \frac{1}{n}\sum_{i=1}^{n}|H_M - H_E| \quad (3.7)$$ where

H_M is the ground-assessed GSR and H_E is the estimated GSR while n is the overall possible observations, for $1 \geq i \geq n$.

Mean bias error (MBE): It is the mean of observable errors between the definite value of a quantity and the estimated value of the quantity. MBE is similar to MAE, but different in the sense that absolute errors are not considered. Also, for MBE, a model can be classified either to a positive direction or to a negative direction (Padhma, 2021). This classification gives room to determine whether a model overestimate or underestimate the value of the quantity in question. A positive bias connotes overestimation, while a negative bias connotes underestimation (Padhma, 2021). Mathematically,

$$\text{MBE} = \frac{1}{n}\sum_{i=1}^{n}(H_M - H_E) \quad (3.8)$$

where H_M is the ground-assessed GSR and H_E is the estimated GSR while n is the overall possible observations, for $1 \geq i \geq n$.

Mean squared error (MSE): Is a measure of the variance of error and it is a differentiable function (Padhma, 2021). MSE is obtained by computing the average of the square of the variation between the definite and the estimated value of a quantity. The metric is worthy for determining the best values for parameters. A MSE value closer to zero signifies a better performance. It is expressed mathematically as:

$$\text{MSE} = \frac{1}{n}\sum_{i=1}^{n}(H_M - H_E)^2 \quad (3.9)$$

where H_M is the ground-assessed GSR and H_E is the estimated GSR while n is the overall possible observations, for $1 \geq i \geq n$.

Root mean squared error (RMSE): This is termed as a measure of accuracy and serves as heuristic approach for training models (Padhma, 2021). As its name implies, it is the

square root of the average of the squared variation between the definite and the estimated value of a quantity. RMSE can simply be attained by computing the square root of MSE. RMSE refers to the standard deviation of estimated errors and reveals the margin between true values and estimated values (Chai and Draxler, 2014; Willmott *et al*., 2009). It is a popular statistical metric tool and often used by researcher to validate experimental observations (Pontius *et al*., 2008). A RMSE value of zero is most desirable, indicating 100% performance accuracy. However, lower RMSE values are of better performance accuracy than higher RMSE values (Padhma, 2021; Hyndman and Koehler 2006). Mathematically,

$$\text{RMSE} = \sqrt{\frac{1}{n}\sum_{i=1}^{n}(H_M - H_E)^2} \tag{3.10}$$

where H_M is the ground-assessed GSR and H_E is the estimated GSR while n is the overall possible observations, for $1 \geq i \geq n$.

Correlation coefficient (R): It is a statistical metric that defines the degree of association between two different variables (Schober *et al*., 2018). The values of R ranges between 1 at the lower boundary, and +1 at the upper boundary. R value of 1 signifies perfection, implying that a noticeable positive increase in one variable will lead to a positive increase of the same measure in the other variable. On the other hand, R value of -1 indicates imperfection, that is, a noticeable positive increase in one variable leads to a negative decrease in the other variable. While R value of 0 indicates no relationship between the variables. Hence, a correlation coefficient value that is closest to unity is applaudable (Schober *et al*., 2018). Mathematically,

$$\text{R} = \frac{\sum[(H_E - \bar{H}_E)(H_M - \bar{H}_M)]}{\sqrt{\sum[(H_E - \bar{H}_E)^2 (H_M - \bar{H}_M)^2]}} \tag{3.11}$$

where H_M is the measured GSR, H_E is the estimated GSR, $\bar{H}_M$ is the mean measured GSR and $\bar{H}_E$ is the mean estimated GSR.

HOMER, the most famous among the renewable energy tools will be used to achieve objectives number three (iii) which is to conduct feasibility study and to evaluate the techno-economic analysis of off-grid solar energy plant for NCSN respectively.

CHAPTER FOUR

4.0 RESULTS AND DISCUSSION

4.1 Preamble

This chapter is divided into three parts which correspondingly satisfy the objectives of the research. The first part deals with the derivation of the proposed soft-computing model. The second part deals with the estimation of GSR and comparison of the performances of GSR models, while the third part features more on the applications of the estimated GSR in enhancing solar energy technologies.

The three parts are further split into sections. Section 4.2 solely addresses objective number one (i) of the research. It entails the development of the proposed model. Section 4.3 of the chapter takes care of a fraction of objective number two (ii). In this section, the developed model (SCM) and some empirical models are used to estimate GSR for the NCSN. Section 4.4, is an extension of section 4.3 and both are classified under the second part of the research. Section 4.4 attempts to compare the estimated GSR for all the considered models. The third part of the research encompasses Sections 4.5 and 4.6 and satisfies objective number (iii). In the two sections, the feasibility and the efficacy of offgrid solar power systems are examined.

4.2 Data Presentation

The meteorological data used for the study comprises monthly mean RH (%), monthly mean minimum temperature (^oC), monthly mean maximum temperature (^oC) and monthly mean all sky insolation incident on a horizontal surface (kW-hr/m^2/day). The data is sourced from the National Aeronautics Space Agency (NASA). The data covered a period of 25 years (from 1993 to 2018), for Abuja city as well for Benue, Kogi, Kwara,

Nasarawa, Niger and Plateau States of Nigeria. The monthly averages of the acquired data are presented for solar insolation, RH, minimum temperature and maximum temperature in Figures 4.1, 4.2, 4.3 and 4.4.

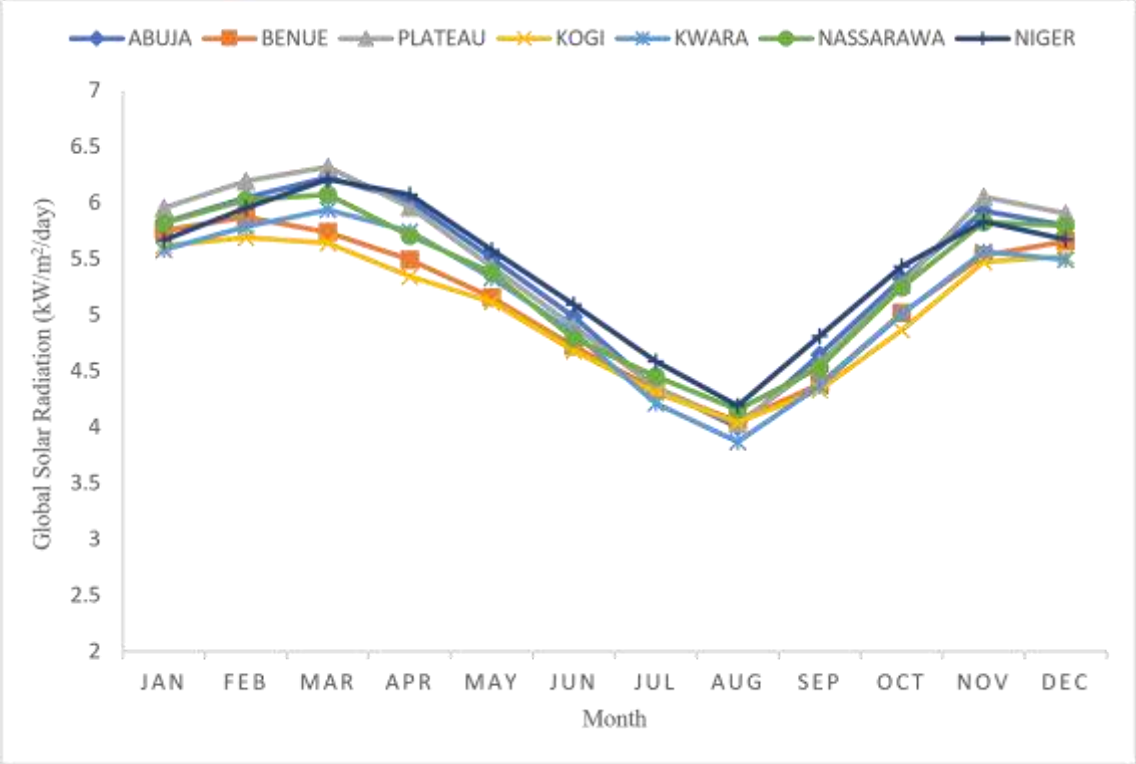

Figure 4.1: Monthly Distribution of Solar Insolation

From Figure 4.1, it could be depicted that the graphs for the seven stations followed a similar trend starting from January to December for an average of 25 years. The measured solar insolation fairly increased between January through to February until peak values are attained in March, it then drops from march and reached a minimum value in August. The solar insolation also rises from August to attain another peak value in November after which it had a partial decrease between November and December.

Solar insolation is maximum in the dry season when there is little or no cloud cover and accompanying rainfall. On the contrary, solar insolation is minimum in the month of August which marks the peak of rainfall activities. At this period, vast cloud cover is recorded which would either absorb or reflect the insolation back to the space.

From the graphs, it is observed that Abuja records the highest solar insolation of 6.22 ($kW/m^2/day$) and a minimum of 3.99 ($kW/m^2/day$). Benue records a peak of 5.87 ($kW/m^2/day$) and a minimum of 4.05 ($kW/m^2/day$). For Kogi, a peak of 5.69 ($kW/m^2/day$) and a minimum of 4.04 ($kW/m^2/day$) were recorded. Kwara recorded 5.94 ($kW/m^2/day$) and 3.87 ($kW/m^2/day$) as the peak and minimum solar insolation respectively. For Nasarawa, a peak of 6.07 ($kW/m^2/day$) and a minimum value of 4.15 ($kW/m^2/day$) were recorded. Niger recorded 6.21 ($kW/m^2/day$) and 4.19 ($kW/m^2/day$) as the maximum and minimum values of solar insolation respectively. Similarly, Plateau recorded a peak and a minimum value of solar insolation as 6.32 ($kW/m^2/day$) and 4.03 ($kW/m^2/day$) respectively.

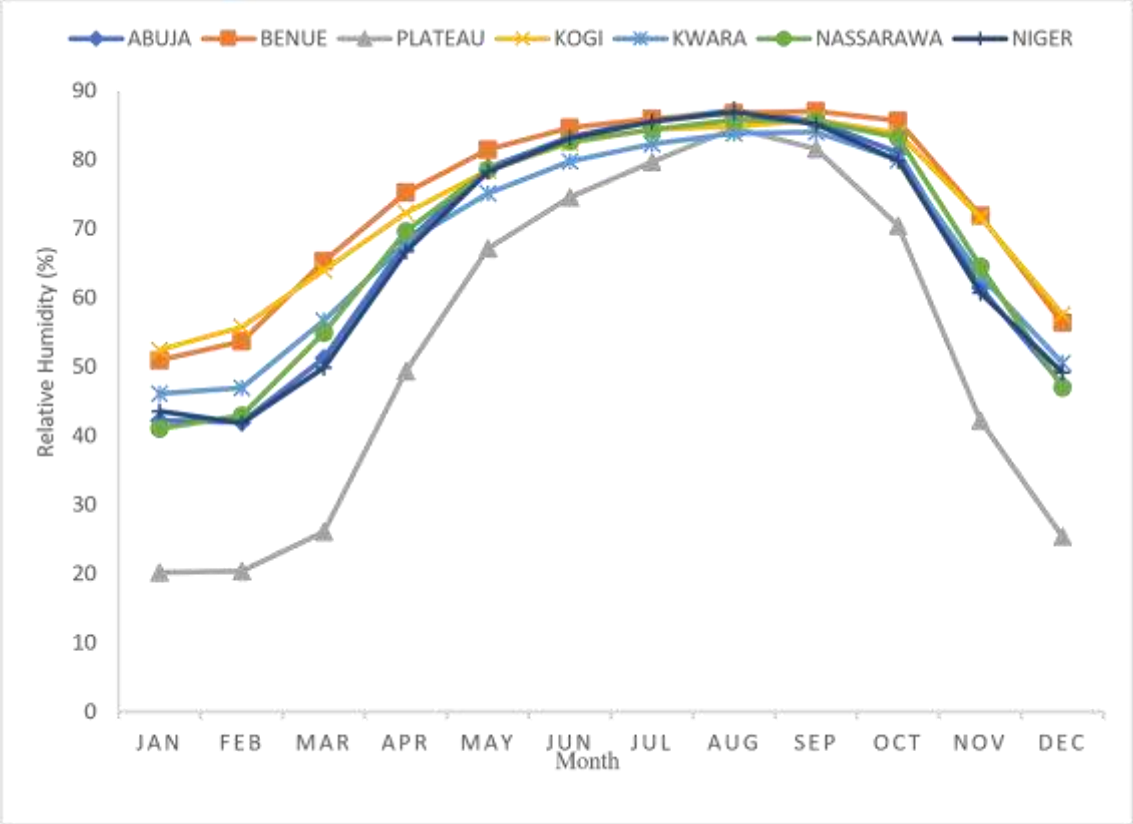

Figure 4.2: Monthly Distribution of RH

The monthly variation of RH on an average of 25 years is presented in Figure 4.2. From the Figure, it is observed that the seven stations recorded analogous weather activities.

This affirmation is deduced from the pattern of the graphs. As also observed from the Figure 4.2, there was a gradual increase of RH between the months of January and February. This was

followed by a steep increase from February through to August, when the highest RH values was recorded. The graphs show that RH fairly decreased between the months of August and October, and sharply decreased to attain another minimum value in the month of December.

RH is a major determinant factor for rainfall. It varies inversely with respect to solar insolation and would attain maximum values with increasing rainfall activities and minimum values with decreasing rainfall activities. On average, Benue records the highest RH as against Plateau with the least record of RH. Kogi state is closest to Benue and recorded the peak values of RH in the first and last quarters of the year.

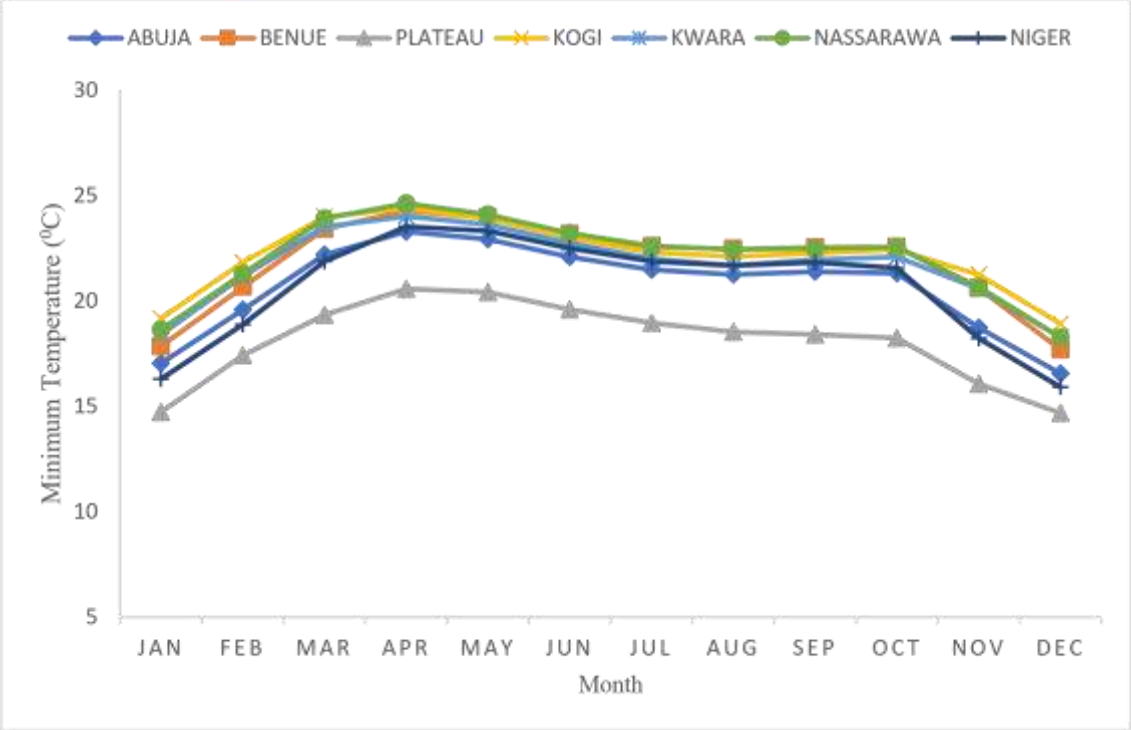

Figure 4.3: Monthly Distribution of Minimum Temperature

The variation T_{min} of with month is presented in Figure 4.3. The distribution of T_{min} shows the same trend for all the examined stations, which implies that there is uniformity in the distribution of atmospheric parameters within the NCSN. Nasarawa records the highest T_{min} between the months of April and mid-October, while Kogi records the peak T_{min} between the months of January and March, and mid-October to December. Plateau on the

other hand recorded the least T_{min} throughout the year, which is as a result of its high altitude above the surface.

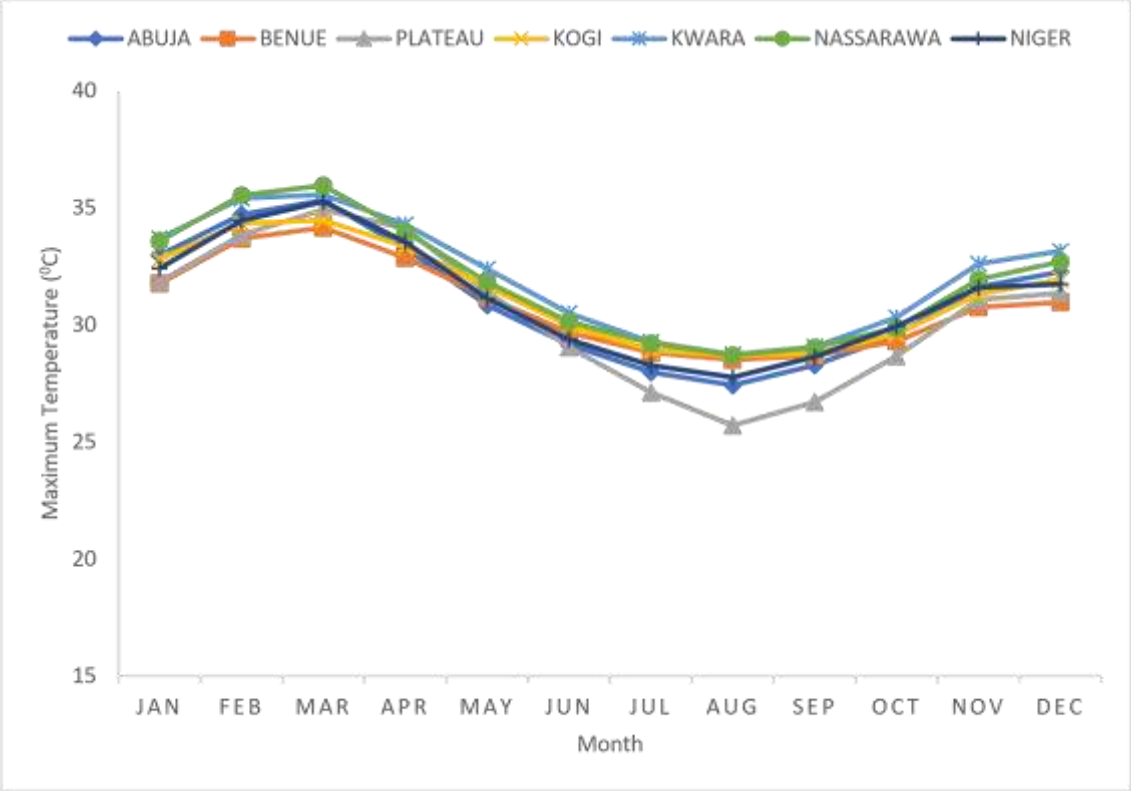

Figure 4.4: Monthly Distribution of Maximum Temperature

Figure 4.4 shows the monthly distribution of T_{max} for Abuja, Benue, Kogi, Kwara, Nasarawa, Niger and Plateau States. On average, Kwara has the maximum record for T_{max} which is closely followed by Nasarawa with a little margin. Also going by average, Plateau recorded the least T_{max} value. This attests to the fact that temperature at the tropospheric layer of the atmosphere increases with decreasing altitude.

Hence, from the distribution of the various measured atmospheric parameters over the months, it is therefore easy to observe that the stations under study displayed similar pattern of weather activities. As a result of this, a generalised model can be adopted for their mensuration.

4.3 Derivation of Model Equation

The model is developed from equations **(**3.2) and (3.4) which are respectively the output of the first layer and the second layer of the ANN network. Equations (4.1) and (4.3) are direct transformation of equations (3.2) and (3.4) correspondingly.

Definition of used parameters:

φ_1 is the activation function of the first layer,

φ_2 is the activation function of the second layer,

$b_j = b_1$ is the input bias that is associated with the j^{th} neuron of the first layer,

$b_k = b_2$ is the output bias that is associated with the k^{th} neuron of the second layer,

w_{ij} is the adjustable weight that connects the input layer to the hidden layer,

w_{jk} is the adjustable weight that connects the hidden layer to the output layer, (for which $1 \leq j \leq m$ and m = 49, that is, the total number of neurons in the hidden layer).

x_i is the set of input data to the ANN (for which $1 \leq i \leq n$ and n = 3).

y_1 is the output of the first layer,

y_2 is the output of the second layer,

LW $\equiv w_{jk}$ IW $\equiv w_{ij}$ z is a derivative of the product of the layered weights and the input biases, it is a 1 by 1 matrix.

p, q, r = constants derived from the layered and input weights
A, B, C = input vectors which represent RH (RH), temperature change (ΔT) and solar flux (I_{rr}) respectively.

$$y = \varphi_1\ (IW \cdot x + b_1) \tag{4.1}$$

the expansion of equation (4.1) gives:

$$y =\ (IW \cdot x\varphi_1 + b_1\varphi_1) \tag{4.2}$$

where φ_1 is a non-linear activation function and $f(x) \neq x$

$$y_2 = \varphi_2[LW\ (y) + b_2] \tag{4.3}$$

the expansion of equation (4.3) gives:

$$y_2 = \varphi_2[LW\ (IW \cdot x\varphi_1 + b_1\varphi_1) + b_2] \tag{4.4}$$

If φ_2 is a linear activation function, such that $f(x) = x = 1$ then

$$y_2 = [LW\ (IW \cdot x\varphi_1 + b_1\varphi_1) + b_2] \tag{4.5}$$

$$y_2 = [(LW \cdot IW \cdot x\varphi_1 + LW \cdot b_1\varphi_1) + b_2] \tag{4.6}$$

$$y_2 = [\varphi_1(LW \cdot IW \cdot x + LW \cdot b_1) + b_2] \tag{4.7}$$

$y_2 =\ [(\ LW \cdot IW \cdot x)\varphi_1 + (LW \cdot b_1\ )\varphi_1 + b_2]$ where IW is a [m × 3] matrix (4.8)

LW is a [1 × m] matrix

$$LW \cdot IW = [1 \times \text{m}]\ [\text{m} \times 3] \text{ matrix} = [1 \times 3] \text{ matrix} \tag{4.9}$$

hence, let

$$LW \cdot IW = [\text{p, q, r}] \text{ matrix} \tag{4.10}$$

$$(\ LW \cdot IW \cdot x)\varphi_1 = [p, q, r]\ \begin{bmatrix} A \\ B \\ C \end{bmatrix} \tag{4.11}$$

$$(LW \cdot IW \cdot x)\varphi_1 = \text{pA} + \text{qB} + \text{rC} \quad (4.12)$$

b_1 is a [m × 3] matrix

$$LW \cdot b_1 = [1 \times \text{m}]\ [\text{m} \times 1] \text{ matrix} = [1 \times 1] \text{ matrix} \quad (4.13)$$

$$(LW \cdot b_1)\varphi_1 = [z] \quad (4.14)$$

Hence, equation 4.8 is transformed to yied:

$$\boldsymbol{y_2} = \text{pA} + \text{qB} + \text{rC} + \text{z} + b_2 \quad (4.15)$$

Summarily, let

$$\alpha = \text{z} + b_2 \quad (4.16)$$

$$\boldsymbol{y_2} = \text{pA} + \text{qB} + \text{rC} + \alpha \quad (4.17)$$

Equation 4.17 is the proposed soft-computing model equation for the estimation of GSR, using relative humidity, temperature difference and solar flux as input parameters for A, B and C respectively. p, q, r, z, b_2 and α are constants which are given by the model.

4.3.1 Training state of the ANN

Some of the basic features of the trained network are presented in the neural network training tool shown in Figure 4.5, in which a training state of 0.98318 regression plot was attained as also represented in Figure 4.6.

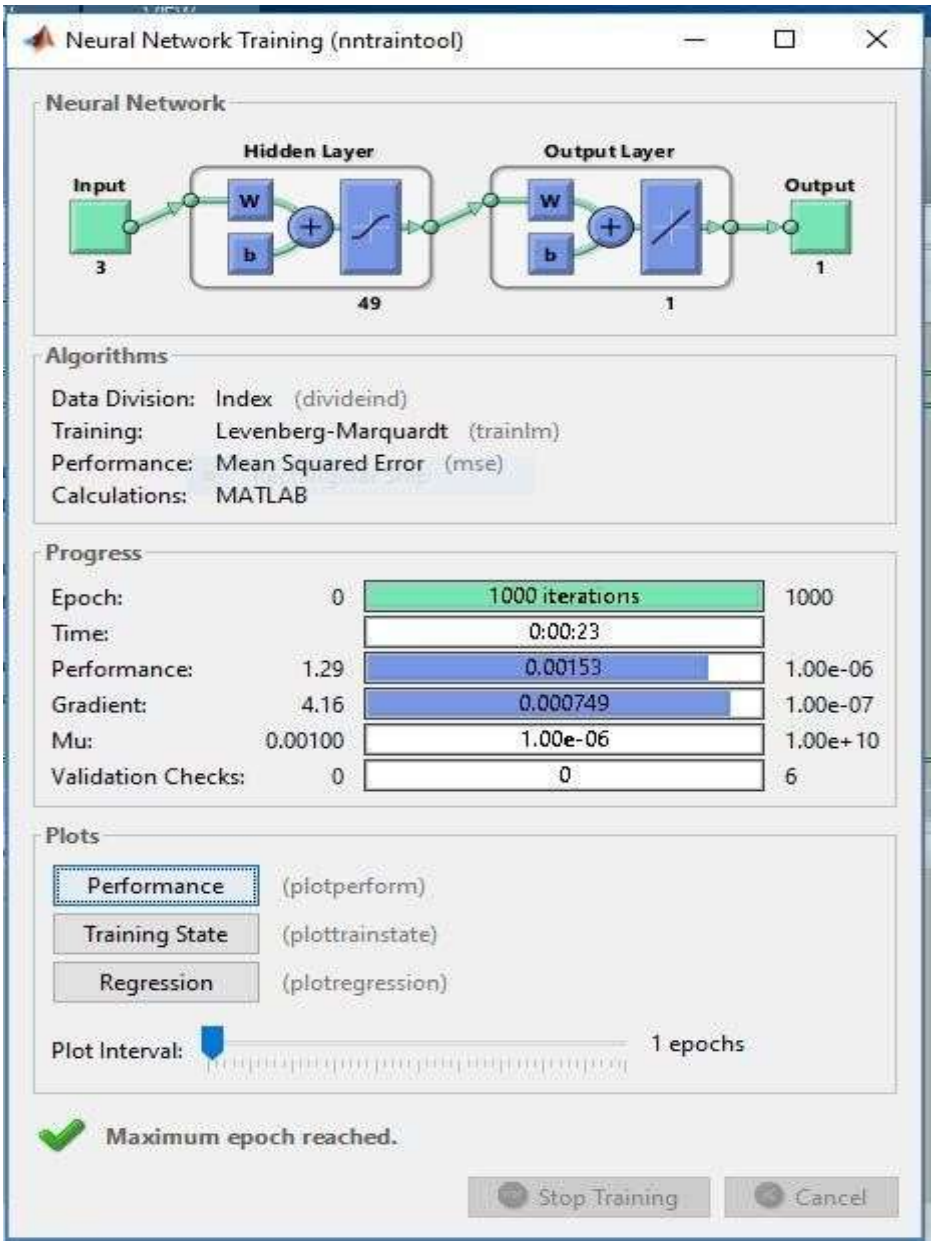

Figure 4.5: Neural Network Training Tool

Figure 4.5 presents some basic properties of the trained network which consists of 3 input vectors, 49 neurons in the hidden layer and 1 output that represents the estimated GSR.

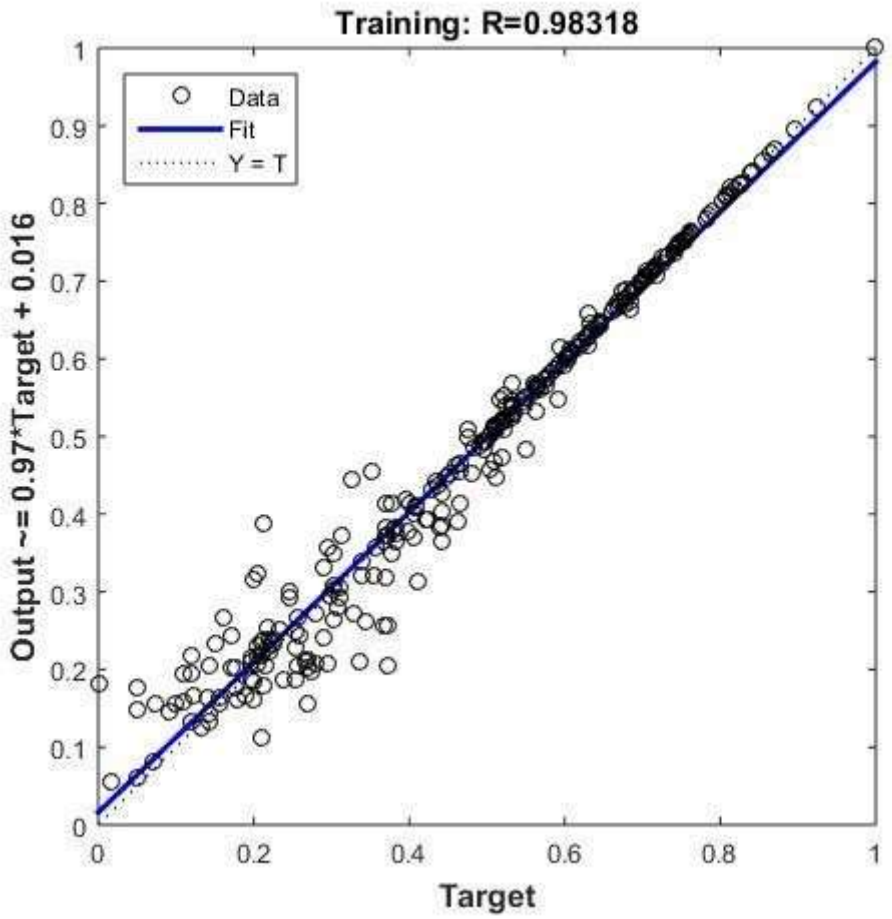

Figure 4.6: Regression Plot of the Training State

Figure 4.6 is a graph of the ANN output (estimated GSR) against the target value (measured / desired GSR). The figure describes the training state of the neural network, in which an approximate regression value of 0.98 was recorded as the optimum possible value for all the training trials. Regression of a particular function appreciates by its closeness to unity (1) and depreciates as it gets closer to zero (0). The regression of the magnitude attained by the network signifies a very good performance. In the same vein, Figure 4.7 portrays the regression of the testing state of the neural network.

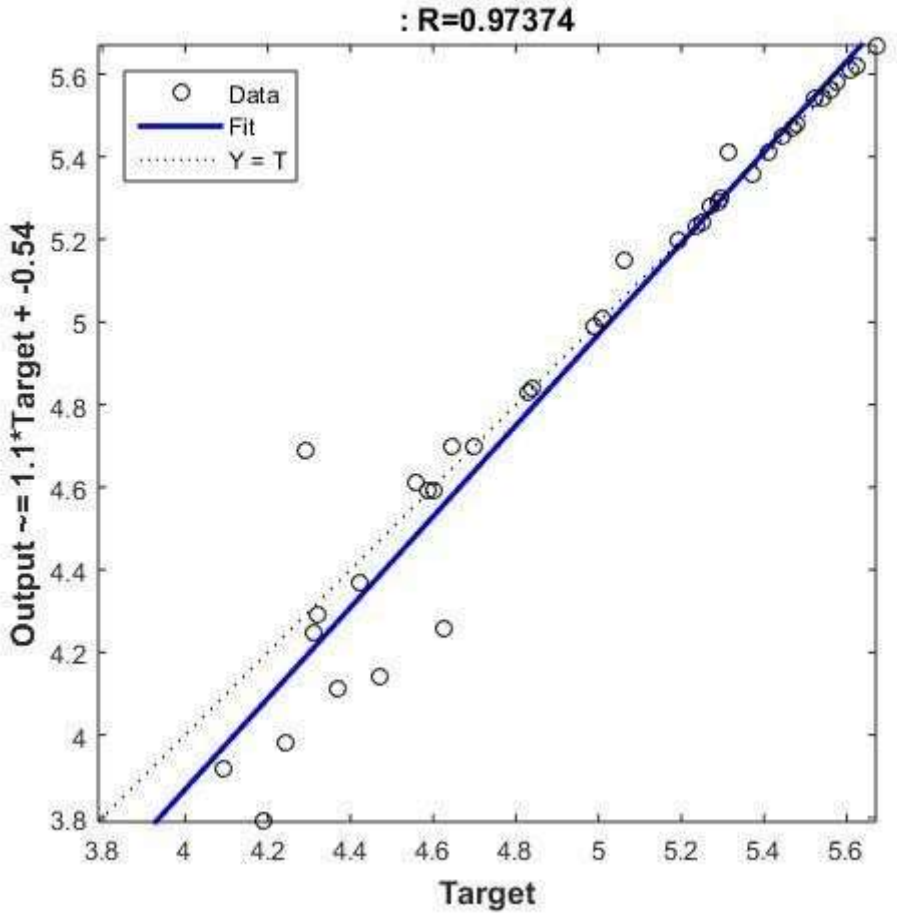

Figure 4.7: Regression Plot of the Testing State

From Figure 4.7, the regression value for the testing state of the network is approximately 0.974, which is an affirmation of the reliability and efficiency of the trained neural network. Other aspects of the performance of the network are presented in Table 1.

Table 4.1: Training Performance of the Neural Network

S/N	Determinant	Abbreviation	Value
1	Mean Square Error	MSE	0.0015
2	Sum Square Error	SSE	0.4775
3	Sum Absolute Error	SAE	6.3124
4	Mean Absolute Error	MAE	0.0210
5	Root Mean Square Error	RMSE	0.1211

For a better performance, low values of MSE, SSE, MAE and RMSE are desirable. In addition, the SAE is also a good result. It can therefore be inferred that models that are developed with minimum errors will have better performance compared to models that are developed with larger errors. In accordance with the above results from the trained neural network, the values of the constants are given as:

p = 0.0181

q = 0.1486

r = 0.0015 z = 0.3876

b_2 = -0.7606 α = -0.373

Therefore, from equation 4.17, the developed model takes the following forms:

$$H = p(RH) + q(\Delta T) + r(I_{rr}) + z + b_2 \quad (4.18)$$

$$H = p(RH) + q(\Delta T) + r(I_{rr}) + \alpha \quad (4.19)$$

where H is the GSR, RH is the relative humidity, ΔT is the change in temperature, I_{rr} is the solar flux, p, q, r, z, b_2 and α are constants.

4.4 Estimation of GSR

In this study, GSR was estimated using fourteen different models, out of which thirteen are existing empirical models, while the fourteenth is the newly developed SCM. The models are highlighted as follows:

Hargreaves and Samani Model (**Md 1**) using equation (2.66)

Bristow and Campbell Model (**Md 2**) using equation (2.67)

Annadale Model (**Md 3**) using equation (2.68)

Allen Model (**Md 4**) using equations (2.69 & 2.70)

Angstrom-Prescott Model (**Md 5**) using equation (2.79)

Glover and McCulloch Model (**Md 6**) using equation (2.80)

Ogleman Model (**Md 7**) using equation (2.81)

Newland Model (**Md 8**) using equation (2.82)

Swartman and Ogunlade Model (**Md 9**) using equation (2.84)

Abdalla Model (**Md 10**) using equation (2.83)

Okundamiya Model (**Md 11**) using equation (2.85)

Olomiyesan and Oyedum (**Md 12**) using equation (2.86)

Badescu Model (**Md 13**) using equation (2.73) and

SCM (**SCM**) using equation (4.19)

4.4.1 Common empirical parameters

Excluding the SCM, other models have some parameters in common, of which some are fixed while some others vary with time and locations. Some common constant / fairly constant parameters include the latitude of location (φ), Γ which is computed from the number of days in a year, the solar constant (I_{sc}), number of days in the year (n) and the sunshine hour (S). These parameters are presented in Table 4.2 for the seven locations.

Table 4.2: Common fixed parameters

	φ (degrees)	Γ	I_{sc} (Wm^{-2})	n	S (hours)
Abuja	9.07	1.033	1,367	365	12.00
Benue	7.73	1.033	1,367	365	12.00
Jos	9.89	1.033	1,367	365	12.00
Kogi	7.75	1.033	1,367	365	12.00
Kwara	8.5	1.033	1,367	365	12.00
Nasarawa	8.48	1.033	1,367	365	12.00
Niger	9.58	1.033	1,367	365	12.00

The first column in Table 4.2 represents the latitude of each location. The values of Γ are computed from the number of days in the year (n) using equation (2.61). I_{sc} represents the solar constant and S is the effective sunshine hour from sunrise to sunset. Results of the computation of the empirical parameters are presented in Tables 4.3 to 4.9 separately for Abuja, Benue, Kogi, Kwara, Nasarawa, Niger and Plateau States.

p

Table 4.3: Empirical arameters for Abuja

Month	dn	I_{rr}(Wm^{-2})	δ	ω_s	S_o	K	H_o (Wm^{-2})
JAN	17	1410.193	-21.2695	86.4373	11.5249	0.8322	8976.10
FEB	47	1398.134	-13.2892	87.8394	11.7119	0.9048	9759.58
MAR	75	1379.455	-2.4177	86.1353	11.4847	0.9744	10509.94
APR	105	1356.422	9.7832	91.5770	12.2103	1.0156	10954.45
MAY	135	1336.148	19.0306	93.1563	12.4208	1.0157	10955.61
JUN	162	1324.669	23.3543	93.9525	12.5270	1.0069	10860.99
JUL	198	1323.485	21.3537	93.5782	12.4770	1.0117	10912.26
AUG	228	1335.033	13.4550	92.1887	12.2918	1.0187	10988.23
SEP	258	1354.919	1.8147	90.2899	12.0387	0.9949	10730.85
OCT	288	1377.955	-9.9663	88.3926	11.7857	0.9301	10032.55
NOV	318	1398.134	-19.3780	86.7811	11.5708	0.850853	9177.58
DEC	344	1409.195	-23.3717	86.0440	11.4725	0.810389	8741.13

From Tables 4.3 to 4.9, dn denotes the day number of the year. I_{rr} represents the solar flux which is calculated using equation (2.61). δ is the solar declination angle which was calculated using equation (2.63). ω_s is the average sunrise hour-angle and was determined using equation (2.64). The sixth column in each tables represents the maximum hours of possible sunshine and was estimated using equation (2.65). The computation of K which is derived from the combination of latitude, solar declination and the mean sunrise hour angle was achieved using equation (2.62) and finally, H_o, the extra-terrestrial solar radiation was estimated using equation (2.60).

p

Table 4.4: Empirical arameters for Benue

Month	dn	I_{rr}(Wm^{-2})	δ	ω_s	S_o	K	H_o (Wm^{-2})
JAN	17	1410.193	-21.2695	86.9710	11.5961	0.8481	9147.39
FEB	47	1398.134	-13.2892	88.1628	11.7550	0.9163	9883.54
MAR	75	1379.455	-2.4177	89.6717	11.9562	0.9811	10582.83
APR	105	1356.422	9.7832	91.3408	12.1788	1.0127	10923.06
MAY	135	1336.148	19.0306	92.6824	12.3577	1.0067	10858.42
JUN	162	1324.669	23.3543	93.3595	12.4479	0.9951	10733.02
JUL	198	1323.485	21.3537	93.0438	12.4058	1.0011	10798.52
AUG	228	1335.033	13.4550	91.8624	12.2483	1.0134	10930.77
SEP	258	1354.919	1.81471	90.2464	12.0329	0.9972	10755.23
OCT	288	1377.955	-9.9662	88.6334	11.8178	0.9397	10135.56
NOV	318	1398.134	-19.3780	87.2637	11.6352	0.8657	9338.08
DEC	344	1409.195	-23.3717	86.6371	11.5516	0.8274	8924.09

p

Table 4.5: Empirical arameters for Kogi

Month	dn	I_{rr}(Wm^{-2})	δ	ω_s	S_o	K	H_o (Wm^{-2})
JAN	17	1410.193	-21.2695	86.9630	11.5951	0.8478	9144.86
FEB	47	1398.134	-13.2892	88.1582	11.7544	0.9161	9881.73
MAR	75	1379.455	-2.4177	89.6705	11.9561	0.9811	10582.08
APR	105	1356.422	9.7832	91.3466	12.1796	1.0127	10923.57
MAY	135	1336.148	19.0306	92.6882	12.3584	1.0068	10859.91
JUN	162	1324.669	23.3543	93.3709	12.4495	0.9952	10734.97
JUL	198	1323.485	21.3537	93.0496	12.4066	1.0013	10800.25
AUG	228	1335.033	13.4550	91.8682	12.2491	1.01345	10931.67
SEP	258	1354.919	1.8147	90.2464	12.0329	0.9971	10754.91
OCT	288	1377.955	-9.9663	88.6299	11.8173	0.9395	10134.06
NOV	318	1398.134	-19.3780	87.2562	11.6342	0.8655	9335.71
DEC	344	1409.195	-23.3717	86.6285	11.5505	0.8271	8921.38

p

Table 4.6: Empirical arameters for Kwara

Month	dn	I_{rr}(Wm^{-2})	δ	ω_s	S_0	K	H_0 (Wm^{-2})
JAN	17	1410.193	-21.2695	86.6646	11.5553	0.8390	9049.46
FEB	47	1398.134	-13.2892	87.9770	11.7303	0.9098	9812.93
MAR	75	1379.455	-2.4177	89.6385	11.9518	0.9784	10552.91
APR	105	1356.422	9.7832	91.4784	12.1971	1.0144	10941.81
MAY	135	1336.148	19.0306	92.9520	12.3936	1.0119	10914.91
JUN	162	1324.669	23.3543	93.6981	12.4931	1.0019	10807.15
JUL	198	1323.485	21.3537	93.3480	12.4464	1.0072	10864.50
AUG	228	1335.033	13.4550	92.0516	12.2736	1.0165	10964.48
SEP	258	1354.919	1.8147	90.2693	12.0359	0.9959	10741.94
OCT	288	1377.955	-9.9663	88.4952	11.7994	0.9342	10077.02
NOV	318	1398.134	-19.3780	86.9866	11.5982	0.8572	9246.38
DEC	344	1409.195	-23.3717	86.2967	11.5062	0.8176	8819.42

p

Table 4.7: Empirical arameters for Nasarawa

Month	dn	I_{rr}(Wm-2)	δ	ω_s	S_o	K	H_o (Wm-2)
JAN	17	1410.193	-21.2695	86.6727	11.5564	0.8392	9052.02
FEB	47	1398.134	-13.2892	87.9822	11.7310	0.9099	9814.78
MAR	75	1379.455	-2.4177	89.6390	11.9519	0.9784	10553.71
APR	105	1356.422	9.7832	91.4727	12.1964	1.0144	10941.35
MAY	135	1336.148	19.0306	92.9463	12.3928	1.0118	10913.47
JUN	162	1324.669	23.3543	93.6924	12.4923	1.0018	10805.24
JUL	198	1323.485	21.3537	93.3422	12.4456	1.0071	10862.80
AUG	228	1335.033	13.4550	92.0459	12.2728	1.0164	10963.63
SEP	258	1354.919	1.8147	90.2693	12.0359	0.9959	10742.31
OCT	288	1377.955	-9.9663	88.4987	11.7998	0.9344	10078.56
NOV	318	1398.134	-19.3780	86.9940	11.5992	0.8574	9248.78
DEC	344	1409.195	-23.3717	86.3059	11.5075	0.8179	8822.14

p

Table 4.8: Empirical arameters for Niger

Month	dn	I_{rr}(Wm^{-2})	δ	ω_s	S_o	K	H_o (Wm^{-2})
JAN	17	1410.193	-21.2695	86.2330	11.4977	0.8260	8909.84
FEB	47	1398.134	-13.2892	87.7156	11.6954	0.9003	9711.09
MAR	75	1379.455	-2.41773	89.5915	11.9455	0.9742	10507.75
APR	105	1356.422	9.7832	91.6675	12.2223	1.0166	10964.88
MAY	135	1336.148	19.0306	93.3365	12.4449	1.0190	10991.21
JUN	162	1324.669	23.3543	94.1806	12.5574	1.0113	10908.41
JUL	198	1323.485	21.3537	93.7843	12.5046	1.0156	10954.21
AUG	228	1335.033	13.4550	92.3154	12.3087	1.0206	11008.61
SEP	258	1354.919	1.8147	90.3037	12.0405	0.9939	10720.03
OCT	288	1377.955	-9.9663	88.3004	11.7734	0.9264	9991.95
NOV	318	1398.134	-19.3780	86.5970	11.5463	0.8451	9115.36
DEC	344	1409.195	-23.3717	85.8171	11.4423	0.8038	8670.51

p

Table 4.9: Empirical arameters for Plateau

Month	dn	I_{rr}(Wm^{-2})	δ	ω_s	S_o	K	H_o (Wm^{-2})
JAN	17	1410.193	-21.2695	86.1083	11.4811	0.8223	8869.28
FEB	47	1398.134	-13.2892	87.6399	11.6853	0.8975	9681.26
MAR	75	1379.455	-2.4177	89.5783	11.9438	0.9729	10494.09
APR	105	1356.422	9.7832	91.7249	12.2300	1.0171	10970.80
MAY	135	1336.148	19.0306	93.4456	12.4594	1.0210	11012.48
JUN	162	1324.669	23.3543	94.3185	12.5758	1.0140	10936.89
JUL	198	1323.485	21.3537	93.9106	12.5214	1.0179	10979.35
AUG	228	1335.033	13.4550	92.3899	12.3187	1.0218	11020.60
SEP	258	1354.919	1.8147	90.3151	12.0420	0.9932	10713.04
OCT	288	1377.955	-9.9663	88.2442	11.7659	0.9240	9966.90
NOV	318	1398.134	-19.3780	86.4844	11.5313	0.8416	9077.24
DEC	344	1409.195	-23.3717	85.6792	11.4239	0.7998	8627.32

p

4.4.2 Results of estimated GSR

The atmospheric data which comprises of RH, T_{min}, T_{max}, I_{rr} and C_{ld} of 25 years average were used to estimate GSR for Abuja, Benue, Kogi, Kwara, Nasarawa, Niger and Plateau using SCM, Hargreaves and Samani Model (Md 1), Bristow and Campbell Model (Md 2), Annadale Model (Md 3), Allen Model (Md 4), Angstrom-Prescott Model (Md 5), Glover and McCulloch Model (Md 6), Ogleman Model (Md 7), and Newland Model (Md 8), Swartman and Ogunlade Model (Md 9), Abdalla Model (Md 10), Okundamiya Model (Md 11), Olomiyesan and Oyedum (Md 12), and Badescu Model (Md 13). Results of the various models are shown in Figures 4.8 to 4.14.

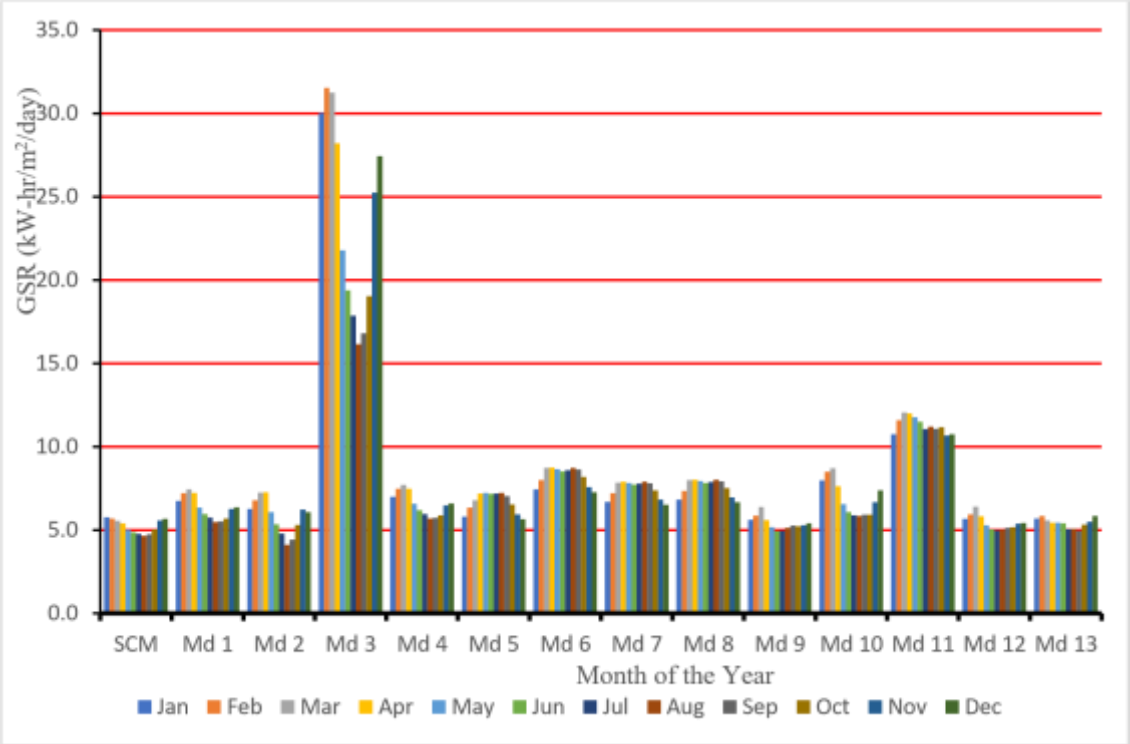

Figure 4.8: Estimated GSR for Abuja

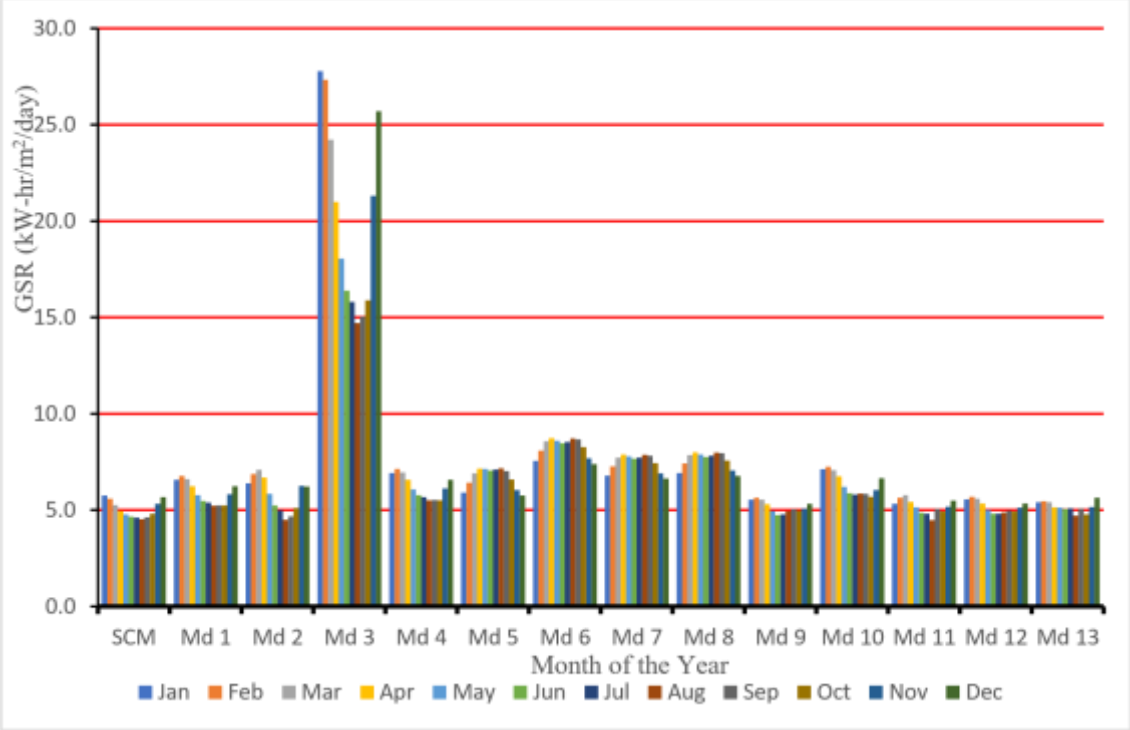

Figure 4.9: Estimated GSR for Benue

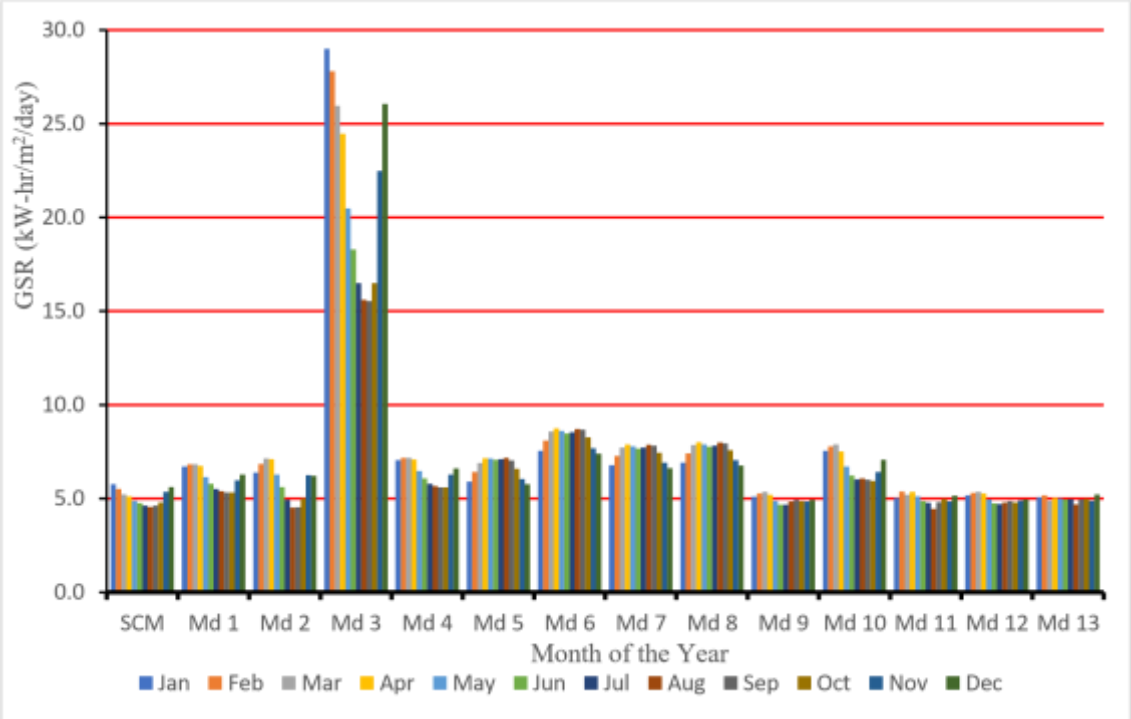

Figure 4.10: Estimated GSR for Kogi

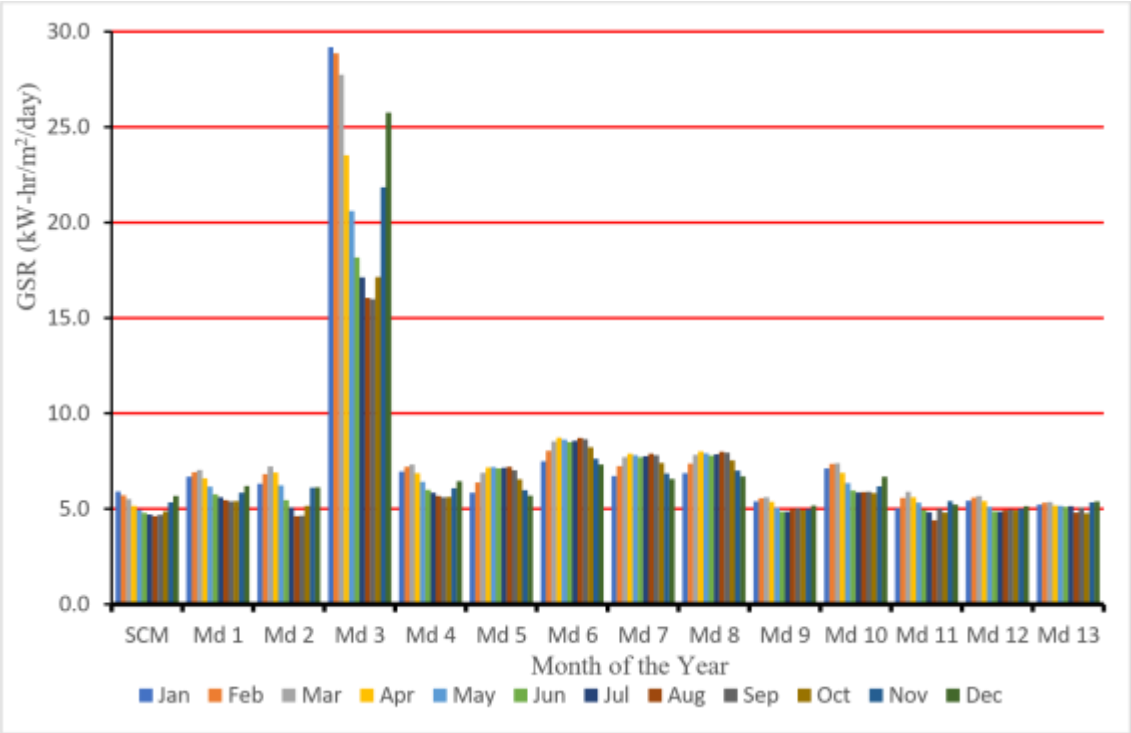

Figure 4.11: Estimated GSR for Kwara

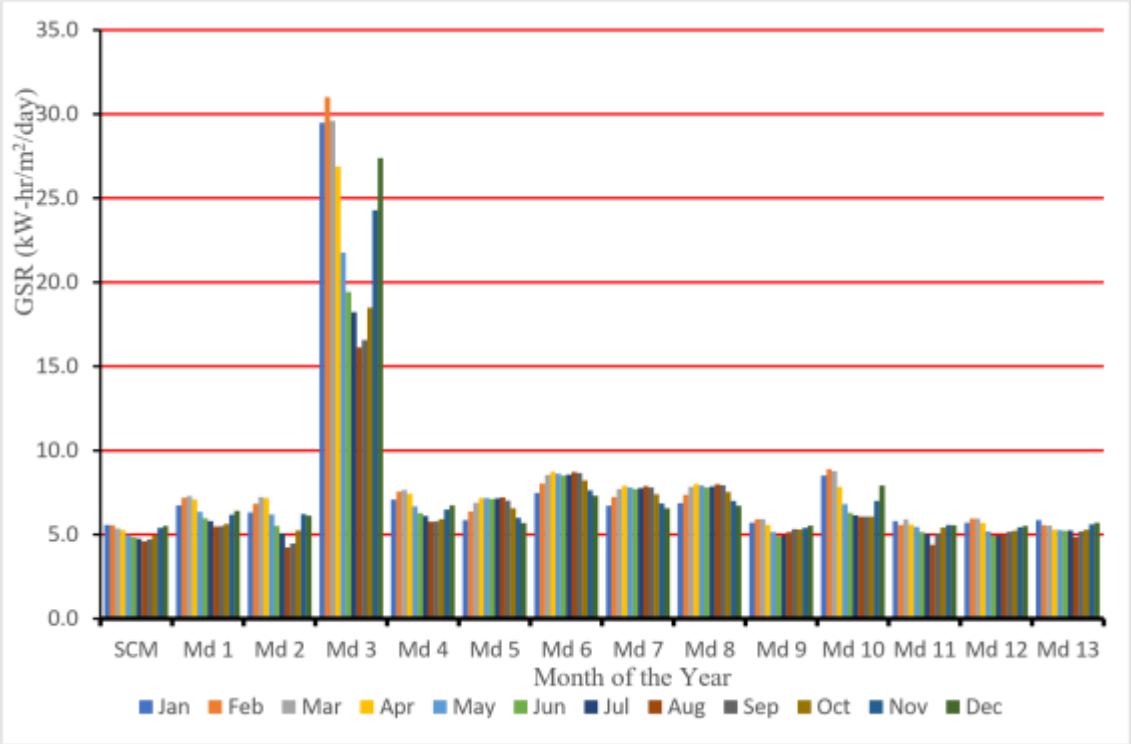

Figure 4.12: Estimated GSR for Nasarawa

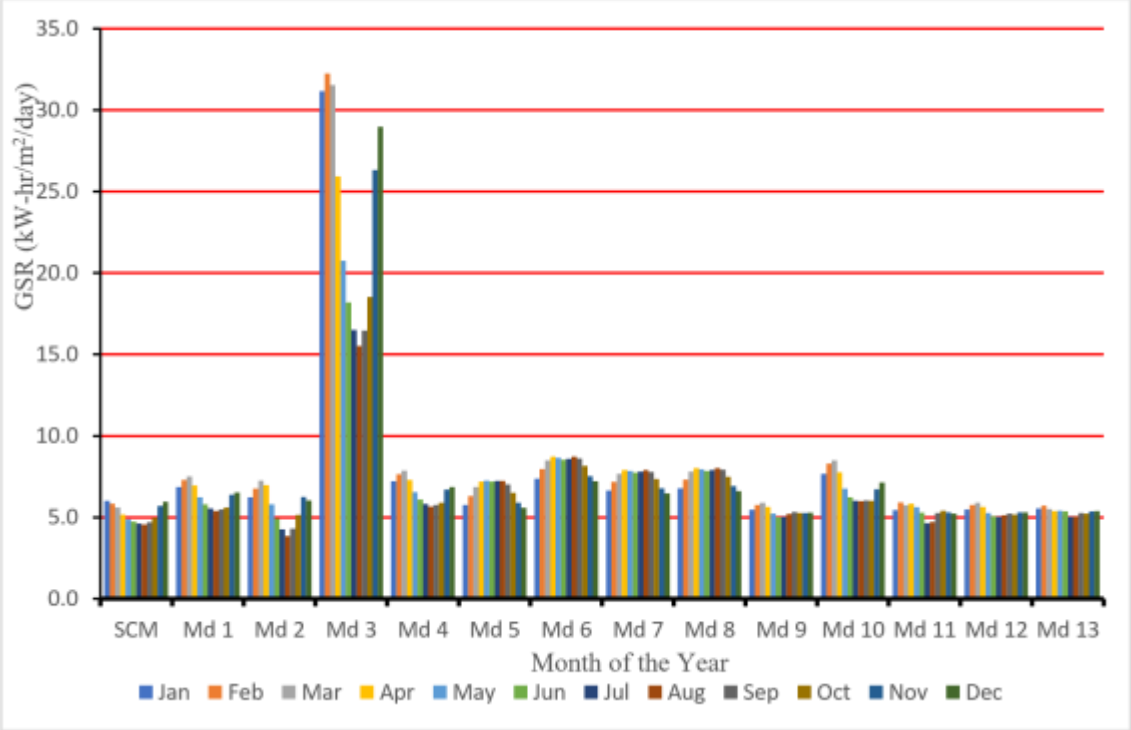

Figure 4.13: Estimated GSR for Niger

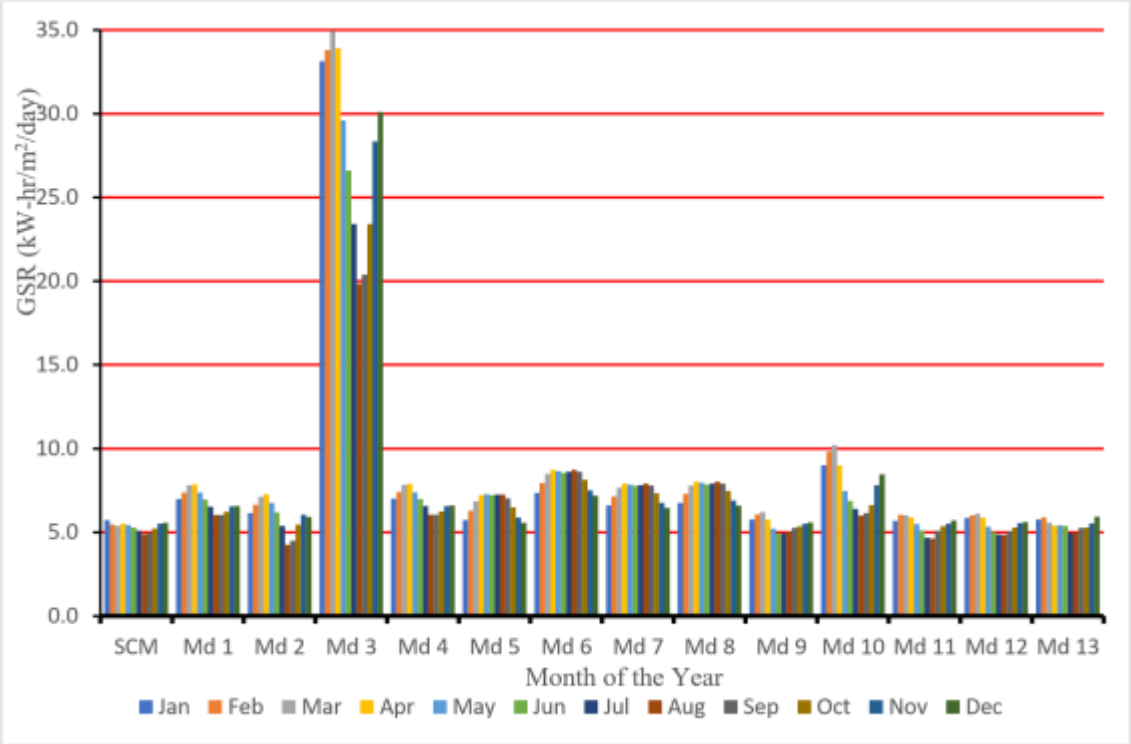

Figure 4.14: Estimated GSR for Plateau

Figures 4.8 to 4.14 present the estimated values of fourteen GSR models including the SCM. Each of the model is represented in series which corresponds to the twelve months of the year. The behaviours of the used models are identical with the distribution of their parameters. SCM and the temperature-based models (Md 1, Md 2, Md 3 and Md 4) showed similar trends. Also, Md 5, Md 6, Md 7 and Md 8 which are sunshine-based models exhibit similar behaviours. While Md 9, Md 10, Md 11 and Md 12 which are multiple parameter-based models and Md 13 which is a cloud-based model have shown similar behaviours. It is therefore worthy of note that the temperature-based, the multiple parameter-based and the cloud -based models showed much similarities in their patterns. However, Md 3 grossly over-predicted GSR for the seven locations considered.

4.5 Comparison of Estimated and Measured GSR

In this section, the Estimated GSR (EGSR) for the different models are compared with the Measured GSR (MGSR) for all the stations under consideration. This comparison is of importance as it determines the margin of the EGSR from the MGSR, as it further

helps to know the model that under-predicted, over-predicted or best-predicted the GSR. However, it is note-worthy that some models performed better in certain locations and seasons of the year compared to other models. The monthly variation of the EGSR and the MGSR is presented in Figures 4.15 to 4.21 respectively for all the examined stations.

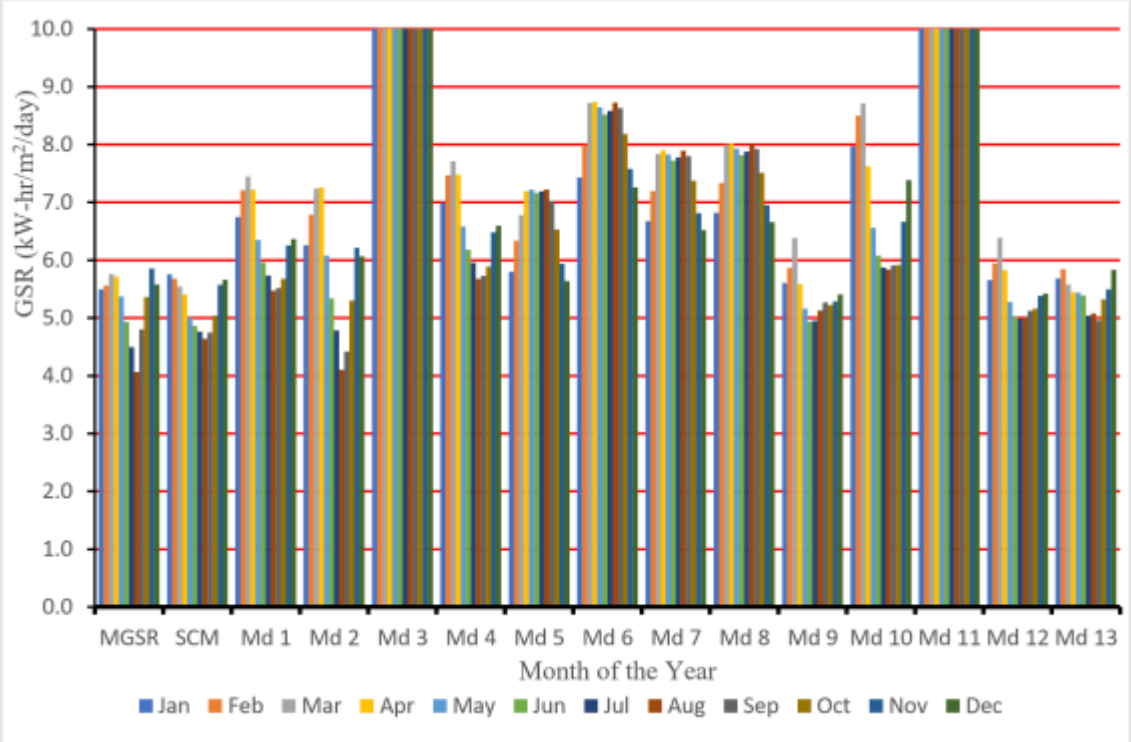

Figure 4.15: Comparison of estimated and measured GSR for Abuja

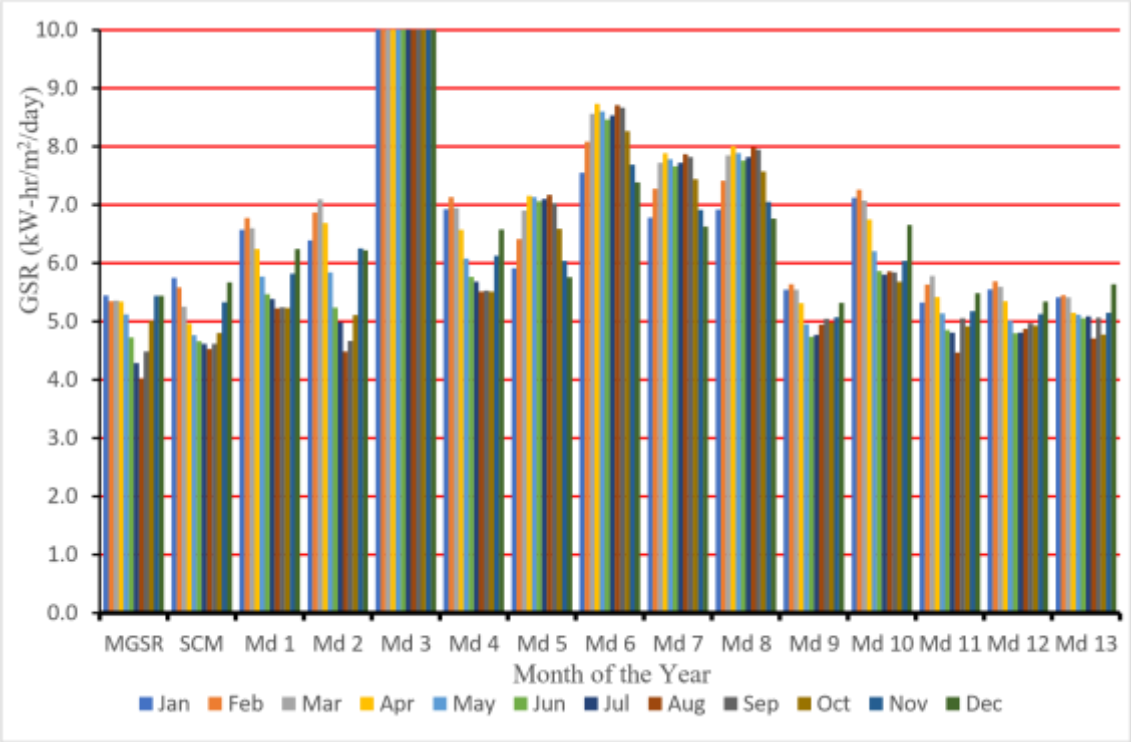

Figure 4.16: Comparison of estimated and measured GSR for Benue

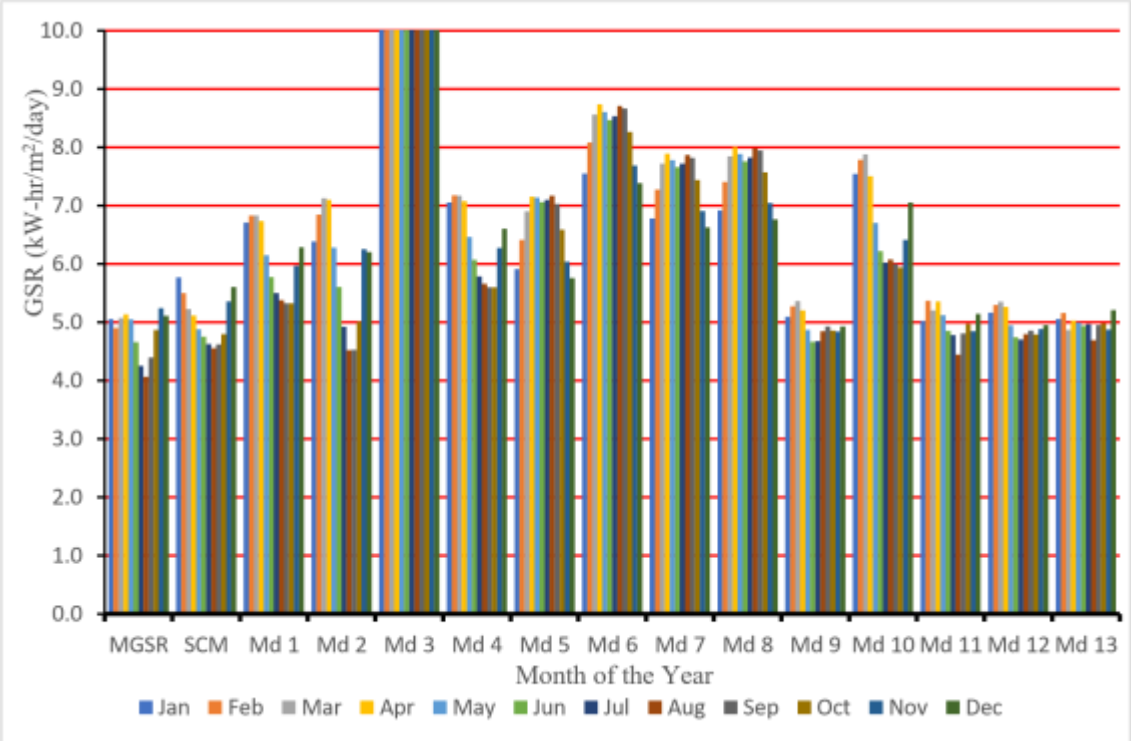

Figure 4.17: Comparison of estimated and measured GSR for Kogi

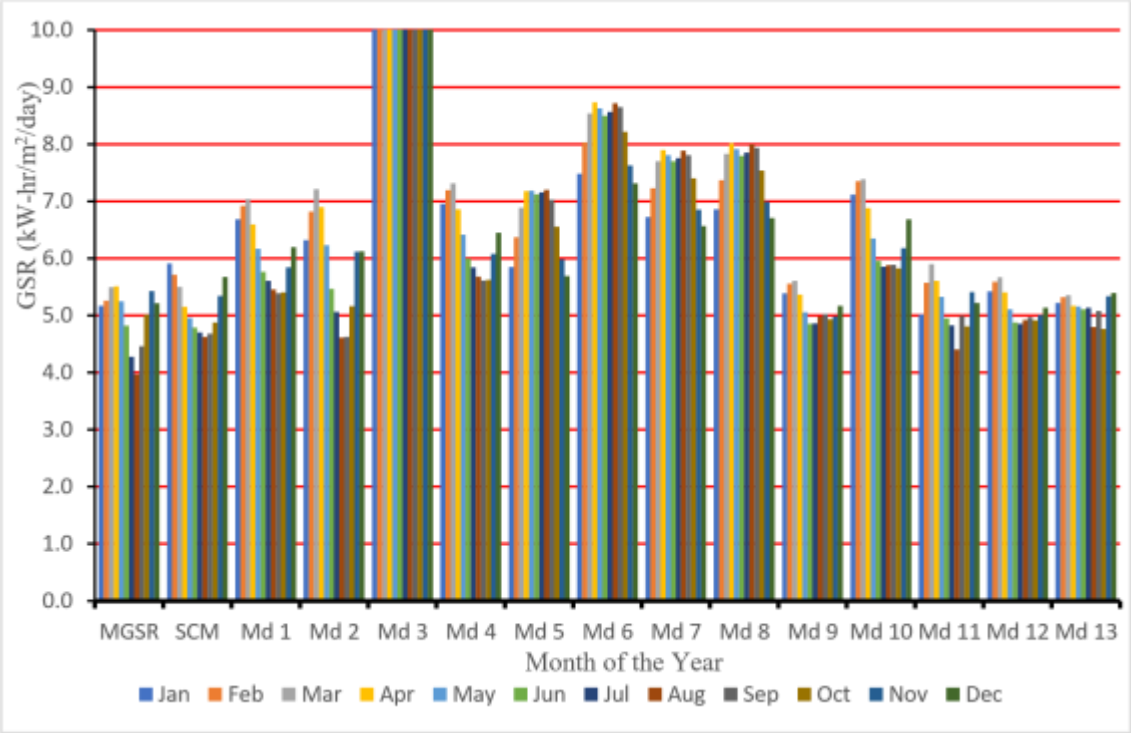

Figure 4.18: Comparison of estimated and measured GSR for Kwara

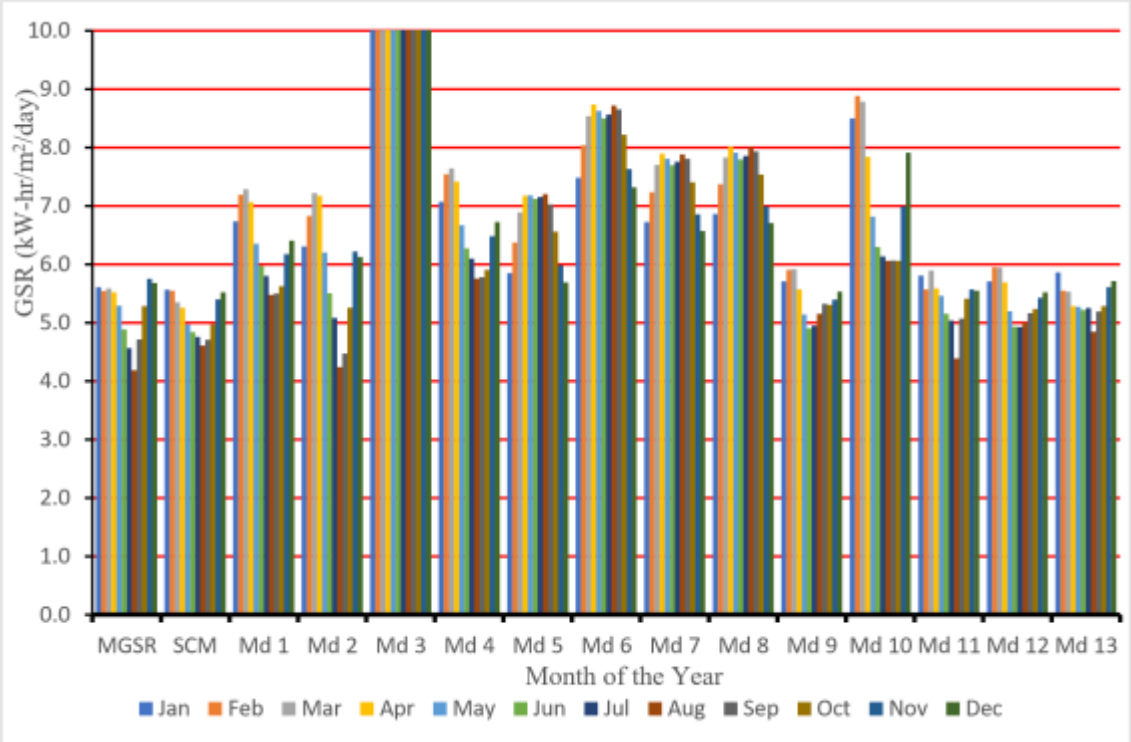

Figure 4.19: Comparison of estimated and measured GSR for Nasarawa

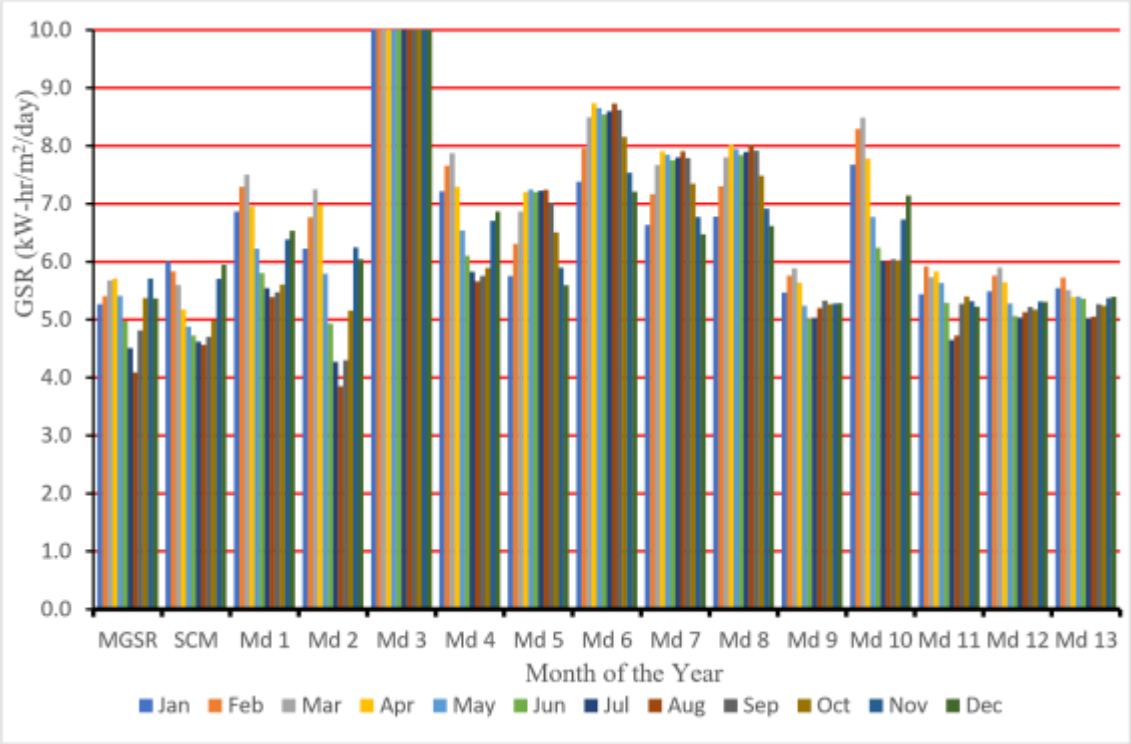

Figure 4.20: Comparison of estimated and measured GSR for Niger

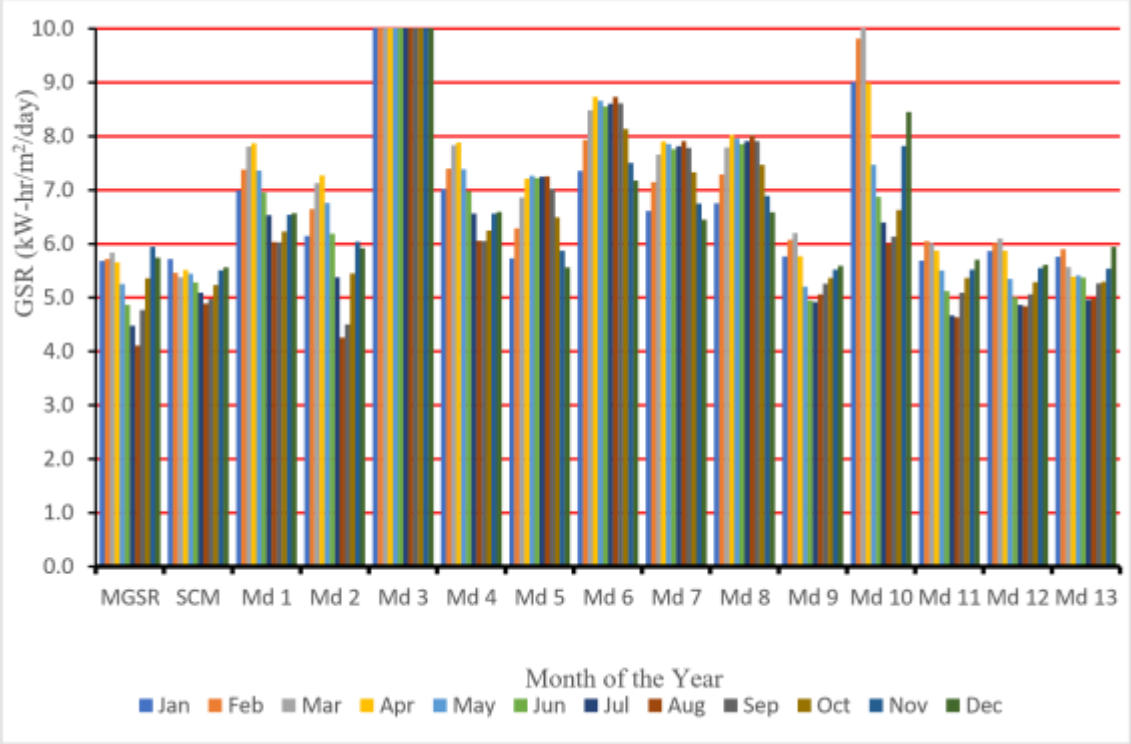

Figure 4.21: Comparison of estimated and measured GSR for Plateau

It could be deduced from Figure 4.15 that SCM, the temperature-based, the cloud-based and the multiple parameter-based models showed similar graphical patterns when

compared with the MSGR. In addition, the values of SCM, Md 9, Md 12 and Md 13 are closest to the MGSR over Abuja, but Md 3 and Md 11 highly over-estimated GSR. Figure 4.16 compares EGSR and MGSR over Benue. The graphical patterns showed similar behaviours for the SCM, the temperature-based model, the multiple parameterbased models and the MGSR. Md 1, Md 2, Md 4, Md 5 and Md 10 showed some notable deviations from the MGSR, while Md 6, Md 7 and Md 8 showed more deviations which is highest for Md 3.

Figure 4.17 compares the results of EGSR and MGSR over Kogi. As shown in the Figure, there are little records of under-estimation which are of negligible figures. But Md 3 grossly over-estimated GSR, followed by Md 6. However, Md1, Md 2, Md 4, Md 5, Md 7, Md 8 and Md 10 showed little deviation from the MGSR, while SCM, Md 9, Md 11, Md 12 and Md 13 recorded the closest values to that of the MGSR.

The comparison between MGSR and EGSR are presented in Figure 4.18 for Kwara. SCM, Md 1, Md 2, Md 3, Md 4, Md 9, Md 10 and Md 11 behaved in much similar ways when compared with the MGSR. It is also good to note that the under-estimation recorded for models are not significant, but a gross over-estimation was recorded for Md 3. In addition, the results of Md 1, Md 2, Md 4, Md 5 and Md 10 recorded a slight deviation from the MGSR, while Md 6, Md 7 and Md 8 recorded more significant deviation from the MGSR.

Figures 4.19 presents the MGSR and EGSR data over Nasarawa. As depicted from the figure, the values of SCM are closest to those of the MGSR. Md 9, Md 11, Md 12 and Md 13 also displayed credible performances as they recorded little deviations from the MGSR values, while Md 1, Md 2, Md 4, Md 5, Md 6, Md 7, Md 8 and Md 10 deviated more from the MGSR which is highest for Md 3. It is also pertinent to note that the underestimation recorded for models are of negligible values.

As shown in Figure 4.20, SCM, Md 1, Md 2, Md 3, Md 4, Md 9, Md 10, Md 11, Md 12 and Md13 showed similar trends when compared with the MGSR. The values recorded for SCM, Md 9, Md 11, Md 12 and Md 13 were closest to the MGSR. Tolerable deviations were also recorded for Md 1, Md 2, Md 4 and Md 5 while Md 6, Md 7, Md 8 and Md 10 recorded values which deviate more from the MGSR. Nevertheless, Md 3 grossly overestimated GSR over Niger.

Figure 4.21 presents the values of MSGR and EGSR for Plateau. The models that are closest to the MGSR include SCM, Md 9, Md 11, Md 12 and Md 13. In addition, the values of Md 1, Md 2, Md 4, Md 5, Md 7 and Md 8 partly deviated from the MGSR values, which is high for Md 6, higher for Md 10 and highest for Md 3. However, it is worthy of note that the level of under-estimations recorded for the models are insignificant.

4.5.1 Evaluation of the models

Apart from the direct comparison made from the various graphical plots, a better way to evaluate the models is to check their performance using a standardised approach. Some statistical metrics which are employed by researchers are used in this study to assess and validate the performances of GSR models. These metrics include Mean Absolute Error (MAE), Mean Bias Error (MBE), Mean Squared Error (MSE), Root Mean Squared Error (RMSE) and the Correlation Coefficient (R). Results of the evaluations are presented in Tables 4.10 to 4.16 for each of the states respectively.

Table 4.10: Evaluation of m odels for Abuja

Sn	Model	MAE	MBE	MSE	RMSE	R
1	Md 1	1.080	-1.080	1.359	1.166	0.753
2	Md 2	0.645	-0.571	0.660	0.812	0.891
3	Md 3	18.475	-18.475	368.24	19.19	0.813
4	Md 4	1.313	-1.313	1.928	1.388	0.752
5	Md 5	1.421	-1.421	2.989	1.729	-0.571
6	Md 6	3.001	-3.001	9.833	3.136	-0.468
7	Md 7	2.196	-2.196	5.607	2.368	-0.486
8	Md 8	2.322	-2.322	6.152	2.48	-0.468
9	Md 9	0.353	-0.151	0.206	0.454	0.609
10	Md 10	1.671	-1.671	3.364	1.834	0.703
11	Md 11	6.045	-6.045	36.957	6.079	0.164
12	Md 12	0.337	-0.185	0.176	0.420	0.710
13	Md 13	0.318	-0.176	0.165	0.406	0.764
14	SCM	0.242	0.026	0.079	0.281	0.856

Table 4.10 presents the results of the statistical evaluation of GSR models over Abuja. Values of MAE, MBE, MSE and RMSE that are closest to zero are desirable, while values that are closest to unity (1) are desirable for R. For the MAE, SCM is the best followed by Md 13, Md 12, Md 9 and Md 5 in that order. For the MBE, SCM is the best model because it records a value that is closest to 0, followed by Md9, Md 13, Md 12 and Md 2. Considering MSE and RMSE, SCM performed best followed by Md 13, Md 12, Md 9 and Md 2 which is ranked fifth. Also, for R, Md 2 is ranked first which is preceded by

m

SCM, Md 3, Md 13 and Md 11.

Table 4.11: Evaluation of odels for Benue

Sn	Model	MAE	MBE	MSE	RMSE	R
1	Md 1	0.881	-0.881	0.896	0.947	0.789
2	Md 2	0.819	-0.819	0.904	0.951	0.887
3	Md 3	15.266	-15.266	252.096	15.878	0.817
4	Md 4	1.195	-1.195	1.558	1.248	0.788
5	Md 5	1.688	-1.688	3.650	1.910	-0.645
6	Md 6	3.270	-3.270	11.401	3.377	-0.603
7	Md 7	2.456	-2.456	6.705	2.589	-0.611
8	Md 8	2.579	-2.579	7.308	2.703	-0.604
9	Md 9	0.273	-0.153	0.142	0.377	0.702
10	Md 10	1.344	-1.344	1.972	1.404	0.707
11	Md 11	0.249	-0.170	0.098	0.313	0.842
12	Md 12	0.269	-0.168	0.129	0.359	0.760
13	Md 13	0.294	-0.167	0.150	0.388	0.705
14	SCM	0.247	-0.043	0.077	0.277	0.825

Table 4.11 presents the performances of GSR models over Benue. SCM came first for MAE, MBE, MSE and RMSE but, came third in R. Md 11 is ranked second for MAE, MSE, RMSE and R but, ranked fifth for MBE. Md 2 is ranked third for MAE, MSE and RMSE and fourth in MBE. Furthermore, Md 9 emerged as fourth position for MAE, second for MBE, fourth for MSE and RMSE. In addition, Md 13 is ranked fifth for MAE, MSE and RMSE, and ranked third for MBE. For other performances of R, Md 1 is ranked fifth, Md 3 fourth while Md 2 is ranked first.

m

Table 4.12: Evaluation of odels for Kogi

Sn	Model	MAE	MBE	MSE	RMSE	R
1	Md 1	1.251	-1.251	1.737	1.318	0.705
2	Md 2	1.082	-1.082	1.580	1.257	0.832
3	Md 3	16.735	-16.735	300.728	17.342	0.745
4	Md 4	1.561	-1.561	2.626	1.620	0.704
5	Md 5	1.871	-1.871	4.103	2.026	-0.555
6	Md 6	3.453	-3.453	12.449	3.528	-0.524
7	Md 7	2.640	-2.640	7.461	2.731	-0.530
8	Md 8	2.763	-2.763	8.111	2.848	-0.524
9	Md 9	0.274	-0.144	0.127	0.357	0.480
10	Md 10	1.945	-1.945	4.105	2.026	0.630
11	Md 11	0.246	-0.176	0.090	0.300	0.754
12	Md 12	0.278	-0.162	0.116	0.340	0.585
13	Md 13	0.281	-0.159	0.130	0.361	0.502
14	SCM	0.294	-0.25	0.136	0.369	0.757

From Table 4.12 and for MAE, it is evident that Md 11, Md 9, Md 12, Md 13 and SCM recorded first, second, third, fourth and fifth positions respectively. For MBE, Md 9, Md 13, Md 12, Md 11 and SCM recorded first, second, third, fourth and fifth positions respectively. It is also shown from the table that Md 11is ranked first for MSE and RMSE, which is followed by Md 12, Md 9, Md 13 and SCM in that order. For the R over Kogi,

m

the first, second, third, fourth and fifth positions respectively are Md 2, SCM, Md 11, Md 3 and Md 1.

Table 4.13: Evaluation of odels for Kwara

Sn	Model	MAE	MBE	MSE	RMSE	R
1	Md 1	1.100	-1.100	1.373	1.172	0.721
2	Md 2	0.899	-0.899	1.034	1.017	0.888
3	Md 3	16.843	-16.843	304.136	17.439	0.727
4	Md 4	1.347	-1.347	1.988	1.410	0.720
5	Md 5	1.694	-1.694	3.638	1.907	-0.439
6	Md 6	3.262	-3.262	11.303	3.362	-0.401
7	Md 7	2.455	-2.455	6.658	2.580	-0.407
8	Md 8	2.578	-2.578	7.258	2.694	-0.401
9	Md 9	0.310	-0.159	0.174	0.417	0.607
10	Md 10	1.457	-1.457	2.308	1.519	0.690
11	Md 11	0.243	-0.181	0.095	0.308	0.856
12	Md 12	0.307	-0.166	0.160	0.400	0.662
13	Md 13	0.316	-0.164	0.179	0.423	0.636
14	SCM	0.323	-0.171	0.156	0.395	0.704

Table 4.13 presents the evaluation report of GSR models over Kwara. From the Table, MAE report showed that the first, second, third, fourth and fifth positions are Md 11, Md 12, Md 9, Md 13 and SCM respectively. While MBE ranked Md 9 as the best, which is preceded by Md 13, Md 12, SCM and Md 11. Still on the note, Md 11, SCM, Md 12, Md

m

9 and Md 13 are the five best models in terms of MSE and RMSE. Nevertheless, Md 2, is ranked first, Md 11 is second, Md 3 is third, Md 1 is fourth and Md 4 is fifth for R over Kwara.

Table 4.14: Evaluation of odels for Nasarawa

Sn	Model	MAE	MBE	MSE	RMSE	R
1	Md 1	1.081	-1.081	1.351	1.162	0.733
2	Md 2	0.714	-0.669	0.793	0.890	0.850
3	Md 3	18.053	-18.053	349.440	18.693	0.838
4	Md 4	1.397	-1.397	2.149	1.466	0.733
5	Md 5	1.466	-1.466	3.049	1.746	-0.675
6	Md 6	3.034	-3.034	9.988	3.160	-0.637
7	Md 7	2.227	-2.227	5.704	2.388	-0.644
8	Md 8	2.350	-2.350	6.245	2.499	-0.637
9	Md 9	0.292	-0.183	0.156	0.395	0.696
10	Md 10	1.979	-1.979	4.533	2.129	0.744
11	Md 11	0.209	-0.158	0.058	0.242	0.936
12	Md 12	0.277	-0.174	0.123	0.350	0.784
13	Md 13	0.241	-0.168	0.116	0.341	0.852
14	SCM	0.195	0.092	0.058	0.240	0.919

As reported in Table 4.14, SCM, Md 11, Md 13, Md 12 and Md 9 are the best five models in terms of MAE. The best five models in terms of MBE are SCM, Md 11, Md 13, Md

m

12 and Md 9. For the MSE and RMSE, the best five models include Md 11, SCM, Md 13, Md 12 and Md 9. While Md 11, SCM, Md 13, Md 2 and Md 3 are ranked first, second, third, fourth and fifth positions respectively in terms of R over Nasarawa.

Table 4.15: Evaluation of odels for Niger

Sn	Model	MAE	MBE	MSE	RMSE	R
1	Md 1	1.105	-1.105	1.449	1.204	0.743
2	Md 2	0.667	-0.459	0.681	0.825	0.898
3	Md 3	18.32	-18.320	370.387	19.245	0.716
4	Md 4	1.422	-1.422	2.275	1.508	0.742
5	Md 5	1.480	-1.480	3.050	1.746	-0.431
6	Md 6	3.024	-3.024	9.869	3.141	-0.388
7	Md 7	2.229	-2.229	5.654	2.378	-0.395
8	Md 8	2.351	-2.351	6.192	2.488	-0.388
9	Md 9	0.318	-0.173	0.185	0.430	0.581
10	Md 10	1.739	-1.739	3.475	1.864	0.664
11	Md 11	0.266	-0.176	0.106	0.325	0.826
12	Md 12	0.309	-0.166	0.164	0.405	0.651
13	Md 13	0.326	-0.164	0.165	0.407	0.717
14	SCM	0.353	-0.035	0.175	0.419	0.665

Table 4.15 shows the statistical evaluation of GSR models over Niger. For the MAE, Md

m

11 is selected as the best, having recorded a value that is closest to 0. This is followed by Md 12, Md 9, Md 13 and SCM. For the MBE, SCM is selected as the best model which is preceded by Md 13, Md 12, Md 9 and Md 11. Also, the best five models in terms of MSE and RMSE include Md 11, Md 12, Md 13, SCM and Md 9. For the R, Md 2, Md 11, Md 1, Md 4 and Md 13 have shown commendable results.

Table 4.16: Evaluation of odels for Plateau

Sn	Model	MAE	MBE	MSE	RMSE	R
1	Md 1	1.574	-1.574	2.780	1.667	0.570
2	Md 2	0.734	-0.689	0.860	0.927	0.739
3	Md 3	22.845	-22.845	543.901	23.322	0.827
4	Md 4	1.597	-1.597	2.854	1.689	0.569
5	Md 5	1.427	-1.386	3.115	1.765	-0.665
6	Md 6	2.922	-2.922	9.561	3.092	-0.624
7	Md 7	2.131	-2.131	5.512	2.348	-0.631
8	Md 8	2.253	-2.253	6.019	2.453	-0.624
9	Md 9	0.291	-0.189	0.152	0.390	0.809
10	Md 10	2.532	-2.532	7.386	2.718	0.821
11	Md 11	0.228	-0.151	0.076	0.275	0.924
12	Md 12	0.266	-0.168	0.101	0.317	0.893
13	Md 13	0.333	-0.165	0.160	0.399	0.825
14	SCM	0.320	-0.053	0.148	0.385	0.871

m

Table 4.16 presents the result of statistical evaluation of GSR models over Plateau. From the Table, it is evident that Md 11, Md 12, Md 9, SCM and Md 13 are of better performances than the other models in terms of MAE. In terms of MBE, SCM, Md 11, Md 13, Md 12 and Md 9 showed brilliant performances. Nonetheless, Md 11, Md 12, SCM, Md 9 and Md 13 have shown remarkable results in terms of MSE and RMSE. For the R, Md 11 is ranked first, followed by Md 12, SCM, Md 3 and Md 13 which is ranked fifth.

4.6.0 Preamble

In this study, standalone off-grid solar power system is designed for a small-scale computer-based business enterprise which is located at Bosso local government area of Niger State for a lifetime of 25 years. The business enterprise has four employees and their activities include but not limited to the following; typesetting, computer training, photostats, printing, book binding, clerical works and different forms of online activities. Business activities begins by 8:00 AM and ends by 6:00 PM, making a total working period of 10 hours. Being a standard business enterprise, a load profile was developed based on its activities for Niger and will be replicated hypothetically for other States in the course of this study. It is also noteworthy that the load profile is not limited to a computer-based enterprise, but can also service a load demand that is within the range of the designed power system.

Table 4.17 and Figure 4.22 present the load description and the daily load profile respectively. The load profile is designed such that some appliances are used intermittently, while some other appliances are used continuously and not necessarily that all the appliances are put to use simultaneously.

Table 4.17: Load description Sn Load Type Quantity

			Rated Power (W)	Total Power (W)	Time of Use (hr)	Energy (kWh/d)
1	Television Set	1	90.00	90.00	9.50	0.86
	Laptop **2** Computer	3	50.00	150.00	7.00	1.05
	Desktop **3** Computer	6	150.00	900.00	8.00	7.20
4	Printer	2	50.00	100.00	3.00	0.30
	Photocopy **5** Machine	2	700.00	1400.00	2.00	2.80
6	Lightening	4	10.00	40.00	10.00	0.40
7	Fan	4	24.00	96.00	10.00	0.96
8	Phone Charging & Others		30.00	30.00	4.00	0.12
	Total			**2806.00**		**13.69**

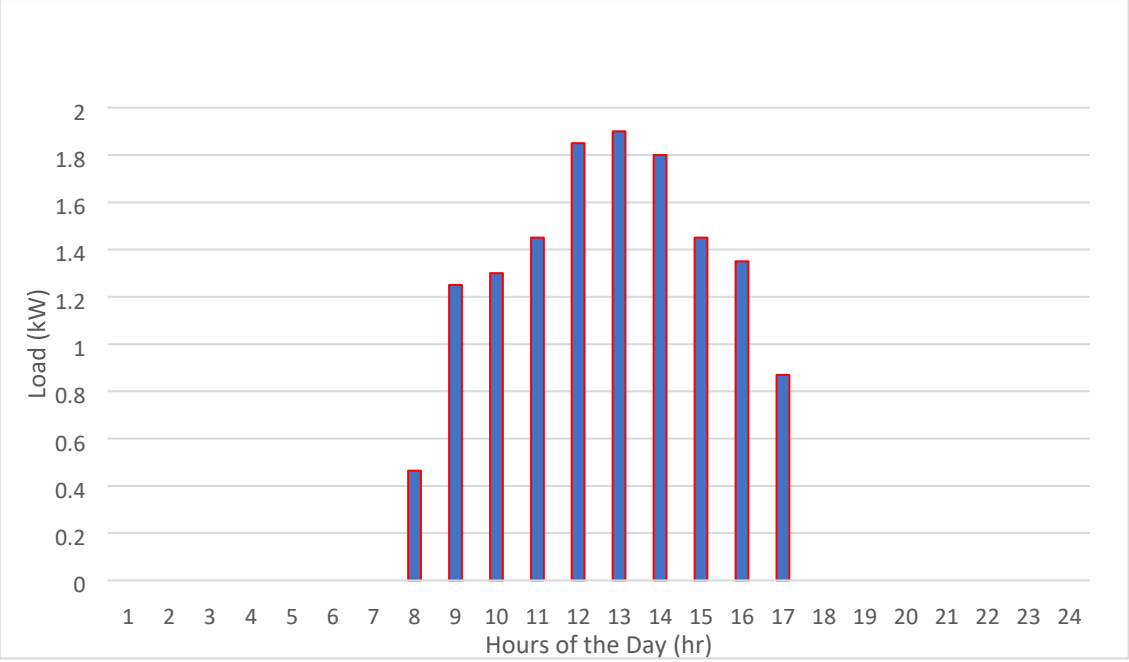

Figure 4.22: Daily load profile

As shown in Figure 4.22, a daily load profile should be dynamic in considering the categories of appliance usages. As a result of this, three categories of appliances are considered. The first category is of those that are used continually, the second category is of those that are used periodically while the last category comprises of those that are used intermittently. This therefore explains the reason why the appliances are not used for equal number of time and also the reason why the daily load profile does not have a constant value throughout the day.

HOMER, a renewable energy tool has been selected to simulate different power system designs, which include both single and hybrid components. In the course of the study, four basic components were selected for the design and they include PV solar module (array), diesel generator, battery and controller. The PV solar module (PV) is the source of the direct current which also serve as the primary producer of electricity through renewable technology. The diesel generator (Gen) is the source of the alternating current through a non-renewable technology and is mainly serving as a backup in the system, to cater for the cloudy hours. The battery (Bat) is primarily used as a backup component for the system, to supply direct current during the non-sunny hours. While the controller (Ctl) functions to balance the activities of the system as a rectifier and as an inverter. The schematic representation of the system set-up is shown in Figure 4.23.

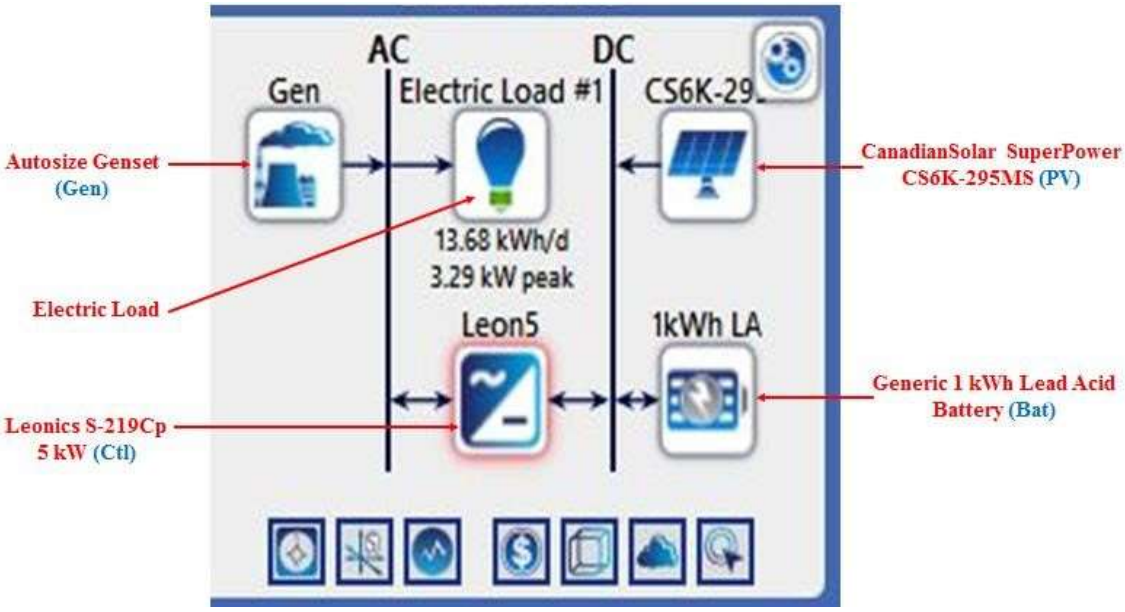

Figure 4.23: Schematic representation of components

The description and specification of each of the components used are presented in Table 4.18. However, the capital cost of the components is not presented in this literature. HOMER has the list of all the required component with their current global prices, which are easily updated through the internet.

Table 4.18: Component, description and specification

Sn	Component	Rated Capacity	Life Span	Technology
1	Canadian Solar Super Power CS6K-295MS	1.18 kW	25 years	Mono-crystalline PV Cells
2	Auto-size Genset	3.70 kW	15, 000 hours	Diesel Engine AC Generator
3	Generic 1kWh Lead Acid Battery	1.001 kWh	10 years	Kinetic Lead Acid Battery
4	Leonics S-219Cp 5kW	5 kW	10 years	Inverter and Rectifier

Temperature and GSR are the two resources used by HOMER for this simulation. Both resources are downloadable from online databases and can be fed into HOMER manually. The monthly average global solar horizontal radiation is given as 5.45 kWh/m^2/day, 5.19 kWh/m^2/day, 5.10 kWh/m^2/day, 5.16 kWh/m^2/day, 5.36 kWh/m^2/day, 5.49 kWh/m^2/day

and 5.47 kWh/m^2/day for Abuja, Benue, Kogi, Kwara, Nasarawa, Niger and Plateau respectively. The designed load profile for the system has a baseline and scaled average energy of 13.69 kWh/d, a baseline and scaled average power of 0.57 kW, a baseline and scaled peak power of 3.29 kW and a baseline and scaled load factor of 0.17.

4.6.1 Feasibility report

HOMER has been used to perform a hourly time series simulation for different system configurations over the 365 days of the year. The calculation report of the simulated system designed for Abuja, Benue, Kogi, Kwara, Nasarawa, Niger and Plateau are presented in Table 4.19.

Table 4.19: Calculation report

Location	Simulated Solutions	Feasible Solutions	Percentage Feasibility (%)
Abuja	1567.0	1137.0	72.56
Benue	1402.0	984.0	70.19
Kogi	1380.0	1004.0	72.75
Kwara	1446.0	1050.0	72.61
Nasarawa	1512.0	1130.0	74.74
Niger	1655.0	1171.0	70.76
Plateau	1545.0	1155.0	74.76

From Table 4.19, the calculation report from HOMER shows the aggregate number of simulated systems configurations, the number of systems configurations that are realistic and those that are not realistic. For Abuja, a total number of 1,567 designs were made out of which only 1,137 are feasible, making up of 72.56 percent of the total. Likewise for Benue, a total of 1,402 designs were simulated and 984 which is made of 70.19 percent of the total simulations were feasible. For Kogi and Kwara, a total of 1,380 and 1,446 system

configurations were considered respectively, while only 1,004 and 1,050 (72.75 and 72.61 percent) of the aggregate fractions were feasible. In addition, 1,512 designs were considered for Nasarawa and only 1,130 were feasible. HOMER also reported 1,655 different system configurations over Niger, out of which only 1,171 (70.76 percent) were feasible. For Plateau, a total of 1,545 system configurations were simulated and only about 74.76 percent (1,155) of the total fraction were feasible. Therefore, the calculation report has shown that the application of off-grid solar power systems is feasible in the NCSN since percentage feasibility varies between 70 % and 74 %. However, the percentage of the simulated systems that were not feasible were linked to capacity shortage.

4.7.0 Preamble

Section 4 subsection 6 satisfies the second part of objective number three (iii) of the study, which is to evaluate the technical and economic values of the simulated systems for proper optimisation. To achieve this, four categories of system configurations were considered and each of the components will be represented by the first letter of its name. That is, Bat, Ctl, Gen and PV will be abbreviated to be B, C, G and P respectively.

Category one combines P with G, B and C. Category two combines P with B and C. Category three combines P with G and C, while category four considers only Gen as 100 percent non-renewable energy source. Different component sizing was also considered (search space) during the simulation process in order to select the best result in terms of cost and technical realisms. The Net Present Cost (NPC) defines the life-cycle cost of the system, which is considered to be 25 years in this study. NPC is made up of the capital cost, replacement cost, fuel cost, operation and maintenance cost. The levelised Cost of Energy (COE) describes the unit cost of energy per 1 kWh. Another important metric of costing in HOMER is the Operation Cost (OC), which is the annual cost of running the

system by considering the capital cost, replacement cost, fuel cost, operation and maintenance cost. The inflation rate is recorded as 22.5 % and diesel price is at $1.83 as recognised internationally for Nigerian market.

4.7.1 Technical, economic and emission report

The optimisation report which comprises of technical, economic and emission reports are presented in Tables: 4.20 to 4.26 respectively for Abuja, Benue, Kogi, Kwara, Nasarawa, Niger and Plateau. From the tables, items number (Sn) 1 to 11 describe technical characteristics. Items from number 12 to 14 designate economic characteristics. On the same note, items from number 15 to 22 describe the volume of fuel consumed and the associated gaseous / particle emissions.

Table 4.20: report for Abuja

Sn	Component / Resource	P+G+B+C	P+B+C	P+G+C	G
1	PV Source (kW)	9.55	19.80	42.00	---
2	Gen Source (kW)	3.70	---	3.70	3.70
3	Battery (Strings)	10.00	9.00	---	---
4	Ctl Source (kW)	3.62	3.53	3.62	---
5	PV Production (kWh/yr)	15,853	32,931	69,752	---
6	Gen Production (kWh/yr)	53.80	---	706.00	5,216.00
7	Total Production (kWh/yr)	15,906	32,931	70,458	5,216
8	Total Consumption (kWh/yr)	4,995	4,994	4,995	4,995
9	Excess Electricity (kWh/yr)	10,661	27,712	65,283	221
10	Renewable Input (%)	99.70	100.00	99.00	0.00
11	Non-Renewable Input (%)	0.34	0.00	1.00	100.00
12	Net Present Cost ($)	24,045.24	104,729.60	281,308.70	1,270,260.00
13	Unit Cost of Energy ($)	0.017	0.076	0.203	0.919
14	Operating Cost ($)	56.66	350.88	980.36	4,581.70
15	Fuel Consumed (Litres)	19.80	0.00	284.00	2,100.00
16	Avg Fuel per Hour (Litres/hr)	0.0023	0.0000	0.0324	0.2400
17	Carbon Dioxide (kg/yr)	51.80	0.00	742.00	5,496.00
18	Carbon Monoxide (kg/yr)	0.326	0.000	4.680	34.600
19	Unburned Hydrocarbon (kg/yr)	0.014	0.000	0.204	1.510
20	Particulate Matter (kg/yr)	0.002	0.000	0.028	0.210

21	Sulphur Dioxide (kg/yr)	0.127	0.000	1.820	13.500
22	Nitrogen Oxides (kg/yr)	0.307	0.000	4.390	32.500

From Table 4.20, it can be inferred that a system combination of PV, Gen, Bat and Ctl gave the least NPC, COE and OC which are $24,045.24, $0.017 and $56.66 respectively. This is preceded by a system combination of PV, Bat and Ctl, having NPC of $104,729.60, COE of $0.076 and OC of $350.88, and followed by a system combination of PV, Gen and Ctl, having NPC of $281,308.70, COE of $0.203 and OC of $980.36. The system having Gen as the sole component has the highest cost in terms of NPC, COE and OC which are $1,270,260.00, $0.919 and $4,581.70 respectively.

It could also be inferred from the table that fuel consumption and emissions increase with increasing percentage of non-renewable energy contribution to the system. A system configuration that is of 100% non-renewable input consumed about 2,100 litres of diesel when used for 3,650 hours (10 hours in a day for a year), thereby emitting about 5,496 kg of Carbon Dioxide gas annually. On the other hand, a system configuration that is of 100% renewable input consumed no diesel and this automatically implies that the system has zero (0) emission.

Furthermore, electricity production outweighs its consumption, which has led to huge excesses in electricity production. This is because HOMER was designed to allow for excesses in order to ensure that the load demand is met at every instant. The excess electricity produced is higher for systems with higher renewable inputs compared to the systems with lower or no renewable inputs. As a result, the excess electricity can be sold out to serve other load demands.

Table 4.21: report for Benue

Sn	Component / Resource	P+G+B+C	P+B+C	P+G+C	G
1	PV Source (kW)	12.60	17.70	42.00	---
2	Gen Source (kW)	3.70	---	3.70	3.70
3	Battery (Strings)	10.00	11.00	---	---
4	Ctl Source (kW)	3.63	3.59	3.65	---
5	PV Production (kWh/yr)	19,838	27,845	66,132	---
6	Gen Production (kWh/yr)	38.30	---	936.00	5,216.00
7	Total Production (kWh/yr)	19,877	27,845	67,068	5,216
8	Total Consumption (kWh/yr)	4,995	4,993	4,995	4,995
9	Excess Electricity (kWh/yr)	14,635	22,617	61,903	221
10	Renewable Input (%)	99.80	100.00	98.60	0.00
11	Non-Renewable Input (%)	0.19	0.00	1.40	100.00
12	Net Present Cost ($)	28,631.45	106,969.40	334,771.10	1,270,260.00
13	Unit Cost of Energy ($)	0.021	0.077	0.242	0.919
14	Operating Cost ($)	71.66	357.74	1,173.42	4,581.70
15	Fuel Consumed (Litres)	14.00	0.00	378.00	2,100.00
16	Avg Fuel per Hour (Litres/hr)	0.0016	0.0000	0.0432	0.2400
17	Carbon Dioxide (kg/yr)	36.50	0.00	989.00	5,496.00
18	Carbon Monoxide (kg/yr)	0.230	0.000	6.240	34.600

Optimisation

19	Unburned Hydrocarbon (kg/yr)	0.010	0.000	0.272	1.510
20	Particulate Matter (kg/yr)	0.001	0.000	0.038	0.210
21	Sulphur Dioxide (kg/yr)	0.090	0.000	2.420	13.500
22	Nitrogen Oxides (kg/yr)	0.216	0.000	5.860	32.500

Inferences drawn from Table 4.21 depicts that a system combination of PV, Gen, Bat and Ctl gave the best optimisation result for Benue, having NPC of $28,631.45, COE of $0.021 and OC of $71.66. Next to the system in term of low cost of operation is that which combines PV, Bat and Ctl with NPC, COE and OC of $106,969.40, $0.077 and $357.74 respectively. This system is followed by a system combination of PV, Gen and Ctl, giving a NPC of $334,771.10, a COE of $0.242 and a OC of $1,173.42. The system with Gen shows the least optimisation value, having NPC, COE and OC of $1,270,260.00, $0.919 and $4,581.70 respectively.

Moreover, the table shows that fuel consumption and emissions increase with increasing use of non-renewable energy source, which is the genset. A system configuration that is of 100% non-renewable input consumed about 2,100 litres of diesel when used for 3,650 hours (10 hours in a day for a year), thereby emitting about 5,496 kg of Carbon Dioxide gas annually. On the other hand, a system configuration that is of 100% renewable input consumed no diesel and this automatically implies that the system has zero (0) emission.

Additionally, electricity production is on the high side compared to its consumption. This has therefore resulted to massive excess electricity production, more especially for systems with high renewable inputs compared to the systems with lower or no renewable inputs. As a result, the excess electricity can be sold out to serve other load demands.

Hence, the excess electricity produced can serve as a source of income generation, if sold out to meet other load demands.

Optimisation r

Table 4.22 eport for Kogi

Sn	Component / Resource	P+G+B+C	P+B+C	P+G+C	G
1	PV Source (kW)	11.00	17.00	41.40	---
2	Gen Source (kW)	3.70	---	3.70	3.70
3	Battery (Strings)	10.00	12.00	---	---
4	Ctl Source (kW)	3.63	4.68	3.65	---
5	PV Production (kWh/yr)	16,847	25,915	63,087	---
6	Gen Production (kWh/yr)	58.80	---	918.00	5,216.00
7	Total Production (kWh/yr)	16,906	25,915	64,005	5,216
8	Total Consumption (kWh/yr)	4,995	4,993	4,995	4,995
9	Excess Electricity (kWh/yr)	11,658	20,685	58,839	221
10	Renewable Input (%)	99.70	100.00	98.60	0.00
11	Non-Renewable Input (%)	0.39	0.00	1.43	100.00
12	Net Present Cost ($)	29,851.09	112,081.4	331,604.8	1,270,260.00
13	Unit Cost of Energy ($)	0.022	0.081	0.240	0.919
14	Operating Cost ($)	76.87	373.13	1,162.31	4,581.70
15	Fuel Consumed (Litres)	21.70	0.00	367	2,100.00
16	Avg Fuel per Hour (Litres/hr)	0.0025	0.0000	0.0418	0.2400
17	Carbon Dioxide (kg/yr)	56.80	0.00	959.00	5,496.00
18	Carbon Monoxide (kg/yr)	0.358	0.000	6.050	34.600
19	Unburned Hydrocarbon (kg/yr)	0.016	0.000	0.264	1.510
20	Particulate Matter (kg/yr)	0.002	0.000	0.037	0.210

21	Sulphur Dioxide (kg/yr)	0.139	0.000	2.350	13.500
22	Nitrogen Oxides (kg/yr)	0.336	0.000	5.680	32.500

The optimisation report presented in Table 4.22 shows that a system combination of PV, Gen, Bat and Ctl is a good option over Kogi. The system has NPC of $29,851.09, COE of $0.022 and OC of $76.87. Next to this in terms of cost reality is a system combination of PV, Bat and Ctl having $112,081.4, $0.081 and $373.13 for NPC, COE and OC respectively. The next system combination to this in terms of cost reality is that of PV, Gen and Ctl, having NPC of $331,604.8, COE of $0.240 and OC of $1,162.31. The last system in terms of cost reality over Kogi that of a Gen. It has NPC of $1,270,260.00, COE of $0.919 and OC of $4,581.70.

Also from Table 4.22, it is evident that fuel consumption and emissions increase with increasing percentage of non-renewable energy contribution to the system. A system configuration that is of 100% non-renewable input consumed about 2,100 litres of diesel when used for 3,650 hours (10 hours in a day for a year), thereby emitting about 5,496 kg of Carbon Dioxide gas annually. On the other hand, a system configuration that is of 100% renewable input consumed no diesel and this automatically implies that the system has zero (0) emission.

Likewise, total electricity production surpasses its total consumption. This therefore implies that the total load demand of the systems was met, having another fraction of unused electricity as excess. The excess electricity produced is higher for systems with high renewable inputs compared to the systems with lower or no renewable inputs. As a result, the excess electricity can be sold out to serve other load demands.

Optimisation r

Table 4.23 eport for Kwara

Sn	Component / Resource	P+G+B+C	P+B+C	P+G+C	G
1	PV Source (kW)	11.50	17.60	41.70	---
2	Gen Source (kW)	3.70	---	3.70	3.70
3	Battery (Strings)	10.00	12.00	---	---
4	Ctl Source (kW)	3.62	3.38	3.65	---
5	PV Production (kWh/yr)	18,047	27,647	65,321	---
6	Gen Production (kWh/yr)	45.40	---	862.00	5,216.00
7	Total Production (kWh/yr)	18,093	27,647	66,183	5,216
8	Total Consumption (kWh/yr)	4,995	4,994	4,995	4,995
9	Excess Electricity (kWh/yr)	12,848	22,419	61,015	221
10	Renewable Input (%)	99.70	100.00	98.70	0.00
11	Non-Renewable Input (%)	0.25	0.00	1.30	100.00
12	Net Present Cost ($)	27,657.85	110,396.40	326,280.00	1,270,260.00
13	Unit Cost of Energy ($)	0.020	0.080	0.236	0.919
14	Operating Cost ($)	68.72	369.52	1,142.91	4,581.70
15	Fuel Consumed (Litres)	16.80	0.00	344.00	2,100.00
16	Avg Fuel per Hour (Litres/hr)	0.0019	0.0000	0.0393	0.2400
17	Carbon Dioxide (kg/yr)	44.00	0.00	901.00	5,496.00
18	Carbon Monoxide (kg/yr)	0.278	0.000	5.680	34.600
19	Unburned Hydrocarbon (kg/yr)	0.012	0.000	0.248	1.510

20	Particulate Matter (kg/yr)	0.002	0.000	0.034	0.210
21	Sulphur Dioxide (kg/yr)	0.108	0.000	2.210	13.500
22	Nitrogen Oxides (kg/yr)	0.261	0.000	5.330	32.500

The optimisation report for Kwara in Table 4.23 explains that a system combination of PV, Gen, Bat and Ctl is most realistic in terms of NPC, COE and OC as $27,657.85, $0.020 and $68.72 respectively. This is followed by NPC, COE and OC of $110,396.40, $0.080 and $369.52 respectively of a system combination of PV, Bat and Ctl. The system combination of PV, Gen and Ctl was ranked third, having NPC of $326,280.0, COE of $0.236 and OC of $1,142.91. While a system of Gen has NPC of $1,270,260.00, COE of $0.919 and OC of $4,581.70.

It could also be established from the table that fuel consumption and emissions increase with increasing percentage of non-renewable energy contribution to the system. A system configuration that is of 100% non-renewable input consumed about 2,100 litres of diesel when used for 3,650 hours (10 hours in a day for a year), thereby emitting about 5,496 kg of Carbon Dioxide gas annually. On the other hand, a system configuration that is of 100% renewable input consumed no diesel and this automatically implies that the system has zero (0) emission.

Also, electricity production outweighs its consumption. As a result, there is surplus electricity supply to the system, which is termed excess electricity. From Table 4.23, the excess electricity produced is higher for systems with high renewable inputs compared to the systems with lower or no renewable inputs. Owing to these established facts, the excess electricity can be sold out to serve other load demands.

Optimisation r

Table 4.24 eport for Nasarawa

Sn	Component / Resource	P+G+B+C	P+B+C	P+G+C	G
1	PV Source (kW)	10.90	18.30	42.00	---
2	Gen Source (kW)	3.70	---	3.70	3.70
3	Battery (Strings)	10.00	10.00	---	---
4	Ctl Source (kW)	3.62	3.56	3.62	---
5	PV Production (kWh/yr)	17,769	29,740	68,405	---
6	Gen Production (kWh/yr)	44.80	---	815.00	5,216.00
7	Total Production (kWh/yr)	17,814	29,740	69,219	5,216
8	Total Consumption (kWh/yr)	4,995	4,994	4,995	4,995
9	Excess Electricity (kWh/yr)	12,571	24,518	64,049	221
10	Renewable Input (%)	99.70	100.00	98.80	0.00
11	Non-Renewable Input (%)	0.25	0.00	1.18	100.00
12	Net Present Cost ($)	25,809.34	104,403.40	316,372.1	1,270,260
13	Unit Cost of Energy ($)	0.019	0.076	0.229	0.919
14	Operating Cost ($)	62.35	349.34	1,107.02	4,581.70
15	Fuel Consumed (Litres)	16.70	0.00	328.00	2,100.00
16	Avg Fuel per Hour (Litres/hr)	0.0019	0.0000	0.0375	0.2400
17	Carbon Dioxide (kg/yr)	43.6.0	0.00	859.00	5,496.00
18	Carbon Monoxide (kg/yr)	0.275	0.000	5.42	34.600

19	Unburned Hydrocarbon (kg/yr)	0.012	0.000	0.236	1.510
20	Particulate Matter (kg/yr)	0.002	0.000	0.033	0.210
21	Sulphur Dioxide (kg/yr)	0.107	0.000	2.100	13.500
22	Nitrogen Oxides (kg/yr)	0.258	0.000	5.090	32.500

From Table 4.24, optimisation of different simulated systems for Nasarawa recognised that a system combination of PV, Gen, Bat and Ctl is optimum for NPC of $25,809.34, COE of $0.019 and OC of $62.35. The system combination of PV, Bat and Ctl is second best with estimated NPC, COE and OC of $104,403.40, $0.076 and $349.34 respectively. Still on the note, the third ranked system combination has NPC of $316,372.1, COE of $0.229 and OC of $1,107.02. While the least cost realistic component has only a Gen with NPC of $1,270,260, COE of $0.919 and OC of $4,581.70.

It was further made known from the table that fuel consumption and emissions increase with increasing use of non-renewable energy source, which is the Gen. A system configuration that is of 100% non-renewable input consumed about 2,100 litres of diesel when used for 3,650 hours (10 hours in a day for a year), thereby emitting about 5,496 kg of Carbon Dioxide gas annually. On the other hand, a system configuration that is of 100% renewable input consumed no diesel and this automatically implies that the system has zero (0) emission.

Moreover, electricity production is on the high side compared to its consumption. This has therefore resulted to massive excess electricity production, more especially for systems with high renewable inputs compared to the systems with lower or no renewable inputs. As a result, the excess electricity can be sold out to serve other load demands. Hence, the excess electricity produced can serve as a source of income generation, if sold out to meet other load demands.

Optimisation r

Table 4.25 eport for Niger

Sn	Component / Resource	P+G+B+C	P+B+C	P+G+C	G
1	PV Source (kW)	9.24	17.00	42.00	---
2	Gen Source (kW)	3.70	---	3.70	3.70
3	Battery (Strings)	10.00	10.00	---	---
4	Ctl Source (kW)	3.62	3.35	3.62	---
5	PV Production (kWh/yr)	15,044	27,622	68,351	---
6	Gen Production (kWh/yr)	53.60	---	706.00	5,216.00
7	Total Production (kWh/yr)	15,097	27,622	69,057	5,216
8	Total Consumption (kWh/yr)	4,995	4,994	4,995	4,995
9	Excess Electricity (kWh/yr)	9,850	22,400	63,883	221
10	Renewable Input (%)	99.60	100.00	99.00	0.00
11	Non-Renewable Input (%)	0.36	0.00	1.00	100.00
12	Net Present Cost ($)	23,139.94	100,071.7	282,099.6	1,270,260.00
13	Unit Cost of Energy ($)	0.017	0.072	0.204	0.919
14	Operating Cost ($)	53.55	334.80	983.22	4,581.70
15	Fuel Consumed (Litres)	19.70	0.00	284.00	2,100.00
16	Avg Fuel per Hour (Litres/hr)	0.0023	0.0000	0.0324	0.2400

17	Carbon Dioxide (kg/yr)	51.60	0.00	744.00	5,496.00
18	Carbon Monoxide (kg/yr)	0.326	0.000	4.690	34.600
19	Unburned Hydrocarbon (kg/yr)	0.014	0.000	0.205	1.510
20	Particulate Matter (kg/yr)	0.002	0.000	0.028	0.210
21	Sulphur Dioxide (kg/yr)	0.126	0.000	1.820	13.500
22	Nitrogen Oxides (kg/yr)	0.306	0.000	4.410	32.500

The optimisation report for Niger in Table 4.25 explains that a system combination of PV, Gen, Bat and Ctl is most realistic in terms of NPC, COE and OC as $23,139.94, $0.017 and $53.55 respectively. This is followed by NPC, COE and OC of $100,071.7, $0.072 and $334.80 respectively of a system combination of PV, Bat and Ctl. The system combination of PV, Gen and Ctl was ranked third, having NPC of $282,099.6, COE of $0.204 and OC of $983.22. While a system of Gen has NPC of $1,270,260.00, COE of $0.919 and OC of $4,581.70.

It was further established from the table that fuel consumption and emissions increase with increasing percentage of non-renewable energy contribution to the system. A system configuration that is of 100% non-renewable input consumed about 2,100 litres of diesel when used for 3,650 hours (10 hours in a day for a year), thereby emitting about 5,496 kg of Carbon Dioxide gas annually. On the other hand, a system configuration that is of 100% renewable input consumed no diesel and this automatically implies that the system has zero (0) emission.

Also, electricity production is far greater than electricity consumption. As a result, there is surplus electricity supply to the system, which is termed excess electricity. From Table 4.23, the excess electricity produced is higher for systems with high renewable

inputs compared to the systems with lower or no renewable inputs. Owing to these established facts, the excess electricity can be sold out to serve other load demands.

Table 4.26 eport for Plateau

Sn	Component / Resource	P+G+B+C	P+B+C	P+G+C	G
1	PV Source (kW)	11.00	18.20	41.50	---
2	Gen Source (kW)	3.70	---	3.70	3.70
3	Battery (Strings)	9.00	10.00	---	---
4	Ctl Source (kW)	3.62	3.39	3.65	---
5	PV Production (kWh/yr)	18,438	30,659	69,762	---
6	Gen Production (kWh/yr)	60.00	---	782.00	5,216.00
7	Total Production (kWh/yr)	18,498	30,659	70,545	5,216
8	Total Consumption (kWh/yr)	4,995	4,994	4,995	4,995
9	Excess Electricity (kWh/yr)	13,260	25,437	65,373	221
10	Renewable Input (%)	99.70	100.00	98.90	0.00
11	Non-Renewable Input (%)	0.32	0.00	1.11	100.00
12	Net Present Cost ($)	24,846.93	103,895.60	306,736.90	1,270,260.00
13	Unit Cost of Energy ($)	0.018	0.075	0.222	0.919
14	Operating Cost ($)	59.93	347.88	1,072.40	4,581.70

15	Fuel Consumed (Litres)	21.30	0.00	317.00	2,100.00
16	Avg Fuel per Hour (Litres/hr)	0.0024	0.0000	0.0362	0.2400
17	Carbon Dioxide (kg/yr)	55.90	0.00	829.00	5,496.00
18	Carbon Monoxide (kg/yr)	0.352	0.000	5.230	34.600
19	Unburned Hydrocarbon (kg/yr)	0.015	0.000	0.228	1.510
20	Particulate Matter (kg/yr)	0.002	0.000	0.032	0.210
21	Sulphur Dioxide (kg/yr)	0.137	0.000	2.030	13.500
22	Nitrogen Oxides (kg/yr)	0.331	0.000	4.910	32.500

The optimisation report presented in Table 4.26 for Plateau shows that a system combination of PV, Gen, Bat and Ctl is the best economic option. The system has NPC of $24,846.93, COE of $0.018 and OC of $59.93. Next to this in terms of cost reality is a system combination of PV, Bat and Ctl having $103,895.60, $0.075 and $347.88 for NPC, COE and OC respectively. The next system combination to this in terms of cost reality is that of PV, Gen and Ctl, having NPC of $306,736.90, COE of $0.222 and OC of $1,072.40. The last system in terms of cost reality over Plateau is that of a Gen. It has NPC of $1,270,260.00, COE of $0.919 and OC of $4,581.70.

Also from Table 4.22, it is evident that fuel consumption and emissions increase with increasing percentage of non-renewable energy contribution to the system. A system configuration that is of 100% non-renewable input consumed about 2,100 litres of diesel when used for 3,650 hours (10 hours in a day for a year), thereby emitting about 5,496 kg of Carbon Dioxide gas annually. On the other hand, a system configuration that is of 100% renewable input consumed no diesel and this automatically implies that the system has zero (0) emission.

Optimisation r

Likewise, total electricity production surpasses its total consumption. This therefore implies that the total load demand of the systems was met, having another fraction of unused electricity as excess. The excess electricity produced is higher for systems with high renewable inputs compared to the systems with lower or no renewable inputs. As a result, the excess electricity can be sold out to serve other load demands.

4.8 Summary of Findings

In this work, an accurate and user-friendly GSR multiple parameter-based model has been developed for the assessment of solar energy resources in the study locations. The model was developed using ANN and it is of the form: $H = pA + qB + rC + \alpha$ where H is the

estimated GSR, p, q and r are constants, A, B and C are input parameters representing relative humidity, temperature difference and solar flux respectively. The developed model alongside thirteen empirical models were used to estimate GSR and compared with ground measured GSR data. Their performances were determined using statistical metrics which include MAE, MBE, MSE, RMSE and R. Inferences drawn from results showed that the developed model is remarkably good for estimating GSR.

Nevertheless, HOMER was used to simulate and optimise different standalone off-grid solar power system configurations. The system is designed for a small-scale computerbased business enterprise. The designed load profile for the system has a baseline and scaled average energy of 13.68 kWh/d, a baseline and scaled average power of 0.57 kW, a baseline and scaled peak power of 3.29 kW and a baseline and scaled load factor of 0.17. From the calculation report, 72.56%, 70.19%, 72.75%, 72.61%, 74.74%, 70.76% and 74.76% fraction of the entire simulated power systems was feasible for Abuja, Benue, Kogi, Kwara, Nasarawa, Niger and Plateau respectively, while the percentage that was not feasible was blamed on capacity shortage. Optimisation report showed that system combination of a PV module, a diesel generator, strings of battery and a controller is the best for the region, with unit cost of energy which ranges between 0.017$ and 0.022$. In addition, a system configuration that is of 100% renewable input consumed no fuel and this automatically implies that the system has zero (0) emission.

Above all, the total load demand of the systems was met, having another fraction of unused electricity as excess which could be sold out to serve other load demands. It is therefore imperative to note that the excess electricity production mainly resulted from high renewable penetration.

CHAPTER FIVE

5.0 CONCLUSION AND RECOMMENDATIONS

5.1 Conclusion

This thesis titled "Development of Artificial Neural Network-Based Model for Assessment of Solar Energy Resources to Implement Off-grid Solar Power System" is focused on proffering the compulsory solutions to GSR data scarcity which will consequently help in solving many other correlational problems such as global warming, lack of electricity, insecurity, unemployment, disasters associated with hydro-dams, poor agricultural produce, storage and preservation. GSR data is also needed in cooling system technologies, passive and active heating systems, irrigation and water pumping systems to mention a few, but the scope of this study is envisioned on power generation owing to its potential in improving lively-hood and national prosperity through engagement in various economic and educational activities. Hence, there is need to provide a clean, cheap, reliable and sustainable source of energy such as solar.

To this effect, a model has been developed to assess the potential of solar energy in the NCSN. The model has been used and compared with other existing models in the said region for proper evaluation and validation. This is preceded by the feasibility study of solar power system, simulation of different system configurations and techno-economic optimisation of simulated systems in providing cheap and efficient power system for a small-scale computer-based business enterprise in the region using HOMER.

In agreement with the objectives of the research, the key findings are presented as follows:

i. The use of SCM (ANN) in modelling and predicting GSR has shown a better performance compared to the empirical models.

ii. An ANN-based model has been developed for estimating GSR in the NCSN.

The model is of the form ($H = pA + qB + rC + \alpha$). It is a multiple parameterbased model.

iii. Estimated GSR data from the developed model and that from thirteen other empirical models were compared with measured GSR data. Result revealed that data from the developed model has shown good accuracy.

iv. The multiple parameter-based models proved better precisions than the single parameter-based models.

v. Both the measured and the estimated values of GSR for the NCSN showed that the seven states in the region are viable for solar power generation. With monthly average GSR of 5.45 $kWh/m^2/day$, 5.19 $kWh/m^2/day$, 5.10 $kWh/m^2/day$, 5.16 $kWh/m^2/day$, 5.36 $kWh/m^2/day$, 5.49 $kWh/m^2/day$ and 5.47 $kWh/m^2/day$ for Abuja, Benue, Kogi, Kwara, Nasarawa, Niger and Plateau respectively.

vi. HOMER considered 1,137, 984, 1,004, 1,050, 1,130, 1,171 and 1,155 feasible solutions for Abuja, Benue, Kogi, Kwara, Nasarawa, Niger and Plateau respectively. This is therefore an affirmation that solar power project is feasible in the NCSN.

vii. Abuja and Niger recorded the least COE of $0.017 for a system combination of photo-voltaic solar arrays, generic genset, strings of battery and controller. While Kogi recorded the highest COE of $0.022 for the same system combination as other states.

viii. Generation of electricity using 100% renewable energy source is much cheaper compared to electricity generation using 100% non-renewable energy source.

ix. A system of 100% renewable energy source emits no green-house gas.

x. Solar resources have the potential of satiating residential and commercial energy demand of citizens in the NCSN.

xi. Through proper implementation and strict adherence to system designs, small scale business owners can manage effective business with constant electric power supply without the use of a power generating set.

5.2 Recommendations

In order to guarantee more credible research as time passes on, the researcher therefore recommends that:

i. the developed model be tested in another region outside the NCSN; ii. further studies should be conducted using other SCMs (not ANN) in the NCSN; iii. there is need to intensify the awareness of the potentials of renewable energy resources to the public; iv. renewable energy resource scheme be incorporated in academic curriculum;

v. and solar energy project is capital intensive and as a result, the Government and interested financial-aid institutions should make efforts to initiate functional financial solution plans that can mitigate capital cost barriers to interested individuals or group.

5.3 Contribution to Knowledge

The contributions of this research to knowledge include but not limited to the development of a mathematical model for accurately predicting GSR values in the study locations. In terms of statistical performance, mean absolute error, mean bias error, mean squared error, root mean squared error and coefficient of correlation values were recorded respectively as: 0.242, 0.026, 0.079, 0.281 and 0.856 for Abuja; 0.247, -0.043, 0.077, 0.277 and 0.825 for Benue; 0.294, -0.25, 0.136, 0.369 and 0.757 for Kogi; 0.323, -0.171,

0.156, 0.395 and 0.704 for Kwara; 0.195, 0.092, 0.058, 0.240 and 0.919 for Nasarawa; 0.353, -0.035, 0.175, 0.419 and 0.665 for Niger; and 0.320, -0.053, 0.148, 0.385 and 0.871 for Plateau State. The model uses most assessable weather parameters, it has good precision and it is user friendly.

In addition, based on good knowledge of GSR, the study provides vital information on how different off-grid power systems have been designed for maximum power availability in which 1,137, 984, 1,004, 1,050, 1,130, 1,171 and 1,155 power system configurations are feasible for Abuja, Benue, Kogi, Kwara, Nasarawa, Niger and Plateau respectively. Also, the optimisation report showed that system combination of a photovoltaic solar module, a diesel generator, strings of battery and a controller is the best for the region, providing unit cost of energy as low as 0.017$, 0.021$, 0.022$, 0.020$, 0.019$, 0.017$ and 0.018$ for Abuja, Benue, Kogi, Kwara, Nasarawa, Niger and Plateau respectively. Hence, conclusion from the study affirms that the inclusion of solar energy technologies in power generation can satiate the demand for effective energy and reduce the dependence on fossil fuels especially in North-central Nigeria.

References

Abdalla, Y. A. G. (1994). New Correlations of Global Solar Radiation with Meteorological Parameters for Bahrain. *International Journal of Solar Energy***,** 16 (11), 1-120. http://dx.doi.org/10.1080/01425919408914270

Abedelhak, B. J., Souad, R., Najib E., Abdelaziz H., Faicel H., & Farouk, Y. (2013). Estimation of GSR using three simple methods. *Energy Procedia Elsevier Ltd.* 42, 406-415.

Adelaja, O. J., Oduola, A. O., Abiodun, O. O., Adeneye, A. K. & Obembe, A. (2021). Plants with insecticidal potential used by ethnic groups in North-Central Nigeria for the management of hematophagous insects. *Asian Journal of Ethnobiology*, 4 (2), 65-75. DOI: 10.13057/asianjethnobiol/y040201.

Ahmet Z. Sahin (2014). Importance of Exergy Analysis in Industrial process. *Research Gate.* https://www.reasearchgate.net/publication/228988818.

Al Shamisi, M. H., Assi, A. H. & Hejase, H. A. (2011). Using MATLAB to develop artificial neural network models for predicting global solar radiation in Al Ain City–UAE, in Engineering education and research using MATLAB: *IntechOpen*.

Allen, R. G. (1997). Self-calibrating method for estimating solar radiation from air temperature. *Journal of Hydrologic Engineering*, 2 (2), 56–67. DOI: 10.1061/(ASCE)1084-0699(1997)2:2(56)

Almorox, J. (2011). Estimating global solar radiation from common meteorological data in Aranjuez, Spain. *Universidad Polit´ecnica de Madrid, School of Agricultural Engineers, Department of Soil Science and Climatology, Ciudad Universitaria s/n, 28040 Madrid-SPAIN*. Turk J Phys 35, 53 – 64.

Andreas, *Z. (1994). Simulation Neuronaler Netze. Simulation of Neural Networks. (in German) (1st ed.). Addison-Wesley, 73.* ISBN 3-89319-554-8.

Angstrom, A. (1924). Solar and terrestrial radiation. *Q J R Meteorol Soc*, 50 (121).

Annandale, J., Jovanovic, N., Benad´e, N. & Allen, R. (2002). Software for Missing Data Error Analysis of Penman-Monteith Reference Evapotranspiration. *Irrigation Science*, 21 (2), 57–67.

Antonanzas, F., Sanz, A., Martínez-de-Pison, F. J, & Perpinan, O. (2013). Evaluation and Improvement of Empirical Models of Global Solar Irradiation: Case Study Northern Spain. *Renew Energy*, 60, 604–614.

Ayaz, A. Khamisani (2018). Design Methodology of Off-Grid PV Solar Powered System. A Case Study of Solar Powered Bus Shelter.

Badescu, V. (2015). Solar Radiation Estimation from Cloudiness Data. Satellite Vs. Ground-Based Observations. *International Journal of Green Energy, 12, 852– 864*. DOI: 10.1080/15435075.2014.888659.

Badrinarayanan, V., Kendall, A. & Cipolla, R. (2016). SegNet: A Deep Convolutional Encoder-Decoder Architecture for Image Segmentation, 10, 3-4. DOI: arXiv:1511.00561v3 [cs.CV]

Bartle, A. (2002). Hydropower potential and development activities. Energy Policy 30. *Elsevier Science Ltd,* PII: S0301-4215(02)00084 – 8, 1231–1239.

Black, J. N. (1956). The Distribution of Solar Radiation ver the Earth's Surface. *Archiv fur Meteorologie, Geophysik, und Bioklimatologie Serie A Meteorologie und Geophysik,* 7, 165–1889.

Bojanowski, J. S., Vrieling, A. & Skidmore, A. K. (2013). Calibration of solar radiation models for Europe using Meteosat Second Generation and weather station data. *Agricultural and Forest Meteorology*, 176, 1-9. DOI: 10.1016/j.agrformet.2013.03.005.

Bonanno, A. Schlattl, H. & Paternò, L. (2008). The age of the Sun and the relativistic corrections in the EOS. *Astronomy and Astrophysics, 390 (3), 1115–1118.* Doi*:*10.1051/0004-6361:20020749.

Bovwe, O., Nwaogazie I. L. & Agunwamba J. C. (2016). Exploratory Factor Analysis and Assessment of Energy Potential of Generated Solid Waste In Nigeria, International Journal of Civil Engineering and Technology, 7 (1), 274-289.

Bristow, K. L. & Campbell, G. S. (1984). On the Relationship Between Incoming Solar Radiation and Daily Maximum and Minimum Temperature. *Agricultural and Forest Meteorology,* 31, 59–166.

Brkic, S. & Tuka, B. (2019). Empirical Model for Estimating Solar Radiation Based on Air Temperature for Sarajevo Area, Bosnia and Herzegovina. *European International Journal of Science and Technology,* 8 (11).

Broggini, C. (2003). Physics in Collision, Proceedings of the XXIII International Conference: Nuclear Processes at Solar Energy. *XXIII Physics in Collisions Conference. Zeuthen, Germany, 20-21.*

Chai, T. & Draxler, R. R. (2014). Root mean square error (RMSE) or mean absolute error (MAE)? – Arguments against avoiding RMSE in the literature, *Geosci. Model Dev*, 7, 1247–1250. https://doi.org/10.5194/gmd-7-1247-2014, 2014.

Chaudhuri, S. & Chattopadhyay, S. (2005). Neuro-computing based short range prediction of some meteorological parameters during the pre-monsoon season. *Soft Comput,* 9, 349–354. https://doi.org/10.1007/s00500-004-0414-3

Chegaar, M. & Guechi, F. (2009). Estimation of Global Solar Radiation Using Meteorological Parameters. *Revue Internationale D'héliotechnique,* 40, 18-23. http:\\www.comples.org

Chieng, H. H., Wahid, N., Pauline, O. & Perla, S. R. (2018). Flatten-T Swish: a Thresholded ReLU-Swish-like Activation Function for Deep Learning. *International Journal of Advances in Intelligent Informatics*, 4, (2), 76-86.

Chowdhury, N., Hossain, C. A., Longo, M. & Yaïci, W. (2020). Feasibility and Cost Analysis of Photovoltaic-Biomass Hybrid Energy System in Off-Grid Areas of Bangladesh. *Sustainability,* 12. Doi:10.3390/su12041568.

Coleman, J. A. & Davidson, G. (2015). The Dictionary of Mythology: An A-Z of Themes, Legends, and Heroes. *London, England: Arcturus Publishing Limited,* 315-316. ISBN 978-1-78404-478-7.

Connolly, D., Lund, H., Mathiesen, B. V. & Leahy, M. (2010). A Review of Computer Tools for Analysing the Integration of Renewable Energy into Various Energy Systems. *Applied Energy*, 87(4).1059–1082.

Crosbie, S. (2000). The Science of Energy: A Cultural History of Energy Physics in Victorian Britain. Bibliovault OAI Repository, *the University of Chicago Press.* 105.

Dagim, K. (2016). Design and Analysis of Solar Thermal System for Hot Water Supply to Minilk II Hospital New Building. *Addis Ababa University Institute of Technology Centre of Energy Technology*, 7-9.

Daily Trust (2018). Over 826,403 people affected by 2018 flooding in Nigeria- UNFPA. Retrieved from https://dailytrust.com/over-826403-people-affected-by-2018 flooding-in-nigeria-unfpa/

Darling, D (2012). The Encyclopedia of Alternative Energy and Sustainable Living. Retrieved from http://www.daviddarling.info/encyclopedia/E/AE_evacuated_tube_collector.html

Dazhia, Y., Jirutitijaroena, P. & Walsh, W. M. (2011). The Estimation of Clear Sky Global Horizontal Irradiance at the Equator. *Published by Elsevier Ltd. PV Asia Pacific Conference 2011*, 25, 141 – 148.

Diarra, C. (2018). Developing Skills to Accelerate Renewable Energy Deployment. Regional Workshop Central Africa. *Sustainable Energy Production and Energy Management.* Doi: 10.1007/s11600-019-00304-3

Dugas, C., Bengio, Y., Belisle, F., Nadeau, C., & Garcia, R. (2001). Incorporating second order functional knowledge for better option pricing, in: *Advances in Neural Information Processing Systems*, 472–478.

Eichie, J. O., Oyedum, O. D., Ajewole, M. O. & Aibinu, A. M. (2016). Artificial Neural Network model for the determination of GSM Rxlevel from atmospheric parameters. *Eng. Sci. Tech., Int. J.*, http://dx.doi.org/10.1016/j.jestch.2016.11.002

El-mohr, I. & Anas, A. (2014). Renewable Energy Systems: Hybrid Energy Systems Applications. Retrieved from https://www.aast.edu

Energypedia (2020). Nigeria Energy Situation. Webinar Series: Sustainable Energy in Humanitarian Settings. Retrieved from https://energypedia.info/wiki/Nigeria_Energy_Situation#citenote.

Enrico, S. & Goran, W. (2007). A brief Commented History of Exergy From the Beginnings to 2004. *Int. J. of Thermodynamics*, 10 (1), 1-26.

Fadare, D. A., Irimisose, I., Oni, A. O. & Falana, A. (2010). Modeling of solar energy potential in Africa using an artificial neural network. *American Journal of Scientific and Industrial Research.* DOI:10.5251/ajsir.2010.1.2.144.157

Fagbenle, R. O., Katende, J., Ajayi, O. O. & Okeniyi, J. O. (2011). Assessment of Wind Energy Potential of Two Sites in North-East, Nigeria. Renewable Energy, 36, 1277-1283.

Folorunso, T. A., Aibinu, A. M., Kolo, J. G., Sadiku, S. O. E. & Orire, A. M. (2018). Effects of Data Normalization on Water Quality Model in a Recirculatory Aquaculture system using Artificial Neural Network, i-manager's Journal on Pattern Recognition, 5 (3), 21-28.

Folorunso T. A., Aibinu, M. A., Kolo, J. G., Sadiku, S. O. &, Orire, A. M. (2019). Water Quality Index Estimation Model for Aquaculture System Using Artificial Neural Network. *Journal of Advanced Computer Engineering Technology*, 5 (3).

Franklin, E. (2017). Solar Photovoltaic (PV) Site Assessment. Retrieved from: https://extension.arizona.edu/sites/extension.arizona.edu/files/pubs/az1697-2017.pdf

Fritz, S. (1957). Solar Energy on Clear and Cloudy Days. *The Scientific Monthly*.

García, R. A., Turck-Chièze, S., Jiménez-Reyes, S. J., Ballot, J., Pallé, P. L., Eff-Darwich, A., Mathur, S. & Provost, J. (2007). Tracking solar gravity modes: the dynamics of the solar core. *Journal of Science*, 15;316 (5831), 1591-1593. DOI: 10.1126/science.1140598.

GCEP (2006). Global Climate & Energy Project: An Assessment of Solar Energy Conversion Technologies and Research Opportunities: *STANFORD UNIVERSITY*.

Gerretsen, I. (2018). Oil-rich Nigeria Turns to Renewable Energy as Population Booms. Retrieved from https://www.zilient.org/article/oil-rich-nigeria-turns-renewable energy-population-booms.

Givler, T. & Lilienthal, P. (2005). Using HOMER Software, NRE 's Micro-power Optimization Model, to Explore the Role of Gen-sets in Small Solar Power Systems.

Glorot, X. & Bengio, Y. (2010). Understanding the Difficulty of Training Deep Feedforward Neural Networks. *In International Conference on Artificial Intelligence and Statistics*, 9, 249–256.

Glover, J & McGulloch, J. D. G. (1958). The Empirical Relation between Solar Radiation and Hours of Sunshine, *Journal of the Royal Meteorological Society*, 84, (360), 172-175. DOI:10.1002/qj.49708436011

Goodfellow, I., Bengio, Y. & Courville, A. (2016). Deep learning. *The MIT Press*, 183 184. DOI:10.1007/s10710-017-9314-z

Goodin, D. G., Hutchinson, J. M. S., Vanderlip, R. L. & M. C. Knapp (1999). Estimating Solar Irradiance for Crop Modeling Using Daily Air Temperature Data. *AGRONOMY JOURNAL*, 91.

Gopinathan, K. K. (1988). A New Model for Estimating Total Solar Radiation. *Solar and Wind Technology*, 5 (107).

Gueymard, C. A. & Myers, D. R. (2009). Evaluation of conventional and high performance Routine solar radiation measurements for improved solar resource, climatological trends, and Radiative modelling. *Journal of Solar Energy*, 83, 171-185.

Han, J. & Moraga, C. (2019). The influence of the sigmoid function parameters on the speed of backpropagation learning, in Natural to Artificial Neural Computation. IWANN 1995. Lecture Notes in Computer Science. *Berlin, Heidelberg: Springer*, 195-201. DOI: 10.20944/preprints201903.0140.v1

Hargreaves, G. H. & Samani, Z.A. (1982). Estimating Potential Evapotranspiration. *Journal of Irrigation and Drainage Engineering*, 108 (IR3), 223–230.

Henderson, H. W., & Wells, R. (1988). Obtaining attractor dimensions from meteorological time series. *Advances in Geophysics. Elsevier*, 30, 205-237.

Herculano-Houzel, S. (2017). Numbers of neurons as biological correlates of cognitive capability, Current Opinion in Behavioural Sciences, 16, 1-7. Retrieved from https://doi.org/10.1016/j.cobeha.2017.02.004.

Hermann, S. (2001). A Solar Manifesto. London: *Published by Earthscan Publications*, ISBN 13: 9781902916248

Hledic R., Chang J. & Lueken R. (2016). NRECA and the National Resources Defence Council (NRDC). *January Council NRDC*, Retrieved from https://doi.org/10.1007/s40095-019- 00326-z

Hodgkin, A. L. & Huxley, A. F. (1952). A quantitative description of membrane current and its application to conduction and excitation in nerve. *Journal of Physiol*, 117 (4), 500-544. DOI: 10.1113/jphysiol.1952.sp004764

Hufbauer, K. (1991). Exploring the sun: solar science since Galileo. *Johns Hopkins University Press, Maryland.*

Hyndman, Rob J. & Koehler, Anne B. (2006). Another look at measures of forecast accuracy. International Journal of Forecasting, 22 (4), 679–688. DOI*:*10.1016/j.ijforecast.2006.03.001

Ideki, O. & Weli, V. (2019). Assessment of Drought Vulnerability and Occurrence Zones in North Central Nigeria. *Journal of Atmospheric and Climate Sciences*, 9, 298 309. Doi: 10.4236/acs.2019.93021.

IEA, (2004). World Energy Outlook. *International Energy Agency, Paris*, IEA/OECD.

Infoguide Nigeria (2020). 38 Power stations in Nigeria locations and their capacities. Retrieved from https://infoguidenigeria.com/power-stations-nigeria/

International Resources Group (2003). World Bank/Sri Lanka Energy Services Delivery Project, Impacts Assessment and Lessons Learned. *Washington, DC*.

Iwayemi, A. (2008). Investment in Electricity Generation and Transmission in Nigeria: Issues and Options. *International Association for Energy Economics,* 37-41.

James M. Fiore (2019). Semiconductor Devices: Theory and Application, Version 1.1.5.

Jeon, I. & Kim, T. (2023). Distinctive properties of biological neural networks and recent advances in bottom-up approaches toward a better biologically plausible neural network. *Brain Science Institute, Korea Institute of Science and Technology, Seoul, Republic of Korea,* 1-18. DOI 10.3389/fncom.2023.1092185.

Jerabaj, S. & Iniyan, S. (2006). Renewable and Sustainable Energy Reviews. *ELSEVIER Renewable and Sustainable Energy Reviews*, 10, 281–311.
DOI: 10.1016/j.rser.2004.09.004

Jiachen, L. (2018). Fusion Reactions in Stars: Proton-Proton Chain and CNO Cycle Reaction. *Stanford University,*1-3.

Jurgen, S. (2015). Deep learning in neural networks: An overview. Neural Networks. DOI*:* 10.1016/j.neunet.2014.09.003.

Kalogirou, S.A. (2004). Solar Thermal Collectors and Applications. *Progress in Energy and Combustion Science,* 30 (3), 231-295.

Kandel, E. R., Schwartz, J. H. & Jessell, T. M. (2000). Principles of Neural Science, 4th Edition. *New York, McGraw-Hill*, 19–20.

Karlik, B. & Vehbi, A. (2011). Performance Analysis of Various Activation Functions in Generalized MLP Architectures of Neural Networks. *International Journal of Artificial Intelligence and Expert Systems*, 1 (4), 111–122.

Kasten, F. & Czeplak, G. (1980). Solar and Terrestrial Radiation Dependent on the Amount and Type of Cloud. *Solar Energy, Pergamon Press Ltd,* 24, 177-189.

Khan, M. F. H. (2019). Islamic University of Technology. RETScreen Report for An Off-grid System. *ResearchGate*. Retrieved from https://www.researchgate.net/publication/334305368

Kittel, C. (2004). Introduction to Solid State Physics. *John Wiley and Sons.* ISBN 0-471-41526 X.

Kostadinov, S. (2019). Understanding Backpropagation Algorithm. *Towards Data Science* Retrieved from https://medium.com/@simonnoff?source=post_page-7bb3aa2f95fd*]*

Kriesel, D. (2005). A brief Introduction to Neural Networks. *dkriesel*, 1-244. Retrieved from https://www.ippp.dur.ac.uk/~mspannow/files/IntroNN_David_Kiesel.pdf Kumar, R., Aggarwal1, R. K. and Sharma, J. D. (2012). Solar Radiation Estimation Using Artificial Neural Network: *Asian Journal of Contemporary Sciences*, 1, 12-17. http://www.parees.co.in/ajcs.htm

Kumar, P., Pukale, R., Kumabhar, N. & Patil, U. (2016). Optimal Design Configuration Using HOMER. *International Conference on Emerging Trends in Engineering, Science and Technology ELSEVIER,* 24, 499 – 504.

Lambert, T., Gilman, P. & Lilienthal, P. (2006). Micropower System Modeling with Homer. Chapter 15. Integration of Alternative Sources of Energy, *John Wiley & Sons, Inc*, 379-418.

Li, C., Ge, X., Zheng, Y., Xu, C., Ren, Y. & Song, C. (2013). Techno-Economic Feasibility Study of Autonomous Hybrid Wind / PV / Battery Power System for a Household in Urumqi, China. *Journal of Energy*, 55, 263-272.

Liu, F., Wang, W., Wang, L. & Yang, G (2012). Working principles of solar and other energy conversion cells. *Nanomaterials and Energy*, *The University of Hong Kong*, 2 (1), 3-10. http://hdl.handle.net/10722/164261

Lumb, F. E. (1964). The Influence of Cloud on Hourly Amounts of Total Solar Radiation at the Sea Surface. *Meteorological Office, Bracknell, Berkshire*, 551.301.45 : 551.521.12 (261) : 551.576.2 (261) . 551.465.71

Luvchik, A. (2015). Conceiving a systemic approach to implement solar energy technology: The case of Israel. *Centre for Environmental Policy Imperial College, London.*

Mallikarjun G. Hudedma, Soppimath, V. & Jambotkar, C. (2017). A Study of Materials for Solar PV Technology and Challenges. *European Journal of Applied Engineering and Scientific Research*, 5 (1), 1-13.

Mandrini C. H. (2012). Solar Structure and Activity: Introduction. *Instituto de Astronomia y Fisica del Espacio, Buenos Aires, Argentina*, 1-43.

Maqsood, I., Khan, M. R. & Abraham, A. (2002). An ensemble of neural networks for weather forecasting. *Neural Comput & Applic*, 13, 112–122. DOI 10.1007/s00521-004-0413-4

Mark, Cullen (2012). Commercial Solar Water Heating Systems. Design review of two of Ireland's largest commercial Solar Water Heating Systems. *Mary Doyle-Kent The School of Engineering Waterford Institute of Technology*, 13-18.

Martinez, I. (2011). Exergy. Retrieved from http://www.webserver.dmt.upm.es/isidoro/

Mathworks, (2005). Getting Started with MATLAB Version 7. *The Mathworks. Inc. Retrieved from* https://www.mn.uio.no/astro/english/services/it/help/mathematics/matlab/getstart.pdf

Menges, H. O., Ertekin, C. & Sonmete, H. (2006). Evaluation of Global Solar Radiation Models for Konya, Turkey. *Energy Conversion and Management*, 47, (18), 3149-3173.

Mohanty, S., Patra, P. K. & Sahoo, S. S. (2016). Prediction and application of solar radiation with soft computing over traditional and conventional approach - A comprehensive Review. *Renewable and Sustainable Energy Reviews*, 56, 778–796.

Muneer, T. & Gul, M. S. (1999). Evaluation of Sunshine and Cloud Cover Based Models for Generating Solar Radiation Data. *Energy Conversion & Management*, 41,

461- 482

Nada, H. A. (2017). Charge Carriers: Electrons and Holes in Semiconductor. *Sudan University of Science and Technology, College of Graduate Studies.*

Nair, V. & Hinton, G. E. (2010). Rectified linear units improve restricted Boltzmann machines. *Proceedings on Machine Learning, Haifa, Israel*, 807–814. DOI/10.5555/3104322.3104425

Namrata, K., Sharma, P. & Saksena, S. B. L. (2013). Comparison of Different Models for Estimation of Global Solar Radiation in Jharkhand (India) Region. *Smart Grid and Renewable Energy*, 4, 348-352. http://dx.doi.org/10.4236/sgre.2013.44041 NASA (2007). NASA/Marshall Solar Physics. *Marshall Space Flight Center.*

NASA (2013). Sun. World Book at NASA. *National Aeronautics and Space Agency.*

National Research Council (2004). Understanding the Sun and Solar System Plasmas: Future Directions in Solar and Space Physics. *The National Academies Press. Washington, DC:* https://doi.org/10.17226/11188.

Neamen, D. A. (2003). Semiconductor Physics and Devices: Basic Principles (3rd ed.). *McGraw-Hill Higher Education. ISBN 0-07-232107-5.*

Newland, f. J. (1989). Study of Solar Radiation Models for the Coastal Region of South China. *Journal of Solar Energy*, 43 (4), 227-235.

Nguyen, H., Bui, X. N., & Moayedi, H. (2019). A comparison of advanced computational models and experimental techniques in predicting blast-induced ground vibration in open-pit coal mine. *Acta Geophysica*, 67 (4), 1025–1037. DOI: 10.1007/s11600-019-00304-3

Njoku, H. (2014). Solar Photovoltaic Potential in Nigeria. *Journal of Energy Engineering.* DOI: 10.1061/(ASCE)EY.1943-7897.0000145

Noor H. Al Dulaimi (2018). Design of an Off-Grid Solar PV System for a Rural Shelter. *German Jordanian University School of Natural Resources Engineering and Management. Department of Energy Engineering*.

Norris, D. J. (1968). Correlation of Solar Radiation with Clouds. *Solar Energy*, 12, 107 112. Perpmon Press, 1965. NREL/TP-710-36774 May 2005.

Nurunnabi, M. & Roy, N. K. (2015). Grid Connected Hybrid Power System Design Using HOMER. *Advances in Electrical Engineering, 2015, Dhaka, Bangladesh,* 18-21.

Nwankpa, C. E., Ijomah, W., Gachagan, A. &Marshall, S. (2018). Activation Functions: Comparison of Trends in Practice and Research for Deep Learning. arXiv:1811.03378v1[cs.LG], 1-14

Nwokolo, S. C. & Ogbulezie, J. C. (2018). A Quantitative Review and Classification of Empirical Models for predicting global solar radiation in West Africa. *Beni-Suef University Journal of Basic and Applied Sciences, Elsevier*, 7, 367–396.

Odin, G. (2018). Business a.m. Nigeria ranked 2nd largest electricity access deficit in world as 80m homes live without power. Retrieved from https://www.businessamlive.com/nigeria-ranked-2nd-largest-electricity-access deficit- in-world-as-80m-homes-live-without-power/

Ogleman, H., Ecevit, A & Tasdemiroglu, E (1984). A New Method for Estimating Solar Radiation from Bright Sun- shine Data, *Solar Energy*, 33, (6), 619-625. DOI:10.1016/0038-092X(84)90018-5

Ojosu, J. O. & Komolafe, L. K. (1987). Models for Estimating Solar Radiation Availability in South-Western Nigeria. *Nigerian Journal of Solar Energy*, 6 (1), 69-77.

Okundamiya, M. S., Emagbetere, J. O. & Ogujor, E. A. (2015). Evaluation of Various Global Solar Radiation Models for Nigeria. *International Journal of Green Energy*, DOI: 10.1080/15435075.2014.968921.

latomiwa, ., Mekhilef, S., Shamshirband, S. & Petković, D. (2015). Adaptive neuro fuzzy approach for solar radiation prediction in Nigeria. *Renewable and Sustainable Energy Reviews*, 51, 1784-1791, https://doi.org/10.1016/j.rser.2015.05.068.

Olayemi, I. K., Idris, B., Ejima, I. A., Adeniyi, K., Ukubuiwe, A. C. & Isah, B. (2014). The Climate of North-central Nigeria and Potential Influence on Mosquito (Diptera: Culicidae) Vectorial Capacity, for Disease Transmission. *Global journal of multidisciplinary and applied sciences.* 2 (2), 26-31.

Olomiyesan, B. M., Oyedum, O. D., Ugwuoke, P. E., Ezenwora, J. A. & Ibrahim, A. G. (2015). Solar Energy for Power Generation: A Review of Solar Radiation Measurement Processes and Global Solar Radiation Modelling Techniques. *Nigerian Journal of Solar Energy,* 26.

Olomiyesan B. M., & Oyedum O. D. (2016a). Comparative Study of Ground Measured, Satellite-Derived, and Estimated Global Solar Radiation Data in Nigeria. *Journal of Solar Energy. Hindawi Publishing Corporation*, 8197389, 1-7.

Olomiyesan, M. B. (2016b). Assessment of Wind and Solar Energy Resources for Implementation of Hybrid Power Systems in North Western States of Nigeria. *Federal University of Technology Minna*, 9-29

Olubusade, J. E., Oyedum, O. D., Aibinu, A. M. & Ezenwora, J. A. (2022). Development of a model for ground measured and satellite-derived GSR data. *International Research Journal of Environmental Sciences*, 11 (3)**,** 27-34.

Osinowo, A. A., Okogbue, E. C., Stephen Bunmi Ogungbenro, S. B. & Fashanu, O. (2015). Analysis of Global Solar Irradiance over Climatic Zones in Nigeria for Solar Energy Applications. *Hindawi Publishing Corporation Journal of Solar Energy*, 819307, 1-9 http://dx.doi.org/10.1155/2015/819307

Otkin, J. A., Anderson, M. C., Mecikalski, J. R. & Diak, G. R. (2005). Validation of GOES- based Insolation Estimates using Data from the U.S. Climate Reference Network. *Journal of Hydrometeorology*, 6 (4), 460–475.

Ouali, K. & Alkama, R. (2014). A new Model of Global Solar Radiation Based on Meteorological data in Bejaia City (Algeria). *Environment and Sustainability, TMREES14. Energy Procedia*, 50, 670 – 676.

Padhma, M. (2021). End to End Introduction to Evaluating Regression Models. Retrieved from https://www.analyticsvidhya.com/blog/2021/10/evaluation metric-for- regression-models/

Pandey, C. K. & Katiyar, A. K. (2013). Solar Radiation: Models and Measurement Techniques. *Hindawi Publishing Corporation. Journal of Energy*, 305207, 1-8. http://dx.doi.org/10.1155/2013/305207

Paluszek, M. & Thomas, S. (2017). Matlab Machine Learning. *Springer Science+Business Media New York, 233 Spring Street, 6th Floor, New York, NY 10013.* DOI 10.1007/978-1-4842-2250-8.

Panhwar, I., Sahito, A. R. & Dursun, S. (2017). Designing Off-Grid and On-Grid Renewable Energy Systems Using HOMER Pro Software. *J. Int. Environmental Application & Science*, 12 (4), 270-276.

Philibert C. (2005). The Present and Future Use of Solar Thermal Energy as a Primary Source of Energy. *Inter Academy Council*.

Phillips, K. J. H. (1995). Guide to the Sun. *Cambridge University Press, 47–53.* ISBN 978-0-521-39788-9.

Pidwirny, M. (2006). Atmospheric Effects on Incoming Solar Radiation. Fundamentals of Physical Geography, Retrieved from http://www.physicalgeography.net/fundamentals/

Pisanty, E. (2018). Why is the silicon crystalline structure is called cubic? Retrieved from https://physics.stackexchange.com/questions/400853/why-is-the-silicon crystalline-structure-is-called-cubic

Pontius, R., Thontteh, O. & Chen, H. (2008). Components of information for multiple resolution comparison between maps that share a real variable. *Environmental Ecological Statistics, 15 (2), 111–142.* DOI:10.1007/s10651-007-0043-y

Prescott, J. A. (1940). Evaporation from Water Surface in Relation to Solar Radiation. *Transactions of the Royal Society of Australia*, 46 (1), 114-118.

Prieto, J. & García, D. (2022). Global solar radiation models: A critical review from the point of view of homogeneity and case study. *ELSEVIER Renewable and Sustainable Energy Reviews,* 155 (111856). https://doi.org/10.1016/j.rser.2021.111856

Punch (2020). Of Nigeria's Dying Factories and Exodus to Ghana. Retrieved from https://punchng.com/of-nigerias-dying-factories-and-exodus-to-ghana/

Punch (2022). 92 million Nigerians lack access to electricity, worst globally – Report. Retrieved from https://punchng.com/92-million-nigerians-lack-access-to electricity-worst-globally-report/

Qiang F. (2003). Radiation (solar). *University of Washington, Seattle, WA, USA. Elsevier Science Ltd*, 1859-1863.

Quej, V. H., Almorox, J., Ibrakhimov, M. & Saito, L. (2016). Empirical Models for Estimating Daily Global Solar Radiation in Yucatán Peninsula, Mexico. *Energy Conversion and Management, Elsevier Ltd,* 110, 448–456.

Quej, V. H., Almoroxa, J., Arnaldob, J. A. & Saitoc, L. (2017). ANFIS, SVM and ANN soft-computing techniques to estimate daily global solar radiation in a warm sub humid environment. *Journal of Atmospheric and Solar–Terrestrial Physics,* 155, 62–70.

Ramachandran, P., Zoph, B. & Le, Q. V. (2017). Searching for Activation Functions. arXiv:1710.05941v2 [cs.NE] 27. Retrieved from http://arxiv.org/abs/1710.05941

Ramli, M. S., Wahid, S. S. & Hassan, K. K. (2017). A Comparison of Renewable Energy Technologies Using Two Simulation Softwares: Homer and Retscreen. *Universiti Teknologi MARA UiTM, MALAYSIA. AIP Conference Proceedings 1875, 030013* https://doi.org/10.1063/1.4998384

Rapier, R. (2020). Fossil Fuels Still Supply 84 Percent of World Energy — And Other Eye peners from BP's Annual Review. Retrieved from https://www.forbes.com/sites/rrapier/2020/06/20/bp-review-new-highs-in global- energy-consumption-and-carbon-emissions-in-2019/?sh=2f3c338466a1

Rawlings, R. (2009). Capturing Solar Energy – CIBSE Knowledge Series*: Hertford: CIBSE Publications*

Razmjoo, A., Mohammadreza, S. H., Ghadimi, M., Qolipour, M. & Nasab, J. R. (2016). Estimating of monthly global Solar Radiation by Angstrom-Prescott (A-P) method for Ahvaz and Abadan cities. *International Journal of Renewable Energy Technology Research,* 5 (2), 1-13.

Reardon C., McGee C. & Milne G. (2013). Your Home. Australia's Guide to Environmantally Sustainable Homes. *Australian Government.* Retrieved from (http://www.gov.au/)

Reliefweb (2022). ACAPS Briefing Note - Nigeria: Country-wide flooding Retrieved from https://reliefweb.int/report/nigeria/acaps-briefing-note-nigeria-country wide-flooding

RETScreen (2015). RETScreen. Retrieved from http://retscreen.net/ang/g_photo.php.
Rietveld, M. R. (1978). A New Method for Estimating the Regression Coefficients in the Formula Relating Solar Radiation to Sunshine, Agricultural Meteorology, 19 (3), 243-252. DOI:10.1016/0002-1571(78)90014-6

Roger, A. H. & Merlin K (2006). Energy its use and the Environment. Thompson Brooks/Cole 2006. Fourth edition, 160-193.

Rojas R. (1996). Neural Networks. A Systematic Introduction, the Backpropagation Algorithm. *Springer-Verlag Berlin Heidelberg New York,* 151-184.

Ruiz, P. F. (2004). European Research on Concentrated Solar Thermal Energy, *European Communities.*

Sabonnadiere, J. C. (2009). Renewable Energy Technologies. *London: Wiley*

Saheb-Koussa, D., Haddadi M. & Belhamel, M. (2009). Economic and technical study of a hybrid system (wind-photovoltaic-diesel) for rural electrification in Algeria. *Applied Energy,* 86 (7), 1024-1030.

Salaris, M. & Cassisi, S. (2005). Evolution of Stars and Stellar Populations. *John Wiley and Sons,* 119–121.

Sambeet M. & Tripathy, P. (2012). Solar Thermal Electricity Generating System. School of Electrical Engineering KIIT University, Bhubaneswar, India. *International Journal of Advancements in Research & Technology*, 1 (3), 2278- 7763.

Sambo, A. S., Garba, B., Zarma I. H. & Gaji, M. M. (2014). Electricity Generation and the Present Challenges in the Nigerian Power Sector. *Energy Commission of Nigeria, Abuja-Nigeria,* Pp 8 -11.

Sanchez, G., Serrano, A. & Cancillo, M. L. (2012). Effect of Cloudiness on Solar Global, Solar Diffuse and Terrestrial Downward Radiation at Badajoz (Southwestern Spain). *Optica Puray Aplicada.*, 45 (1), 33-38.

Schober, P., Boer, C. & Schwarte, L. (2018). Correlation Coefficients: Appropriate Use and Interpretation. *Anesthesia & Analgesia,* 126 (5), 1763-1768 DOI:10.1213/ANE.0000000000002864

Scofield, J. H. (2009). The Solar Spectrum. *Dept. Physics & Astronomy, Oberlin College.* PHYS-068, 1-9.

Sen, Z. (2008). Solar energy Fundamentals and Modelling Techniques. *Springer Verlage Limited, London.*

Shahin, M. A., Jaksa, M. B., & Maier, H. R. (2008). State of The Art of Artificial Neural Networks in Geotechnical Engineering. *Electronic Journal of Geotechnical Engineering* 8 (1), 1–26.

Sharifi, M. B., Georgakakos, K. P., & Rodriguez-Iturbe, I. (1990). Evidence of deterministic chaos in the pulse of storm rainfall. *Journal of Atmospheric Sciences*, 47 (7), 888-893.
DOI: https://doi.org/10.1175/1520-0469(1990)047<0888:EODCIT>2.0.CO;2

Sharston, R. & Murray, S. (2019). The combined effects of thermal mass and insulation on energy performance in concrete office buildings. *Advances in Building Energy Research,* DOI: 10.1080/17512549.2018.1547220

Shepehered, G. M. (2004). The Synaptic organization of the Brain. *Oxford University Press, USA, 2004.* ISBN 019515956X, 9780195159561. 719 pages

Sivakumar, B., Liong, S. Y. & Liaw, C. Y. (1998). Evidence of chaotic behaviour in Singapore rainfall. *Journal of the American Water Resources Association*, 34 (2), 301-310.

Sivakumar, B. (2020). Chaos theory in hydrology: important issues and interpretations. *Journal of Hydrology*, 227 (4), 1-20. https://doi.org/10.1016/S00221694(99)00186-9

Smith, C. (1998). The Science of Energy - a Cultural History of Energy Physics in Victorian Britain. *The University of Chicago Press. ISBN 0-226-76420-6*.

Solar Choice (2016). Why even partial shading is bad for solar power systems. Retrieved from https://www.solarchoice.net.au/blog/partial-shading-is-bad-for-solar panels- power

Solar Server (2011). Online Portal to Solar Energy. Retrieved from http://www.solarserver.com/knowledge/basic-knowledge/solar-collectors.html

Solar Thermal, (2012). Solar Thermal – Concentrated. Retrieved from http://www.solarthermalmagazine.com/Solar Thermal/concentrated-solar-power-2/

Stehlik, J. (1999). Deterministic chaos in runoff series. J. *Journal of Hydrol. Hydromech*, 47 (4), 271–287.

Streetman, B. G. (2006). Solid State Electronic Devices, 6th ed. *Upper Saddle River, NJ: PrenticeHall, Inc.*

Suckling, P.W. (1983). Extrapolation of Solar Radiation Measurements: Mesoscale Analyses from Arizona and Tennessee Valley Authority regions. *Journal of Climate & Applied Meteorology*, 22 (3), 488–494.

Suleiman, L. N. (2010). Renewable Energy as a Solution to Nigeria Energy Crisis. The Africa Report 2019. *University of Applied Science*. Nigeria's oss is Ghana's Gain. Retrieved from https://www.theafricareport.com/21326/nigerias-loss-is ghanas-gain/

Sutskever, I. (2013). Training Recurrent Neural Networks. A thesis submitted in conformity with the Requirements for the Degree of Doctor of Philosophy, *Graduate Department of Computer Science University of Toronto*, 1-49.

Suzuki, K. (2013). Artificial Neural Networks – Architectures and Applications. *InTech Janeza Trdine 9, 51000 Rijeka, Croatia*, 1-264.

Swartman, R. K. & Ogunlade, O. (1967). Solar Radiation Estimates from Common Parameters. *Solar Energy*, 11, 170–172.

Sze, S. M. & Kwok K. Ng (2007). Physics of Semiconductor Devices. *John Wiley & Sons, Inc., Hoboken, New Jersey. Third Edition*. ISBN-I 3: 978-0-47 1-14323-9

Sze, S. M. (1981). Physics of Semiconductor Devices (2nd ed.). *John Wiley and Sons (WIE).* ISBN 0-471-05661-8

Teke, A., Yildirim, H. B. & Celik, O. (2015). Evaluation and performance comparison of different models for the estimation of solar radiation. Renewable and Sustainable Energy Reviews, 50, 1097-1107. DOI: 10.1016/j.rser.2015.05.049.

Telesur (2022). Flood Across Nigeria. Retrieved from https://www.telesurenglish.net/news/612-People-Killed-in-Floods-Across Nigeria-20221026-0002.html

The Guardian (2022). Flooding world climate crisis. Retrieved from https://www.theguardian.com/ environment/2022/oct/20/flooding- world-climate-crisis-australia-venezuela-nigeria

Thevenard, D., Driesse, A., Pelland, S., Turcotte, D. & Poissant, Y. (2010). Uncertainty in Long-term Photovoltaic Yield Predictions, Report # 2010-122 (RP-TEC), *Canmet ENERGY, Varennes Research Centre, Natural Resources Canada*, 1-52.

Thomas Y. (1807). A Course of Lectures on Natural Philosophy and the Mechanical Arts, 1-52.

Tobias, S. M. (2005). The solar tachocline: Formation, stability and its role in the solar dynamo. *Fluid Dynamics and Dynamos in Astrophysics and Geophysics. CRC Press, 193–235.*

Torres, A. F., Garcia, S. A., Pison, S. F. J. & Lamigueiro, P. O. (2013). Evaluation and Improvement of Empirical Models of Global Solar Irradiation: Case Study Northern Spain. *Renewable Energy*, 60, 604-614.
DOI: 10.1016/j.renene.2013.06.008

Turkay, B. E. & Telli, A. Y. (2011). Economic analysis of standalone and grid connected hybrid energy systems. *Renewable Energy*, 36 (3), 1931-1943.

Uchegbulam, O., Opeh, R. N. & Atenaga, M. O. (2014). Assessment of Power Generation Resources in Nigeria. *IOSR Journal of Applied Physics (IOSR-JAP) e-ISSN: 2278-4861*. 6 (2) 44-50.

Udo, B. (2013). Nigerian government ratifies sale of PHCN successor firms to Emeka Offor, 13 others, amid controversies. Retrieved from https://www.premiumtimesng.com/business/145115-nigerian-government- 1

Ullah, K. R., Saidur, R., Ping, H.W., Akikur, R. K. & Shuvo, N. H. (2013). A Review of Solar Thermal Refrigeration and Cooling Methods. *Renewable Sustainable Energy Rev*. 24, 499-513.

USAID (2020). U.S. Agency for International Development. Power Africa in Nigeria. *Energy Sector Overview*. Retrieved from https://www.usaid.gov/powerafrica/nigeria

Utuk, M. (2017). Current Power Generation in Nigeria. Retrieved from www.nigeriaelectrictyhub.com

Vanguard (2018). Rains of Fury: Nigeria loses 141 lives to rainstorm, flood in 2018. Retrieved from https://www.vanguardngr.com/2018/08/rains-of-fury-nigeria loses-141-lives-to-rainstorm-flood-in-2018/

Veeraboina, P. & Guduri, G.Y. (2014). Analysis of yearly solar radiation by using correlations based on ambient temperature: *India. Sustainable Cities and Society*, 11, 16-21. DOI: 10.1016/j.scs.2013.

Vernay C, Blanc P, & Pitaval S. (2013). Characterizing Measurements Campaigns for An Innovative Calibration Approach of the Global Horizontal Irradiation Estimated by HelioClim-3. *Renewable Energy*, 57, 339-347.

Vernay, C., Pitaval, S & Blanc, P. (2014). Review of satellite-based surface solar irradiation databases for the engineering, the financing and the operating of photovoltaic systems. *ELSEVIER Science Direct Energy Procedia*, 57, 1383 – 1391.

Vigneswaran, A., Majid, M. S., Rahman, H. A., Hassan, M. Y. & Hamzah, M. K. (2008). Cost comparison between amorphous silicon and cadmium telluride for stand alone photovoltaic system in Malaysia. *Power Energy Conf.*, no. PECon 08, 468–472.

Wald, L. (2018). Basics in Solar Radiation at Earth Surface. Retrieved from https://hal mines-paristech.archives-ouvertes.fr/hal-01676634

Washington State University (2009). Solar Electric System Design, Operation and Installation. An Overview for Builders in the Pacific Northwest. *Washington State University Extension Energy Program. 905 Plum Street SE, Bldg 3 Olympia*, WA 98504-3165.

Weis, C. (2013). Considerations for Off-Grid PV Systems. Retrieved from https://www.homepower.com/articles/solarelectricity/designinstallation/consider ations-grid-pv-systems

Wikipedia (2021). States of Nigeria and the Federal Capital Territory. Retrieved from https://en.wikipedia.org/wiki/List_of_capitals_of_states_of_Nigeria.

Wilcox Solar Observatory (2006). The Mean Magnetic Field of the Sun. Retrieved from http://wso.stanford.edu/#MeanField

Willmott, C. J., Matsuura, K. & Robeson, S. M. (2009). Ambiguities Inherent in Sums of Squares Based Error Statistics. *Atmos. Environ*., 43, 749–752.

World Economic Forum (2022). Nigeria's worst floods in a decade have displaced over a million people. Retrieved from https://www.weforum.org/agenda/2022/10/nigeria- flood-rain- climate

Xinhua, X. & Hongwei, Z (2019). Soft Computing Methods for Predicting Daily Global Solar Radiation, Numerical Heat Transfer, Part B: DOI:10.1080/10407790.2019.1637629.

Yadav, A. K. & Chandel, S. S. (2013). Solar Radiation Prediction using Artificial Neural Network Techniques: A review. A Review. *Renewable and Sustainable Energy Reviews*. http://dx.doi.org/10.1016/j.rser.2013.08.055i

Younes, S. & Muneer, T. (2006). Improvements in Solar Radiation Models Based on Cloud Data. *Building Services Engineering Research and Technology*, 27 (1), 41–54.

Zambolin, E. & Del Col, D. (2009). Experimental analysis of thermal performance of flat plate and evacuated tube solar collectors in stationary standard and daily conditions. *Solar Energy*, 84 (3), 1382–1396.

Zamfirescu C. & Dincer I. (2009). How Much Exergy One Can Obtain from Incident Solar Radiation. *Journal of Applied Physics*, 105 (044911), 044911-1 to 044911-5. http://dx.doi.org/10.1063/1.3081637

Zargut S. Jan, David R. Morris & Frank R. Steward (1988). Exergy Analysis of Thermal, Chemical and Metallurgical Processes. *Hemisphere Publishing Corporation*. ISNB 0-89116-574-6.

Zgut S. Jan, David R. Morris & Frank R. Steward (1988). Exergy Analysis of Thermal, Chemical and Metallurgical Processes. *Hemisphere Publishing Corporation*. ISNB 0-89116-574-6.

Zhang, D., Wang, J., Linb, Y., Si, Y., Huang, C., Yang, J., Huang, B. & Li, W. (2017). Present Situation and Future Prospect of Renewable Energy in China. *Renewable and Sustainable Energy Reviews ELSEVIER*, 76, 865–871. https://doi.org/10.1016/j.rser.2017.03.023.

Zheng, H.. Yang, Z., Liu, W., Liang, J. & Li, Y. (2015). Improving deep neural networks using softplus Units. *International Joint Conference on Neural Networks*, 1–4. DOI: 10.1109/IJCNN.2015.7280459